The effect of extracellular Hsp90β and TGF-β1 on colon cancer biology

A thesis submitted in the fulfilment of the requirements for the degree of

Master of Science in Biochemistry

of

Rhodes University

by

Tamarin Perks

January 2015

Abstract

The TGF-β signaling pathway is known to be one of the most commonly mutated pathways in human cancers, while Hsp90 is a *bone fide* drug target that is involved in regulating the conformation and activity of many oncoproteins. The role of intracellular Hsp90 in cancer has thus far been established and there is a growing link between extracellular Hsp90 and cancer metastasis, as well as the role of TGF-β in metastasis. This study aimed to analyse the interaction between Hsp90 (both intracellular and extracellular) and the TGF-β machinery in cancer cells, as well as to determine the effect of these proteins on cellular responses on the biology of cancer cells. This was achieved by studying the expression of Hsp90; TGF-βRII and TGF-β1 in cancer cell lines of various origins using flow cytometry, ELISA, and western blot analysis. The genetically paired SW480 and SW620 colon cancer cell lines, derived from a primary tumour and lymph node metastasis, respectively, were selected for further study due to differences in expression levels and activation of the TGF-β1 pathway. SW480 cells expressed double the level of TGF-βRII compared to SW620 cells, while SW620 expressed two times more extracellular TGF-β1 than SW480 cells. A direct interaction between TGF-β1 and Hsp90β was determined *in vitro*, and confirmed *in vivo* in SW620 cells. Growth, adhesion and migration were analysed in SW480 and SW620 cells. SW480 cells adhered significantly faster than SW620 cells, while SW620 cells had a greater rate of migration. Inhibiting the TGF-β pathway, specifically TGF-βRI, using SB 431542, as well as inhibiting Hsp90 with novobiocin, caused an increase in migration in SW480 cells. Only the addition of TGF-β1 in combination with Hsp90 as well as SB 431542 caused an increase in migration in SW620 cells. The canonical TGF-β1/TGF-βRI/TGF-βRII pathway may be constitutively active in SW620 cells and the inhibition of TGF-βRI may suggest an alternate pathway or receptor in both SW480 and SW620 cells.

Declaration

I declare that this thesis is my own, unaided work. It is being submitted for the degree of Master of Science of Rhodes University. It has not been submitted before for any degree or examination at any other university.

Miss Tamarin Perks
January 2015
Grahamstown

Table of Contents

List of Figures

List of Tables

List of Abbreviations

17-AAG	17-allylamino-17-demethoxygeldanamycin
17-DMAG	17- dimethylamino-17-demethoxygeldanamycin
Ab	Antibody
ADP	Adenosine diphosphate
Akt/PKB	Protein kinase B
Aha1	Activator of heat shock protein 90
ANOVA	Analysis of variance
ATCC	American Type Culture Collection
ATP	Adenosine triphosphate
BMP	Bone morphogenetic protein
BSA	Bovine serum albumin
C-terminal	Carboxy terminal
CD95	Cluster of differentiation 95
Cdc37	Cell division cycle 37
CFS	Carboxyfluorescein
CO_2	Carbon dioxide
DAPK	Death-associated protein kinase
DEN Virus	Dengue Fever virus
DMEM	Dulbecco's Modified Eagle Medium
DMSO	Dimethyl sulfoxide
DTSSP	3,3'-Dithiobis[sulfosuccinimidyl]propionate
DOC	Deoxycholate
ECACC	European Collection of Cell Cultures
ECM	Extracellular matrix
ECL	Enhanced chemiluminescence
EDTA	Ethylenediaminetetra-acetic Acid
EEVD	glutamate-glutamate-valine-aspartate motif
EGF	Epithermal growth factor
ELISA	Enzyme-linked immunosorbent assay

ERK	Extracellular signal-regulated kinase
FAK	Focal adhesion kinase
FCS	Fetal calf serum
FITC	Fluorescein isothiocyanate
FoxP3	Forkhead box protein P3
GDF	Growth differentiation factor
Grp	Glucose-regulated protein 94/78
H_2SO_4	Sulfuric acid
HCl	Hydrochloric acid
HEK293T	Human embryonic kidney 293 cells
HEPES	4-(2-hydroxyethyl)-1-piperazine-ethanesulfonic acid)
HER-2	Human epidermal growth factor receptor-2
HIF-1	Hypoxia-Inducible Factor-1
Hip	Hsc70-interacting protein
Hop	Hsp70/Hsp90 organising protein
HRP	Horse radish peroxidase
HSE	Heat shock elements
HSF	Heat shock factor
Hsp	Heat shock protein
IC_{50}	Half maximal inhibitory concentration
IMM	Immunophilins
IgG	Immunoglobulin
JNK	c-Jun N-terminal kinase
LAP	Latency-associated peptide
LIF	Leukemia inhibitory factor
LLC	Large latent complex
LRP-1	Low density lipoprotein receptor-related protein-1
LTBP	latent TGF-1 binding protein
MAPK	Mitogen activated protein kinase
MEK	Mitogen-activated protein/Extracellular regulated kinase
MMP	Matrix metalloproteinase
NIH	National Institutes of Health
N-terminal	Amino terminal
p15	Cyclin-dependent kinase 4 inhibitor B

p21	Cyclin-dependent kinase inhibitor 1
p23	Prostaglandin-E synthase
PBS	Phosphate buffered saline
PBS-T	Phosphate buffered saline with Tween-20
PDM	Product of the differences from the mean
PI3K	Phosphatidylinositide 3-kinase
PMSF	Phenylmethanesulfonylfluoride
PSA	Penicillin, Streptomycin, Amphotericin
Rac	Ras-related C3 botulinum protein
RGD	Arg-Gly-Asp
RhoA	Ras homologous A protein
RIPA	Radio-immunoprecipitation assay
RPMI	Roswell Park Memorial Institute
SDS	Sodium dodecyl sulphate
SDS-PAGE	Sodium dodecyl sulphate-polyacrylamide gel electrophoresis
SLC	Small latent complex
SOX4	(Sex determining region Y)-box 2
SMAD	Mothers against decapentaplegic homolog
Sulfo-NHS	Sulfo- *N*-hydroxysulfosuccinimide
TMB	3,3',5,5'-Tetramethylbenzidine
TBS	Tris-buffered saline
TBS-T	Tris-buffered saline with Tween-20
TGF	Transforming growth factor
TGF-β	Transforming growth factor-beta
TGF-βRI	Transforming growth factor-beta type 1 receptor
TGF-βRII	Transforming growth factor-beta type 2 receptor
TPR	Tetratricopeptide repeat
TRAP1	Tumor necrosis factor type 1 receptor-associated protein
VEGF	Vascular endothelial growth factor
WHO	World Health Organization

List of Symbols

α	Alpha
β	Beta
°C	Degrees Celsius
g	Grams
kDa	Kilodaltons
µg	Micrograms
µl	Microlitres
µm	Micrometres
µM	Micromolar
mg	Milligrams
ml	Millilitres
mM	Millimolar
min	Minutes
M	Molarity
MW	Molecular weight
ng	Nanograms
nm	Nanometres
nM	Nanomolar
N	Normality
%	Percent or g/100 ml
pg	Picograms
x g	Relative centrifugal force to gravity
U	Units
V	Volts
v/v	Volume per volume
w/v	Weight per volume

Acknowledgements

I would firstly like to thank **my supervisor Dr Adrienne Edkins,** for believing in me, without you I would never have made it this far. You are an absolute inspiration to me and your passion for science has pushed me to strive for excellence. You have helped build the foundations to my career and I will forever be grateful to you for all your support, insight, guidance and encouragement.

To **my co-supervisor Dr Jo-Anne de la Mare,** you are the greatest. Without your support, guidance, insight and friendship I may have fallen to pieces. Thank you for always being there to help guide me and keep my feet on the ground. I was honoured to be your first student; I truly believe that you will make an incredible supervisor. I will miss you the most.

My biggest supporter and **my best friend, Scott Jurgens,** thank you for letting me live out my dreams. There is no one I would rather have at my side. Thank you for loving me and always being my rock.

To **my amazing parents Maureen and Peter,** without your constant love and support I would not be where I am today. You are always there for me, no matter what, believing in me wholeheartedly, encouraging me to reach for the stars. You are incredible role models and I am privileged to call you my parents. I love you both so much, I hope I make you proud. This one is for you.

I would like to give a special thank you to **my labby Sam.** We did it!! Thanks for all the laughs, tears and special times. You are literally my other half, and one in a million; I will cherish your friendship forever. Thank you to all the members of **my lab BioBRU,** for all your friendship, support and guidance. Your craziness and willingness to help made my time at BioBRU memorable and I believe that being part of an incredible team makes all the difference in the world.

Finally, I would like to thank my funders **The Ernst and Ethel Eriksen Trust and the National Research Foundation** for giving me this opportunity to make a difference in the world. Without this funding this would never have been possible.

Chapter 1
Introduction

1 Introduction

1.1 Cancer as a biological phenomenon

1.1.1 Definition and significance of cancer

According to the World Cancer Report released in 2014, cancer is one of the leading causes of mortality throughout the world. There were 8.2 million cancer related deaths in 2012 alone, with more than 14 million new cases reported in the same year. Colorectal cancer is in the top five most prevalent cancers for both men and woman and accounted for around 700 000 cancer deaths in 2012 (World Health Organization (WHO), 2014). Cancer may be considered as a genetic disease, in which alterations or mutations in genes that are important for regulation of cellular homeostasis, namely oncogenes and tumour suppressors, can cause the progression of cancer from the benign stage to the malignant stage (Hanahan and Weinberg, 2011; Martin, 2003; Sidera and Patsavoudi, 2009). These mutations may in turn alter the expression or activation of downstream components in a number of signal transduction pathways. This allows cancer cells to override the controlling mechanisms that regulate cell survival, growth, differentiation, motility, and proliferation in normal cells (Martin, 2003).

Hanahan and Weinberg (2000) proposed that there are several cancer hallmarks, which are phenotypes that most cancer cells display (Hanahan and Weinberg, 2000). These traits include: (1) evasion of apoptosis or programmed cell death, an essential process without which tumours are able to grow rapidly; (2) self sustained supply of growth signals i.e. the ability to produce the mitogenic growth signals that are needed to start proliferation; (3) independence of extracellular growth signals or anti-growth signals allowing cancer cells to continually proliferate; (4) angiogenesis, in that cancer cells have the ability to develop their own blood supply/vascular system when it is needed, and thus have a continual supply of oxygen and nutrients; (5) limitless proliferation potential which, with the combination of the first three hallmarks, allows cancer cells to divide indefinitely; and (6) metastasis, in which cells move out of the primary tumour and invade nearby cells, moving to different sites in the body to form new tumours. The latter capability allows the cells to find new areas where there are more nutrients and more space to grow (Hanahan and Weinberg, 2000). Each of

these physiological changes shows a breach against the defense mechanisms that cells and tissues have against cancer. In 2011, Hanahan and Weinberg proposed four more hallmarks that needed to be considered when defining a cancer, these are: (7) the deregulation of cellular metabolism, (8) the avoidance of immune destruction, (9) the instability and mutation level of the genome, which links to the classification of cancer as a genetic disease discussed above, and finally (10) the development of tumour-promoting inflammation (Hanahan and Weinberg, 2011).

1.1.2 Cancer metastasis

The major cause of cancer-associated mortality is often not the primary tumour, but rather metastasis of cancer cells to tissues elsewhere in the body (Chaffer and Weinberg, 2011; WHO, 2014). Currently there are few standardised therapies available to prevent or treat cancer metastasis; even though these treatments have the potential of providing relapse-free survival for cancer patients (Tsutsumi *et al*., 2009). Metastasis, one of the ten cancer hallmarks mentioned above (Hanahan and Weinberg, 2000, 2011), occurs so that cancer cells in the tumour can escape the tumour microenvironment and spread to establish at another site where they can proliferate (Gupta and Massagué, 2006). For metastasis to occur there are a series of sequential processes which must take place and these are shown in Figure 1 (Tsutsumi *et al*., 2009; Gupta and Massagué, 2006). The cancer cells in the primary site of the tumour proliferate to increase the tumour mass (Figure 1, step 1). At the same time, angiogenesis, which is a vital process that provides blood flow and thus nutrients to the growing group of cells, occurs at this site. New blood vessels and capillaries form from vasculature that is already present, with the help of angiogenic growth factors, such as vascular endothelial growth factor (VEGF), which in turn is regulated by hypoxia-inducible factors (e.g. HIF-1) (Gupta and Massagué, 2006). Invasion of the surrounding tissues occurs by proteolysis whereby cell impermeable barriers, such as the basement membrane, are broken down by the cancer cells (Figure 1, step 2). What follows is the complex process of migration involving assembly and disassembly of cell adhesions and rearrangement of the actin cytoskeleton. Actin forms a complex with focal adhesions on the extracellular matrix and depolarisation and repolarisation of adhesions within the cell then causes directional movement of the cell (Fidler, 2003; Gupta and Massagué, 2006; Tsutsumi *et al*., 2009). Extracellular matrix proteins are degraded by proteases allowing the

lagging edges of the cell to move through the tissue stroma (Reing *et al*., 2009; Sottile and Chandler, 2005) (Figure 1, step 3). After detaching from the primary site, an embolism of tumour cells enters the capillaries in a process called intravasation to be transported to the new site (Figure 1, step 4). The cells are able to survive in the bloodstream in suspension and adhere to the capillary endothelial cells or the basement membrane of the new tumour site (Figure 1, step 5). This is modulated by signals from extracellular matrix proteins (Hanahan and Weinberg, 2011; Schwartz and Ginsberg, 2002). Extravasation from the blood vessels then occurs, using a similar mechanism to intravasation (Figure 1, step 5). Finally, proliferation and angiogenesis occurs at the secondary site in order to produce a new tumour (Figure 1, step 6) (Fidler, 2003; Gupta and Massagué, 2006; Tsutsumi *et al*., 2009).

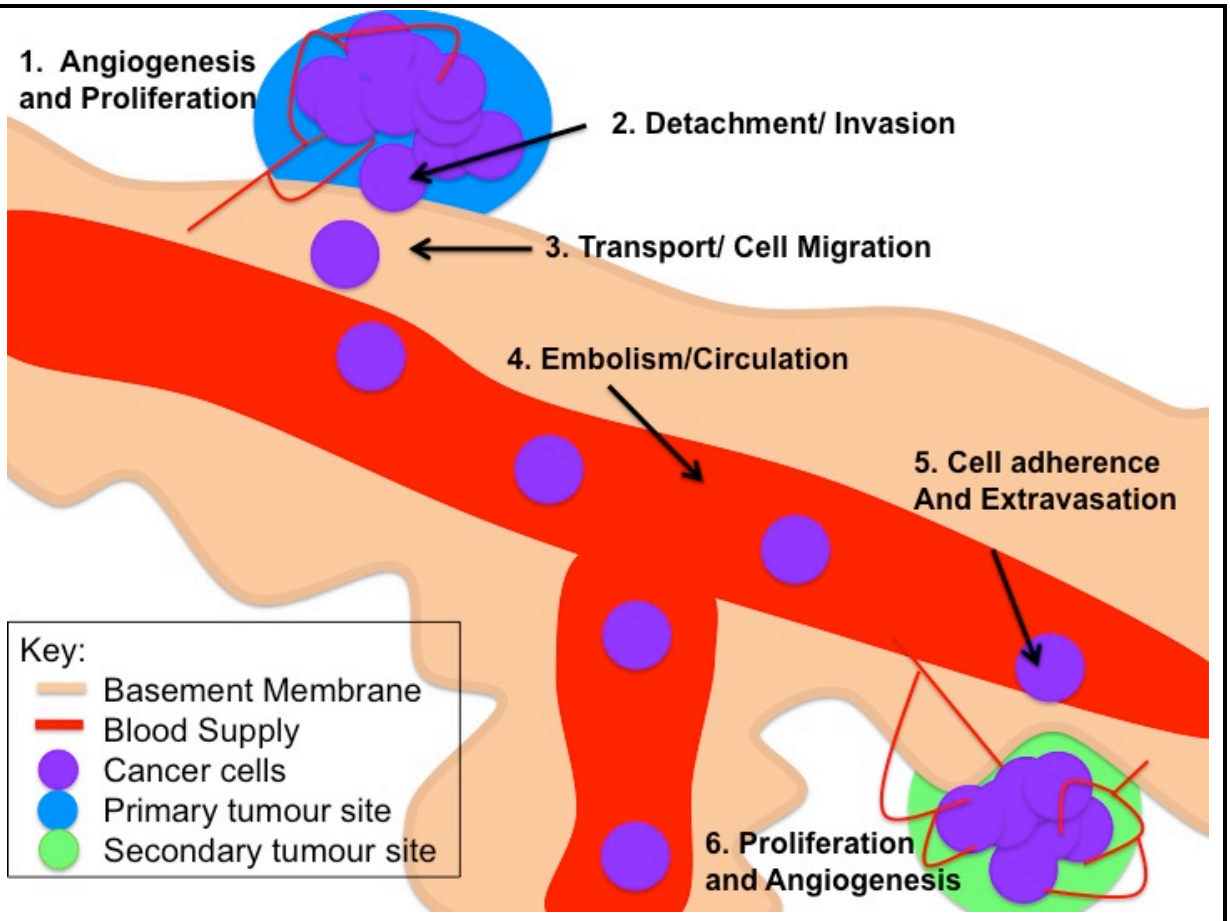

Figure 1. Schematic diagram showing the six steps involved in the metastasis of cancer using the blood stream as a transport system. Steps 1-6 of cancer metastasis are shown and include (1) angiogenesis and proliferation, (2) detachment from the primary site and invasion into the basement membrane, (3) transport using cell migration to the blood vessels, (4) embolism and circulation through the blood stream, (5) cell adherence to the blood vessel, extravasation, and (6) proliferation and angiogenesis at the secondary site (Adapted from: Fidler, 2003; Gupta and Massagué, 2006; Lee and Lim, 2007; Tsutsumi *et al*., 2009).

The processes described above are regulated by several proteins, many of which are activated, overexpressed or mutated in cancer cells (Sidera and Patsavoudi, 2009). One of these proteins is Hsp90, and it has been linked to fundamental metastatic processes *in vitro* and *in vivo*, like cell migration (Annamalai *et al*., 2009; Tsutsumi *et al*., 2009).

1.2 Heat shock proteins

1.2.1 History of Heat Shock Proteins

Heat shock proteins (Hsps) were first discovered over 60 years ago when *Drosophila* cells were subjected to heat stress (Ritossa, 1962; Tissieres *et al*., 1974). It was found that an increase in temperature induced variations in the puffing patterns of the chromosomes of the *Drosophila* cells (Ritossa, 1962). The cellular response to stress has since been studied extensively, with specific focus on the role of some Hsps as molecular chaperones, which will be discussed further below (Schlesinger, 1990). In particular, the gene sequences encoding these Hsps were determined and it was noted that many of them had regulatory signals for their own activation, when certain protein factors were present (Schlesinger, 1990). In addition, it was proposed that Hsps may have many different roles, not only those that are stress-related, as they were also present in cells under normal conditions (Schlesinger, 1990; Sorger and Pelham, 1988).

There are several classes of molecular chaperones that ensure correct and efficient protein folding of newly synthesised proteins, which need to be folded into a unique three-dimensional structure encoded in the amino acid sequence of each protein (Hartl, 2002; Pauwels *et al*., 2007). The refolding process occurs after stress, both spontaneously and with the help of chaperones (Didenko *et al*., 2012; Hartl, 2002; Makhnevych and Houry, 2012; Young, 2001). Some Hsps are molecular chaperones that are constitutively expressed, but whose expression can also be increased under stress conditions such as an increase in temperature (Hartl, 2002; Johnson, 2012). The Hsps can be induced in response to physiological changes such as cell division, apoptosis, tissue development, growth factor activity, as well as many stimuli (other than heat shock) such as amino acid analogs, heavy metals, protein kinases, hormones, infections, alcohol, hypoxia, acidosis, nutrient deprivation and cancer (Calderwood *et al*., 2006; Sarto *et al*., 2000). Hsps also transport polypeptides to

target organelles so that they can be packaged, degraded or repaired, therefore functioning as a quality control system for global protein homeostasis. These Hsps occur in almost every cellular compartment (Altieri *et al*., 2012; Johnson, 2012; Li *et al*., 2012; Marzec *et al*., 2012; Sarto *et al*., 2000). There are specific transcription factors called heat shock factors (HSFs) for the regulation of the expression of these Hsps, which act as activators that bind to specific heat shock elements (HSEs) on the genome (Morimoto *et al*., 1992; Sarto *et al*., 2000; Smith and Workman, 2007; Sreedhar *et al*., 2004).

1.3 Heat Shock Protein 90

1.3.1 Structure and Function of Hsp90

Hsp90 is a highly conserved, ubiquitously expressed molecular chaperone that is particularly abundant in the cytoplasm of stressed cells (Sidera *et al*., 2004). Hsp90 functions mostly include stability and activation of client proteins, which are cellular proteins that require Hsp90 to function. Hsp90 also participates in the assembly, folding, maturation, degradation and proteolytic turnover of these proteins (Hartl, 2002; Sidera *et al*., 2004; Young, 2001). The majority of Hsp90 clients include signal transduction molecules from protein groups like transcription factors, soluble and transmembrane kinases, growth factor receptors and other chaperones (Taipale *et al*., 2012; Tsutsumi *et al*., 2009; Young, 2001).

Hsp90 has mostly been found to exist as a constitutive homodimer (Minami *et al*., 1991), but monomers and heterodimers have also been found (Li *et al*., 2012a; Maruya *et al*., 1999; Minami *et al*., 1991). The general structure of this protein consists of three well-conserved domains. The N-terminal domain is around 25 kDa in size and this is where the ATP-binding occurs. There is a 35 kDa middle domain, and 12 kDa C-terminal domain where dimerisation occurs (Terasawa *et al*., 2005). Hsp90 is ATP-dependent and functions as a chaperone by repeated ATP-dependent cycles (Figure 2) (Cheng *et al*., 2008). The C-terminal domains on Hsp90 are constitutively dimerised and when this dimer of Hsp90 is in an open conformation (with the N terminal domains separated), it has a high affinity for misfolded proteins due to hydrophobic regions on the client protein being exposed. Upon ATP binding to the N-terminal domain the hydrolysis of ATP to ADP drives a conformational change of Hsp90 resulting in its closed conformation and this causes it to clamp down on the client protein (Figure 2)

(Cheng *et al*., 2008; Maruya *et al*., 1999; Meyer *et al*., 2003; Terasawa *et al*., 2005). This closed conformation is induced by a co-chaperone, Activator of heat shock protein 90 (Aha1), by orientating the domains and this increases the rate of ATPase activity (Li *et al*., 2012a).

Co-chaperones are important for Hsp90 function in facilitating activation of the client proteins and regulating the ATPase activity of Hsp90 as demonstrated in Figure 2. There are numerous co-chaperones, the core of which include Hsp70-Hsp90 Organising Protein (Hop), Prostaglandin-E synthase (p23), Cell division cycle 37 (Cdc37), Hsc70-interacting protein (Hip) and immunophilins (IMM), as well as Hsp70, which is also a chaperone in its own right (Li *et al*., 2012a; Pratt and Toft, 2003; Terasawa *et al*., 2005). These proteins coordinate into a multi-chaperone complex (Eustace and Jay, 2004; Pratt and Toft, 2003; Sidera and Patsavoudi, 2009). A client protein attached to Hsp70 will be passed onto an open, nucleotide free Hsp90, facilitated by Hop, which is able to bind simultaneously to both Hsp90 and Hsp70 at different domains. The other co-chaperones p23 and IMM stabilise the closed state of Hsp90 and help with the maturation of the complex (Terasawa *et al*., 2005). When ATP hydrolysis occurs, the complex dissociates and the client protein and co-chaperones are released. Hsp90 is now ready to interact with the next client protein (Figure 2) (Cheng *et al*., 2008; Meyer *et al*., 2003; Terasawa *et al*., 2005).

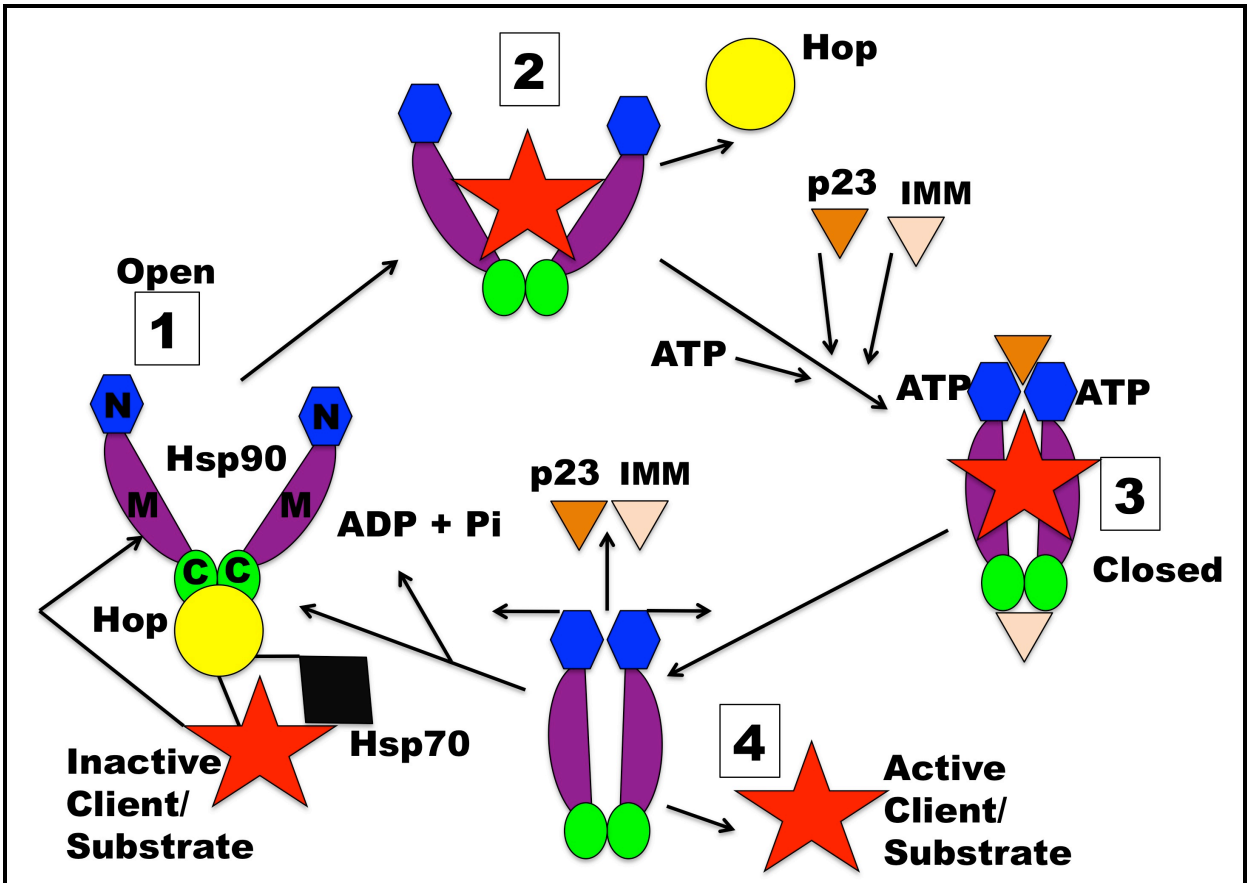

Figure 2. The ATPase cycle of Hsp90 and its interaction with client proteins. (1) The substrate or client (red star) is transferred from Hsp70 (black square) via the co-chaperone Hop (yellow circle) to the open, nucleotide free form of Hsp90. The structure of Hsp90 is depicted with its three domains as follows: the N-terminal (N, blue hexagons), C-terminal (C, green circles) and middle domains (M, purple extended ovals). (2) In this open state Hsp90 binds to the inactive client. (3) ATP binds to the N-terminal domains of Hsp90 causing them to dimerise, allowing p23 (orange triangle) and immunophilins ((IMM) pale pink triangles) to bind. This holds the substrate in place like a clamp. (4) ATP hydrolysis releases the substrate by inducing a conformational change, which opens the clamp releasing the now active client as well as p23 and IMM. Hsp90 is now ready to receive a new client from Hsp70. (Adapted from: (Li *et al*., 2012a; Maruya *et al*., 1999; Terasawa *et al*., 2005; Young, 2001)

1.3.2 Hsp90 Isoforms

Hsp90 occurs in four or five isoforms, according to different literature sources, that have different subcellular localisations. Two of these are cytosolic and extracellular forms (α and β) and they are 85% identical in amino acid sequence (Millson *et al*., 2007; Minami *et al*., 1991; Sreedhar *et al*., 2004; Young, 2001). Hsp90α has been found to be the inducible form of the protein and has been linked to enhanced cell cycle regulation. It has been described as a fast-response, cytoprotective isoform. Hsp90β on the other hand, is constitutive and is involved in normal cellular functions, long-term cellular adaptation and cellular evolution (Millson *et al*., 2007; Sreedhar *et al*., 2004). Both the α and β isoforms have been linked to cancer (Biaoxue *et al*., 2012; Ciocca and Calderwood, 2005; Eustace *et al*., 2004; Hunter *et al*., 2014). A

biochemical difference between the isoforms that has been identified is that the α isoform dimerises more efficiently than the β isoform (Csermely *et al*., 1998; Sreedhar *et al*., 2004). There are a few amino acid variations in certain areas of each isoform, which may be linked to isoform-specific functions. The expression of Hsp90α is lower in comparison to the β isoform but is highly inducible and studies have shown that Hsp90β is essential in human cells, while Hsp90α is not (Grad *et al*., 2010; Millson *et al*., 2007; Voss *et al*., 2000; Young, 2001).

Other Hsp90 isoforms include glucose-regulated protein 94 (Grp94) and Tumor Necrosis Factor Receptor-Associated Protein 1 (TRAP-1)/Hsp75 (Sreedhar *et al*., 2004). Grp94 is located in the endoplasmic reticulum and although it has a very similar domain organisation to Hsp90α and Hsp90β cytosolic isoforms (i.e. N-terminal domain, middle domain and C-terminal domain), it is structurally different at the N terminal and at the C-terminal domains. This implies that the dimerisation of the N-terminal domains during ATP binding may be different and specific to its own client proteins (Marzec *et al*., 2012). TRAP-1, on the other hand, is found in the mitochondria and is similar to Hsp90α and Hsp90β in that it can be inhibited by geldanamycin (see section 1.3.5 and 1.3.6 below), but functional differences are prominent. These include the fact that TRAP-1, as well as Grp94, does not bind to the traditional co-chaperones associated with cytosolic Hsp90. It is also missing the C-terminal tetratricopeptide repeat (TPR) recognition sequence (EEVD) that Hsp90 uses for binding co-chaperones containing this TPR domain (Altieri *et al*., 2012; Li *et al*., 2012a). Both the latter isoforms have been flagged as important due to the potential that they hold for subcellular targeted cancer therapeutics (Altieri *et al*., 2012; Marzec *et al*., 2012).

The final isoform, although quite controversial, is Hsp90N, a truncated 75 kDa Hsp90 lacking the N terminal domain. It has been associated with cellular transformation and appears to be membrane associated (Grammatikakis *et al*., 2002). Since a later study was unable to reproduce the results of Grammatikakis *et al.* (2002), it has been suggested that Hsp90N is probably a result of post-translational modification rather than an independent isoform (Zurawska *et al*., 2008). Thus the classification of Hsp90N as an isoform has been under debate, although no further studies have been performed since 2008.

1.3.3 Extracellular Hsp90

Hsp90 is most well-known to function in the intracellular compartments of the cell, specifically the nucleus, lysosomes, endoplasmic reticulum, cytoplasm and mitochondria (Eustace and Jay, 2004). In the last decade, however, Hsp90 has increasingly been found to activate signaling pathways outside the cell, on the cell surface facing the extracellular space and in the extracellular media (Chen *et al*., 2013; Eustace and Jay, 2004; Hance *et al*., 2014; Hunter *et al*., 2014; Li *et al*., 2007; Li *et al*., 2012b; Sims *et al*., 2011; Suzuki and Kulkarni, 2010). As a result, the role of extracellular Hsp90 is now being studied more intensely (Tsutsumi and Neckers, 2007). The origin of extracellular Hsp90 is also being researched. In particular, the controversial isoform Hsp90N was identified as being associated with the cell membrane (Grammatikakis *et al*., 2002). The secretion of the Hsp90α isoform into the extracellular space has been shown to occur via exosomes and, furthermore, the presence of Hsp90α and Hsp90β was found on the surface of cancer cells, specifically breast cancer (Hunter *et al*., 2014; McCready *et al*., 2010).

In comparison to intracellular Hsp90, which has more than 300 different clients that are known and are currently being studied (Picard, 2014; Sidera *et al*., 2008; Trepel *et al*., 2010; Tsutsumi and Neckers, 2007), there are only a handful of extracellular Hsp90 client proteins that have been elucidated and these are listed in Table I.

Table I. Currently known extracellular Hsp90 Clients*

Client Protein	Classification	Function	Reference
J1pA	Bacterial protein	Mediation of bacterial infection	(Jin *et al*., 2003)
MMP-2 and MMP-9	Serine protease	Tissue invasion and metastasis	(Eustace *et al*., 2004; Stellas *et al*., 2010)
TLR4	Hsp90 receptor	Activity of NK cells; response to LPS	(Triantafilou and Triantafilou, 2004)
Annexin II	Phospholipid binding protein	Generation of Plasmin	(Lei *et al*., 2004; McCready *et al*., 2010)
DEN Virus Receptor	Virus receptor	Interaction with DEN E protein	(Reyes-Del Valle *et al*., 2005)
HER-2/ErbB2	Transmembrane kinase	Cell motility	(Sidera *et al*., 2008)
TGF-βRI/RII	Transmembrane kinase receptor	Phosphorylation of SMAD2 and SMAD3	(Wrighton *et al*., 2008)
LRP1/CD91	Hsp90 receptor	Activity of NK cells	(Cheng *et al*., 2008; Gopal *et al*., 2011)
Latency-associated peptide (LAP)	Precursor domain	Inactivation of TGF-β1	(Suzuki and Kulkarni, 2010)
Fibronectin	Extracellular matrix protein	Cell motility and differentiation	(Hunter *et al*., 2014)

*For a comprehensive and regularly updated list of intracellular and extracellular Hsp90 clients see http://www.picard.ch/downloads/Hsp90facts.pdf

1.3.4 Hsp90 and cancer

Hsp90 has become known as the “cancer chaperone” because the majority of its client proteins are often activated, overexpressed or mutated in cancer cells (Sidera and Patsavoudi, 2009). Hsp90 also stabilises mutant proteins, therefore promoting cancer development (Sidera *et al*., 2008). Many Hsp90 client proteins have been found to have overlapping functions, examples of which include Protein kinase B (Akt), Human Epidermal Growth Factor Receptor-2 (HER-2) and HIF-1α, as well as over 50 others, which are all involved in the control of the cell cycle and cell growth. These proteins have been labeled oncogenic clients (Annamalai *et al*., 2009; Neckers and Ivy, 2003; Sidera *et al*., 2008; Sidera and Patsavoudi, 2009; Taipale *et al*., 2012). Hsp90 is thus involved in many of the fundamental cellular processes involved in oncogenesis.

1.3.5 Extracellular Hsp90 and cell migration

Extracellular Hsp90 has been implicated in the processes involved in cancer cell metastasis, specifically migration and invasion, due to its putative chaperoning activity on the surface of the cell (Annamalai *et al*., 2009; Tsutsumi *et al*., 2009). In 2004, Sidera and colleagues discovered extracellular Hsp90 on the surface of neurons and Schwann cells and showed its involvement in migration and cell motility (Sidera *et al*., 2004). The same group also found that melanoma migration was inhibited by a neutralising antibody purported to be specific for cell surface Hsp90 (Stellas *et al*., 2010). Eustace and colleagues found extracellular Hsp90 on the surface of fibrosarcoma cells and demonstrated that it was linked to invasion. They showed that matrix metalloproteinase 2 (MMP-2), which has been shown to be crucial in cell invasion due to its role in extracellular matrix degradation, was inhibited with geldanamycin, a known inhibitor of Hsp90 (Eustace *et al*., 2004) discussed in section 1.3.6 below. Extracellular Hsp90 has also been demonstrated to regulate motility in dermal fibroblasts (Lei *et al*., 2004). The latter studies showed that neutralising Hsp90 antibodies inhibited cell motility and that the addition of recombinant Hsp90 stimulated motility. Overall, these studies in a range of cells (Eustace *et al*., 2004; Lei *et al*., 2004; Sidera *et al*., 2004; Stellas *et al*., 2010) revealed that extracellular Hsp90 was involved specifically in molecular pathways leading to cell migration and invasion.

1.3.6 Current Hsp90 Inhibitors

Hsp90 inhibitors interact with Hsp90 to inactivate and destabilise the interaction between the chaperone and its client proteins, causing the client proteins to dissociate and be degraded due to the disruption of the folding cycle (Neckers and Ivy, 2003). There are currently four classes of Hsp90 inhibitors, based on their different mechanisms of inhibition (Li *et al*., 2009). These classes are as follows: (1) agents which block the ATP binding site to prevent the clamping of the client protein; (2) those which disrupt the interaction between the co-chaperone and Hsp90, as a more specific approach which will achieve a similar effect as direct inhibition of Hsp90; (3) antagonists of the association between client proteins and Hsp90, providing the best selectivity; and lastly (4) molecules which interfere with the post-translational modifications of Hsp90 for an indirect approach, inhibiting processes such as hyperphosphorylation and hyperacetylation which have been linked to the regulation of co-chaperone association and ATP binding (Li, *et al*., 2009).

The first inhibitor of Hsp90 identified was geldanamycin, derived from the antibiotic group ansamycin, which was originally proposed as an anti-tumour agent because it was found to decrease the activity of receptor tyrosine kinases like HER-2 known to be involved in cancer progression (Holzbeierlein *et al*., 2010; Sidera and Patsavoudi, 2009). Bagatell and colleagues reported in 2004 that geldanamycin bound to the ATP binding site on the N-terminal of Hsp90, which inhibited its chaperone function (Bagatell and Whitesell, 2004). This allowed the clients to be ubiquitinated and degraded by proteolysis. Many Hsp90 inhibitors are currently in clinical trials; a few examples include 17-allylamino- 17-demethoxygeldanamycin (17-AAG), which is currently in Phase II clinical trials for the treatment of kidney cancer (Linehan, 2012) and 17- dimethylamino-17-demethoxygeldanamycin (17-DMAG), which is in Phase I clinical trials for several metastatic cancers and lymphomas (Belani, 2013; Ramanathan *et al*., 2010). These are both analogues of geldanamycin with lower liver toxicity than the original compound (Neckers and Ivy, 2003; Sidera and Patsavoudi, 2009). AUY922 is another Hsp90 inhibitor that binds to the ATP binding site, although it is not an analogue of geldanamycin. This drug is the focus of a number of studies including one which is currently recruiting for Phase II trials on lung cancer (Garon *et al*., 2013) and Phase I trials to treat breast cancer (Jensen *et al*., 2008). Most anti-tumour drugs are aimed at the N-terminal ATP binding site, since replacement of ATP by the drug disrupts the chaperone cycle (Sidera and Patsavoudi, 2009; Trepel *et al*., 2010). This binding site is well conserved in both α and β isoforms (Trepel *et al*., 2010). C-terminal Hsp90 inhibitors have also been studied, of which novobiocin, an analogue of coumarin, was the first to be described. This compound was found to block the dimerisation of Hsp90 (Yu *et al*., 2005), prevent co-chaperone binding and affect client binding (Blagg and Kerr, 2006; Holzbeierlein *et al*., 2010).

1.3.7 Inhibition of Extracellular Hsp90

It has been shown that the level of Hsp90 on the cell surface is greater in cancer cells than in normal cells (Barrot and Haystead, 2013). Blocking secreted Hsp90, especially the α isoform, has been shown to inhibit cell motility and thus extracellular Hsp90 has been linked to the regulation of cell metastasis and motility (Annamalai *et al*., 2009; Li *et al.,* 2012b) and has become an important target for new anti-metastatic drugs in the form of cell-impermeable Hsp90 inhibitors (Sidera and Patsavoudi, 2008). Tsutsumi

and colleagues discovered an inhibitor specifically designed for extracellular Hsp90 in 2009 (Tsutsumi, *et al.,* 2009). It is a small molecule DMAD-N-oxide, which is a derivative of 17-DMAG that has completed Phase I clinical trials, funded by the National Cancer Institute, for metastatic cancer treatment (Belani, 2013; Ramanathan *et al*., 2010). The drug inhibits focal adhesion complex formation and rearrangement of the actin cytoskeleton, thus inhibiting cell migration and invasion. Tsutsumi and colleagues showed that this molecule significantly retarded tumor cell migration and integrin/extracellular matrix-dependent cytoskeletal reorganisation without inducing the degradation of a cohort of intracellular Hsp90 client proteins (Tsutsumi, *et al.,* 2009). These findings prove that extracellular Hsp90 is involved in cell migration and invasion and that these drugs could be used for anti-metastatic cancer therapy.

1.4 Growth factors and cancer

Growth factors are polypeptides that stimulate intracellular signaling pathways by binding to transmembrane receptors, which encompass kinase activity (Witsch *et al*., 2013). While growth factors may not necessarily instigate oncogenesis, they are involved in the regulation of various steps throughout the progression of tumours via downstream signaling pathways (Witsch *et al*., 2013). After several years of studies showing that a range of growth factors were present in cancer cells, it was shown that these growth factors secreted from human tumours are often responsible for autonomous cell growth. A study by Ullrich and colleagues (1984) analysed the intracellular mechanisms of growth factor function and showed that their receptors are usually single pass transmembrane proteins with an intracellular tyrosine kinase domain (Ullrich *et al*., 1984). Another finding showed that growth factors are often the link between tumours and the extracellular matrix and other non-malignant cells (Lee *et al*., 1984). These studies began to explain how growth factors have an important role in tumour progression. In particular, growth factors are involved in proliferation, angiogenesis, invasion, intravasation and extravasation, which are all important steps in the metastasis process (Hanahan and Weinberg, 2011; Witsch *et al*., 2013). Examples of growth factor families that are involved in tumour progression include epidermal growth factors, insulin-like growth factors, transforming growth factors and vascular epithelial growth factors (Witsch *et al*., 2013).

1.5 Transforming Growth Factors (TGFs)

1.5.1 Structure and function of TGFs

Transforming Growth Factors (TGFs) are a class of growth factors divided into TGF-α and TGF-β. Although these two proteins are not structurally or genetically similar and use completely different receptor systems, they are both upregulated in some human cancers (Fallon *et al*., 2000). TGF-α, which is approximately 6 kDa in size, is similar in structure to Epidermal Growth Factor (EGF), both of which bind and compete for the same EGF receptor (Massagué, 2008; Xu and Pasche, 2007). TGF-β on the other hand is a disulphide-linked homodimer around 390 amino acids in length and approximately 13 kDa in size. It is a dual function cytokine/chemokine, which has been shown to regulate a variety of biochemical processes including cell proliferation, differentiation, motility, adhesion, organisation and programmed cell death (Massagué, 2008; Xu and Pasche, 2007). Under normal conditions, TGF-β is primarily involved in the inhibition of proliferation and induction of apoptosis and functions as a tumour suppressor (Massagué, 2008). However, under cancer conditions, the TGF-β pathway is often mutated causing contrasting results compared to healthy cells including becoming a promoter of proliferation and migration (Elliott and Blobe, 2005).

1.6 Transforming Growth Factor Beta (TGF-β)

1.6.1 Activation of TGF-β1 and the TGF-β signaling pathway

Mature TGF-β1 is synthesised within the cell in combination with a signal peptide and an amino-terminal propeptide region called the latency associated peptide (LAP), which together is around 100 kDa in size, as seen in Figure 3 (Annes, 2003; Fontana *et al*., 2005; Munger *et al*., 1999). The mature TGF-β1 homodimer is cleaved from the LAP homodimer but remains strongly bound by a non-covalent bond. This complex is known as the small latent complex (SLC). The SLC binds to the latent TGF-β1 binding protein (LTBP), once both proteins have been secreted, to form a large latent complex (LLC) (Step 1, Figure 3) (Annes, 2003; Miyazono *et al*., 1988; Munger *et al*., 1999; Wipff and Hinz, 2008). The LLC binds to the extracellular matrix (Step 2, Figure 3) and remains bound here until it is activated and this scenario prevents TGF-β1 from binding to the TGF-β type II receptor (TGF-βRII) until it is stimulated to do so. The activation of TGF-β1 by release from LAP and LTBP of a mature 26 kDa active dimer occurs by acid or alkaline pH, increases in temperature, proteases, integrins, thrombospondin 1, reactive oxygen species (Annes, 2003; Munger *et al*., 1999) as

well as by proteolytic cleavage by several MMPs, like MMP2, MMP3, MMP9 and MMP13 (Wipff and Hinz, 2008). Several integrins have also been found to activate latent TGF-β1, specifically αv integrins (Wipff and Hinz, 2008). TGF-β1 LAP has been found to bind to αvβ6 integrin, which provides Arg-Gly-Asp (RGD) sites for this binding and induces activation of TGF-β1 in a protease dependent manner (Munger *et al*., 1999; Sheppard, 2005). The αvβ6 integrin is said to utilise cell traction to spatially regulate the LLC, while also binding to MMPs, allowing a conformational change and refining the location and availability of TGF-β1 (Sheppard, 2005; Wipff and Hinz, 2008).

Once the mature TGF-β1 protein is activated, the TGF-β1 signaling pathway is initiated by the binding of this TGF-β1 ligand to its cognate TGF-β receptors (Rich, 2003; Witsch *et al*., 2013) (Step 4, Figure 3). The TGF-β superfamily consists of a number of related ligands namely TGF-β1, TGF-β2, TGF-β3, Bone morphogenetic proteins (BMP), activin, nodal and Growth and Differentiation Factors (GDFs) each with specific receptor affinities. In particular, the binding of TGF-β1 to TGF-βRII then recruits the type I receptor (TGF-βRI) forming a heterodimeric complex (Step 5, Figure 3), which stimulates receptor-associated protein kinase activity (Rich, 2003; Witsch *et al*., 2013). This phosphorylates the transcription factors SMAD2 (Mothers against decapentaplegic homolog 2) and SMAD3 (Mothers against decapentaplegic homolog 3), resulting in the binding of SMAD2 and SMAD3 to SMAD4 (Mothers against decapentaplegic homolog 4). These complexes translocate into the nucleus (Step 6, Figure 3) where target genes involved in both the promotion and/or suppression of tumours are transcribed. Examples of such target genes include MMP-2, MMP-9, VEGF, (sex determining region Y)-box 2 (SOX4) and Leukemia inhibitory factor (LIF), which are involved in tumour promoting functions; and cyclin-dependent kinase 4 inhibitor B (p15), cyclin-dependent kinase inhibitor 1 (p21), cluster of differentiation 95 (CD95), death-associated protein kinase (DAPK) and forkhead box P3 (FoxP3), which are proteins that take on a tumour suppressing role. A number of other signaling pathways are co-activated as a result of this TGF-β1 signaling pathway (Step 7, Figure 3), for example the Ras/MAPK, RhoA/JNK, PI3 kinase/Akt and Rac/ERK systems (Elliott and Blobe, 2005; Xu and Pasche, 2007). Mutations causing upregulation or downregulation of these pathways are often found in cancers as they are involved in cell growth, division and survival (Witsch *et al*., 2013).

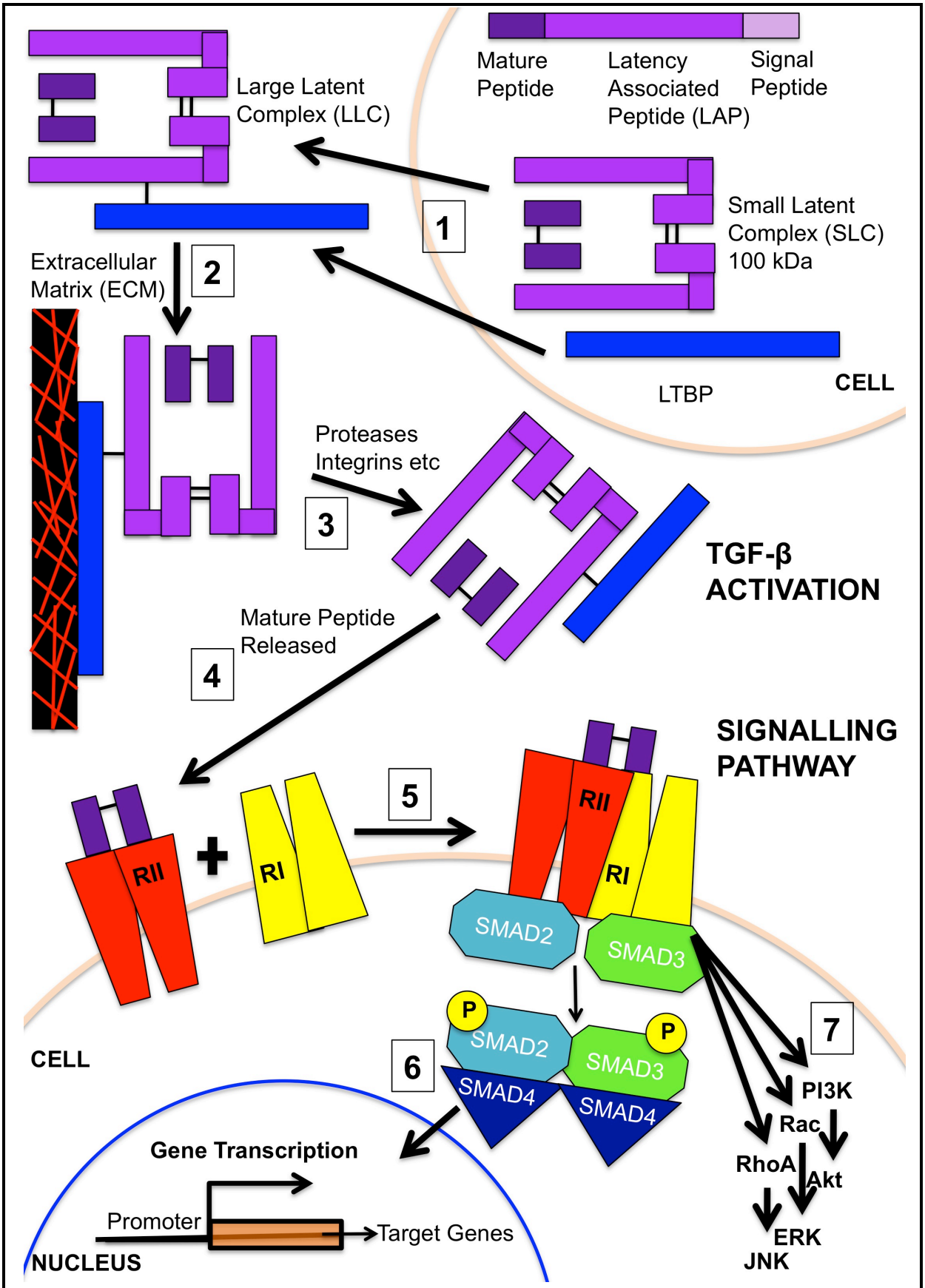

Figure 3. The activation of TGF-β1 and the canonical TGF-β signaling pathway.

Figure 3. (Continued) The activation of TGF-β1 and the canonical TGF-β signaling pathway. TGF-β1 (26 kDa) is co-transcribed with a signal peptide and the latency associated peptide (LAP, 75 kDa) as a proprotein (in dark purple, light purple and lilac, respectively). TGF-β1 is secreted in a small latent complex (SLC, 100 kDa) containing a dimer of the mature TGF-β1 peptide (dark purple rectangles) and a dimer of LAP (light purple rectangles), which binds to the latent TGF-β1 binding protein (LTBP, blue rectangle) creating the large latent complex (LLC) which is around 250 kDa in size (1). The LLC binds to the extracellular matrix (black rectangle with red lines) (2) until it is activated by proteases, acid pH or integrins (3). The released mature peptide (dark purple rectangles) binds to the TGF-β type 2 receptor (RII, red trapezium) (4), which recruits the TGF-β type 1 receptor (RI, yellow trapezium) (5). This initiates the SMAD pathway by phosphorylating SMAD2 (teal octagon) and SMAD3 (green octagon), which bind to SMAD4 (dark blue triangle) and translocate to the nucleus (blue ring) where the complex regulates gene transcription (6). Here target genes involved in tumour promotion (eg. MMP-2, SOX4) and suppression (eg. p15, Fas) are transcribed. Other pathways influenced by the TGFβ machinery are shown to the right in black arrows (7); these include RhoA/JNK, Rac/ERK, and PI3 kinase/Akt. (Adapted from: Annes, 2003; Hui and Friedman, 2003; Rich, 2003; Witsch *et al*., 2013; Xu and Pasche, 2007)

1.6.2 TGF-β and cancer

The TGF-β signaling pathway is known to be one of the most commonly mutated pathways in human cancers (Akhurst, 2004; Massagué, 2008). The role that TGF-β plays in cancer appears to change depending on the stage of the cancer. In particular, the protein takes on the role of tumour suppressor in the early stages of the disease, thereby inhibiting growth, but switches to a tumour promoter in the later stages where it has been linked to metastasis (Bierie and Moses, 2006; Sheppard, 2005). The mechanisms controlling this process are poorly understood, but it has become clear that the way in which TGF-β functions is highly dependent on the microenvironment and the level of progression of the cancer cell (Padua and Massagué, 2009; Simms *et al*., 2012; Xu and Pasche, 2007).

1.6.3 TGF-β and extracellular Hsp90

In recent years a link has been made between the regulation of TGF-β signaling and Hsp90 (Wrighton *et al*., 2008). By using the small molecule inhibitor 17AAG, Hsp90 function was inhibited and it was shown that this caused the degradation of TGF-β receptors (TGF-βR) in Mv1Lu lung epithelial cells and HaCaT keratinocytes, thus preventing TGFβ-mediated transcription (Wrighton *et al*., 2008). This study showed that an element of the TGF-β signaling pathway, specifically TGF-βR, may be regulated by Hsp90 as well as a direct interaction between Hsp90 and the two TGF-β receptors using co-immunoprecipitation (Wrighton *et al*., 2008). Four years later the same chaperone activity was shown in SW480 colon cancer, U2OS osteosarcoma and A549 lung cancer cells using geldanamycin treatments, where TGF-β signaling (also at the TGF-β receptor) was destabilised, and thus found to be dependent on Hsp90 chaperoning (Haupt *et al*., 2012). A study by Suzuki and Kulkarni (2010) showed that Hsp90β was secreted into the extracellular space of osteosarcoma cells where it inhibited the activation of the latent form of TGF-β1, thus decreasing proliferation. This was the first study to link Hsp90 to TGF-β and not the receptor. By stimulating the cells with TGF-β1, an increase in cell surface Hsp90β was also identified. This revealed that Hsp90β was able to function as a negative regulator of the activation of TGF-β1 (Suzuki and Kulkarni, 2010). The other form of TGF, TGF-α, has also been linked to Hsp90, specifically the α isoform, by acting as a trigger for human keratinocytes to secrete intracellular Hsp90α (Cheng *et al*., 2008). The latter

study also suggested that Hsp90α was secreted via the exosome pathway, effectively assisted by TGF-α, and this promoted migration through the LRP1 (LDL receptor-related protein 1)/CD91 cell surface receptor (Cheng *et al*., 2008).

Considering the established interaction between Hsp90 and the TGF-β receptors as well as between Hsp90 and LAP, together with the link between both Hsp90 and the TGF-β pathway and cancer metastasis, it is possible that Hsp90, in particular extracellular Hsp90, interacts directly with the TGF-β1 ligand to regulate biological processes such as migration.

1.7 Problem statement

Intracellular Hsp90 is a *bone fide* drug target that is involved in regulating the conformation and activity of over 300 client proteins, many of which are oncoproteins. Extracellular Hsp90 is also being assessed as a drug target specifically for metastatic tumours. However, in contrast to intracellular Hsp90, the client proteins that interact with extracellular Hsp90 are poorly defined. Given the established role of Hsp90 in cancer and the growing link between extracellular Hsp90 and cancer metastasis, as well as the role of TGF-β in metastasis, it is important to analyse the relationship and interaction between Hsp90 (both intracellular and extracellular) and the TGF-β machinery. This will extend our fundamental understanding of cancer cell biology and may identify novel strategies for anti-metastatic drug development in the future.

1.8 Hypothesis

There is a direct interaction between extracellular Hsp90 and element(s) of the TGF-β signaling pathway in cancer cells *in vitro* and this interaction influences the migration and growth of these cells.

1.9 Aim and Objectives

1.9.1 Broad aim

To characterise the TGF-β1/Hsp90 machinery in cancer cells *in vitro* in terms of their interactions and effect on key biological processes.

1.9.2 Objectives

1. Analysis of the expression of TGF-β1, TGF-βRII and Hsp90 isoforms in a range of cancer cell lines
2. Analysis of potential interactions between intracellular and extracellular Hsp90β and TGF-β1 in cancer cells
3. Determination of the role of TGF-β1 and Hsp90 in growth and migration of cancer cells
4. Investigation of the effect of the addition and inhibition of TGF-β1 and Hsp90β on the downstream TGF-β signaling pathway

Chapter 2
Materials and Methods

2 Materials and Methods

2.1 Materials

2.1.1 Reagents

Reagents specific to each experiment are described in the Methods section below. All other general reagents, including tissue culture reagents and additives, proteins and antibodies, together with supplier information, are listed in Appendix 1.

2.1.2 Cell lines

The MDA-MB-231 (American Type Culture Collection [ATCC]: HTB-26) and the MCF-7 (ATCC: HTB-22) breast carcinoma cell lines were a gift from Associate Professor Sharon Prince (University of Cape Town, South Africa), while the HeLa (ATCC: CCL-2) cervical cancer cell line was a gift from Professor Rosemary Dorrington (Rhodes University, South Africa). The A549 (European Collection of Cell Cultures [ECACC]: 86012804 and ATCC: CCL-185) lung carcinoma cell line as well as the paired colon cancer cell lines SW480 (ECACC: 87092801 and ATCC: CCL-228) and SW620 (ECACC: 87051203 and ATCC: CCL-227), from a colon adenocarcinoma and the lymph node metastasis respectively, were purchased from the European Collection of Cell Cultures (ECACC).

2.2 Methods

2.2.1 Culture maintenance of cell lines

A549 lung cancer cells, MDA-MB-231 and MCF-7 breast cancer cells as well as HeLa cervical cancer cells were cultured in Dulbecco's Modified Eagle Medium (DMEM) supplemented with 5% [v/v] fetal calf serum (FCS), 2 mM L-glutamine, and 100 U/ml Penicillin, 100 µg/ml Streptomycin and 12.5 µg/ml Amphotericin (PSA). SW480 and SW620 colon cancer cells were maintained in Leibovitz's L-15 Medium with GlutaMAX™, 5% [v/v] FCS and 100 U/ml PSA. All cell lines, except the SW480 and SW620 lines, were cultured at 37°C with 9% CO_2 in a humidified incubator. The latter were cultured at 37°C without CO_2.

2.2.2 Surface staining of cells for flow cytometry

Cells were harvested using 1X Accutase® solution (A6964, Sigma-Aldrich), washed twice with phosphate-buffered saline (PBS, pH 7.4; 137 mM NaCl, 27 mM KCl, 4.3 mM Na_2HPO_4, 4 mM KH_2PO_4), collected by centrifugation at 720 x *g* and resuspended to a final concentration of 5 x 10^6 cells/ml. Thereafter 1 µg Fluorescein isothiocyanate (FITC)-conjugated mouse anti-human TGF-βRII antibody was added to 200 µl of cell suspension (1 x 10^6 cells). The sample was vortexed briefly and incubated at 4°C for 60 minutes in the dark. The stained cell suspension was washed twice with PBS, collected by centrifugation at 720 x *g* and resuspended in 200 µl PBS once more. The final cell suspension was analysed using a FACSAria™ III flow cytometer, specifically the 488 nm Coherent® laser (BD Biosciences) using wavelengths of 488 nm and 519 nm for excitation and emission, respectively. A FITC-conjugated mouse IgG_1 isotype control was used to account for any non-antigen non-specific binding of primary antibodies. A further negative control without primary antibody was used to assess cell autofluorescence. Data was analysed using FlowJo software version 10.0.4 (Tree Star Inc., 2013).

2.2.3 Collection of spent media and cell lysis

The spent media was removed from confluent 6-well plates and centrifuged at 13 800 x *g* for 5 minutes to remove cell debris before storing at -80°C for later use. Lysis buffer (0.05 M Tris-HCl, 10% [v/v] glycerol, 2% [w/v] SDS) was added to the cells and incubated for 10 minutes. Cells were scraped gently to form a lysate, boiled for 5 minutes and stored at -20°C. The total protein content of cell lysates was determined using a NanoDrop 2000™ (Thermo Scientific) at an absorbance of 280 nm.

2.2.4 Enzyme-linked Immunosorbent Assay (ELISA)

A human TGF-β1 DuoSet Development ELISA kit (DY240, R&D Systems Inc.) was utilised to analyse the expression of TGF-β1 in the cell culture supernatant (spent media) of a column of cancer cell lines. This was carried out according to manufacturer's specifications. Briefly, the wells were coated with a capture antibody overnight at room temperature, washed with PBS containing Tween-20 (PBS-T: 0.05% [v/v] Tween-20 in PBS) and then blocked for 1 hour in PBS containing 5% [v/v] Tween-20. The TGF-β1 present in cell supernatants was activated using 1 N HCl and

neutralised with a 1.2 N NaOH/0.5 M HEPES buffer before use. After further washing steps, 100 µl of cell supernatant was added to the wells and incubated for 2 hours at room temperature. The wells were washed once more, followed by incubation for 2 hours with the detection antibody. Streptavidin-horseradish peroxidase (HRP) was added to each well and incubated at room temperature for 20 minutes. Each well was washed and developed using 1 mg of 3,3', 5,5'-Tetramethylbenzidine (TMB) (T5525, Sigma-Aldrich). One tablet of TMB (1 mg) was dissolved in 1 ml of DMSO and added to 9 ml of 0.05 M Phosphate-Citrate Buffer (0.2 M Na_2HPO_4, 0.1 M citric acid, pH 5.0) and 2 µl of 30% [v/v] hydrogen peroxide was added immediately prior to use. To stop the reaction, 2 M H_2SO_4 was added and the colour development was recorded at 450 nm and 540 nm using a microtitre plate reader (PowerWaveX^{TM}, BioTek). Samples were assayed in triplicate and the concentration of TGF-β1 determined from a standard curve generated by assaying purified recombinant human TGF-β1 diluted to an eight-point range between 0 pg/ml and 2000 pg/ml in duplicate.

2.2.5 Sodium Dodecyl Sulphate-Polyacrylamide Gel Electrophoresis (SDS-PAGE), western blot analysis and chemiluminescent detection of proteins

The method described by Laemmli (1970) was used to separate proteins by denaturing electrophoresis according to size. SDS-PAGE sample buffer (0.05 M Tris-HCl, 10% [v/v] glycerol, 2% [w/v] SDS, 1% [w/v] bromophenol blue, 5% [v/v] β-mercaptoethanol) was added to samples, followed by boiling for 5 minutes (or longer where needed). Acrylamide gels were made up of 4% [v/v] stacking gel in 0.5 M Tris-HCl (pH 6.8), and either 8%, 10% or 12% [v/v] resolving gel in 1.5 M Tris-HCl (pH 8.8), and elecrophoresed between 120-160V in SDS-PAGE running buffer (0.25 mM Tris, 192 mM glycine, 1% [w/v] SDS pH 8.3). Pierce Prestained Protein MW Marker (26612, Thermo Scientific) was used to approximate sizes of resolved proteins.

Western blotting was performed according to Towbin *et al*. (1979). Protein samples resolved using SDS-PAGE were transferred onto a nitrocellulose membrane for 2 hours at 120 V using transfer buffer (13 mM Tris-HCl, 100 mM glycine, 20% [v/v] methanol). Ponceau S staining (0.5% [w/v] Ponceau S, 1% [v/v] glacial acetic acid) was used to confirm protein transfer from the gel to the membrane. Destaining was achieved using deionised water or Tris-Buffered Saline (TBS; 50 mM Tris, 150 mM NaCl, pH 7.5). Membranes were blocked using 5% milk (5% [w/v] fat-free milk powder

in TBS), 1% BLOTTO (1% [w/v] BLOTTO [sc-2325, Santa Cruz Biotechnology] in TBS;) or 5% [w/v] Bovine Serum Albumin (BSA) in TBS. Incubation with primary antibody diluted in the appropriate blocking agent was carried out overnight at 4°C with gentle agitation. Washing of the membrane was done three times with TBS-T (0.05% [v/v] Tween-20 in TBS) to remove unbound primary antibody. Membranes were incubated for 1 to 2 hours with secondary antibodies conjugated to HRP in 5% BLOTTO or TBS-T. Again, washing of the membrane three times in TBS-T ensured removal of excess antibody.

Proteins were visualised using Clarity Western Enhanced Chemiluminescence [ECL] substrate (Bio-Rad) and detected using the ChemiDoc™ XRS+ system (Bio-Rad) or the film exposure method (Agfa HealthCare). The film was placed in developer solution [25% [v/v] G138i 'A', 2.5% [v/v] G138i 'B', 2.5% [v/v] G138i 'C', 2.5% [v/v] G138Si starter (Agfa)] for 1 minute, then washed in stopper solution (2% [v/v] glacial acetic acid), placed in fixer solution [20% [v/v] G334i 'A', 5% [v/v] G334i 'B', 15% [v/v] G334i 'C' (Agfa)] for 1 minute and finally rinsed with water before drying.

2.2.6 Fluorescence Microscopy

SW480 and SW620 cells were lifted with 1X trypsin in 0.3% [w/v] Ethylenediaminetetraacetic acid (EDTA), seeded at a density of 1 x 10^4 cells/ml on gelatin-coated coverslips and incubated for 72 hours at 37°C. The cells were washed in PBS, flash-treated with ice-cold methanol, and allowed to air-dry. Coverslips were blocked with 1% [w/v] BSA in PBS for 45 minutes at room temperature and incubated with appropriate primary antibodies in 1% [w/v] BSA/PBS overnight at 4°C. Cells were washed with 0.1% [w/v] BSA/PBS followed by incubation with the respective secondary antibodies for 1 hour in the dark at room temperature. Cells were again washed with 0.1% [w/v] BSA/PBS and nuclei stained with Hoechst-33342 dye (1 µg/ml) (H1399, Invitrogen) for a few seconds at room temperature. The coverslips were mounted onto microscope slides with fluorescent mounting medium (Dako Mounting Medium [S3023]). Immunofluorescence was visualised using the Zeiss AxioVert.A1 Fluorescence LED and the images analysed using Zen Lite Software 2011 (Zeiss). Images were captured using the 100x oil objective.

2.2.7 Cytotoxicity studies of TGF-βRI and Hsp90 inhibitors on colon cancer cell lines

Half maximal inhibitory concentration (IC_{50}) values of SB 431542, novobiocin and geldanamycin against SW480 and SW620 cells were determined using the WST-1 cytotoxicity assay (Roche Applied Sciences) according to manufacturer's specifications. Briefly, cells were seeded at a density of $6x10^3$ cells/well in 96-well plates at 37°C and allowed to adhere for 48 hours. This was followed by treatment with a range of concentrations (as indicated in figure legends) of SB 431542, novobiocin and geldanamycin for 96 hours. After the addition of 10 µl/well WST-1 reagent and incubation for 3 hours at 37°C, the absorbance at 440 nm was measured using a microtitre plate reader (PowerWaveX^{TM}, BioTek). Data were analysed using KC Junior software (Bio-Tek Instruments) prior to the determination of percentage cell viability relative to vehicle treated cells.

2.2.8 *In vitro* pull down assay

Purified recombinant human Hsp90β and TGF-β1 proteins (2 µg each) were added to 100 µl TBS containing 0.5% [v/v] protease inhibitor cocktail (P8340, Sigma Aldrich) and allowed to interact for one hour at 4°C with gentle agitation. Goat anti-Hsp90α/β antibody (2 µg) was added and allowed to interact with the two recombinant proteins in solution for a further hour at 4°C with gentle agitation. Resuspended Protein A/G PLUS-Agarose (sc-2003, Santa Cruz Biotechnology) (20 µl) was added to the mixture and agitated overnight at 4°C. A negative control containing all components of the interaction except the antibody was used to account for non-specific binding to the agarose beads. Immunoprecipitates were collected by centrifugation at 1000 x *g* for 5 minutes at 4°C. The supernatant was stored at -20°C for analysis at a later stage. The pellet was washed four times with TBS, with centrifugation as described above at each step. After the final wash the pellet was resuspended in SDS-PAGE sample buffer, boiled and centrifuged as before to pellet out the agarose beads. The supernatant, along with samples from the flow through and wash steps, were analysed using western blot analysis as described in Section 2.2.5 above.

2.2.9 *In vivo* pull down assay

SW620 cells were seeded into a T150 flask and, when confluent, placed at 4°C for 1 hour, before washing twice with PBS. DTSSP [3,3´-Dithiobis (sulfosuccinimidyl)propionate], which contains an amine-reactive *N*-hydroxysulfosuccinimide (sulfo-NHS) (21578, Thermoscientific) at a concentration of 3 mg/ml, as well as 1% [v/v] Triton-X was added to the cells and incubated at 4°C for 2 hours. The DTSSP was quenched using 1 M Tris-HCl (pH 7.5) for 15 minutes at 4°C. The cells were lysed with 1 ml Radio-Immunoprecipitation assay (RIPA) buffer (50 mM Tris-HCl [pH 7.4], 150 mM NaCl, 1 mM EDTA, 1 mM Na_3VO_4, 1 % [v/v] NP40, 1 mM sodium deoxycholate [DOC], 1 mM phenylmethanesulfonylfluoride [PMSF] and 0.05 % [v/v] protease inhibitor cocktail) and gentle scraping. Goat anti-Hsp90α/β antibody (5 µg) or goat IgG (5 µg), as an isotype negative control, was added to 1 mg of cell lysate and allowed to interact for an hour at 4°C with gentle agitation. Resuspended Protein A/G PLUS-Agarose was added to the mixture and processed as above (see 2.2.8) with the exception of using TBS-T as the wash buffer.

2.2.10 Confocal microscopy

Gelatin (5% [w/v]) was used to coat 15-well µ-Slide angiogenesis plates (81506, Ibidi) and left to set overnight at 4°C. SW480 and SW620 cells were lifted with 5% trypsin-EDTA, seeded at a density of 1.5 x 10^4 cells/well and incubated for 24 hours at 37°C. The slides were kept in an Olaf humidifying chamber (80008, Ibidi) to prevent evaporation. Cells were treated with varying concentrations of TGF-β1, Hsp90β, SB 431542 and novobiocin for 24 hours at 37°C. The cells were washed, flash treated and stained as in section 2.2.6 above, after which Dako mounting medium (30 µl) was added to each well. Immunofluorescence was detected using the Zeiss LSM 780 laser scanning confocal microscope and the images analysed using Zen Lite Software 2012 (Zeiss) and the intensity of pSMAD2/3 and nuclei in SW480 and SW620 cells was determined as shown in Appendix 3. Images were captured using the 63x oil objective.

2.2.11 Growth Assay

SW480 and SW620 cells were seeded at a density of 1.2 x 10^4 cells/well into 96-well plates and treated immediately with a range of concentrations of TGF-β1, Hsp90β, SB 431542, novobiocin and geldanamycin (as indicated in figure legends). The percentage cell proliferation relative to untreated cells at 24 hours was determined by WST-1 assay as described in section 2.2.7 above.

2.2.12 Crystal violet adhesion assay

SW480 and SW620 cells were seeded at a density of 1.2 x 10^6 cells/ml into a 96-well plate and treated with combinations of TGF-β1, Hsp90β, SB 431542, novobiocin and αvβ6 integrin blocking antibody as indicated in figure legends. The cells were left to adhere for 8 hours at 37°C before decanting the media and washing the wells with PBS three times. Adherent cells were fixed with 4% [v/v] paraformaldehyde in PBS for 15 minutes before washing with deionised water and staining with 10% [w/v] crystal violet in 5% [v/v] ethanol for 20 minutes with gentle agitation. Wells were again washed with deionised water, allowed to air-dry and crystal violet dye solubilised overnight in 5% [w/v] SDS and 1% [v/v] Triton-X with gentle agitation. Absorbance was read at 590 nm using a microtitre plate reader (PowerWaveX^{TM}, BioTek).

2.2.13 Migration assay

SW480 and SW620 cells were seeded at a density of 1.2 x 10^6 cells/ml into each individual well of a micro-insert 4-well chamber (80409, Ibidi) and left to adhere overnight. Each insert was filled with L-15 medium containing combinations of TGF-β1, Hsp90β, SB 431542, novobiocin or an αvβ6 integrin blocking antibody as indicated in figure legends. After 24 hours, the inserts were lifted and the cell area was washed four times to remove floating cells. Photos of the intersection between the vertical and horizontal wounds generated by the micro-inserts were taken under a 10x objective using an iPhone 5 in conjunction with the SkyLight microscope adapter at 0, 12, and 24 hours. Images were analysed in Image J (National Institutes of Health (NIH)) as indicated in figure legends and described in Appendix 2 to quantify migration of cells.

2.2.14 Statistical Analysis

Where relevant, statistical analysis was carried out using GraphPad Prism 4.03 software (GraphPad Inc., 2005). IC_{50} values were calculated by non-linear regression. T-Test was performed when comparing two cell lines. Two-way ANOVA, with Bonferroni post tests, were performed where many treatments were being compared.

Chapter 3

Results

3 Results

3.1 Characterisation of diverse cancer cell lines for expression of TGF-βRII, TGF-β1 and Hsp90

SW480 and SW620 colon cancer cells, MDA-MB-231 and MCF-7 breast cancer cells, A549 lung cancer cells and HeLa cervical cancer cells were analysed to determine the extracellular expression levels of a key TGF-β cell surface receptor, TGF-βRII. This was achieved by fluorescent staining using an anti-human TGF-βRII antibody followed by analysis by flow cytometry. Histograms from isotype controls were gated using FlowJo software, for a total of 5% TGF-βRII positive events and then copied onto the histograms for their corresponding stained samples (Figure 4). The histograms (solid black line) in Figure 4 illustrate the TGFβ-RII staining compared to the isotype control (grey shading) for each cell line. The histograms for the SW480, SW620, MDA-MB-231, MCF-7, and A549 cell lines showed a clear shift in fluorescence associated with an increase in TGF-βRII staining, relative to the isotype control, which indicates that these cell lines expressed the receptor. In contrast, the histogram for TGFβ-RII staining in the HeLa cell line showed only a slight shift in fluorescence relative to the control suggesting low levels of the receptor (Figure 4). The comparison of the percentage of positive events in each population revealed that SW480 cells had the highest expression of TGF-βRII of all the cell lines analysed, with 50.5% positive events (Figure 4). SW620, MDA-MB-231, MCF-7, and A549 cells all had a similar level of TGF-βRII expression (between 24.1% and 31.3%), while HeLa cells had very little expression of TGF-βRII (Figure 4). Considering their identical genetic background it is interesting to note that the SW480 colon adenocarcinoma line displayed double the TGF-βRII expression level of the SW620 line derived from a lymph node metastases.

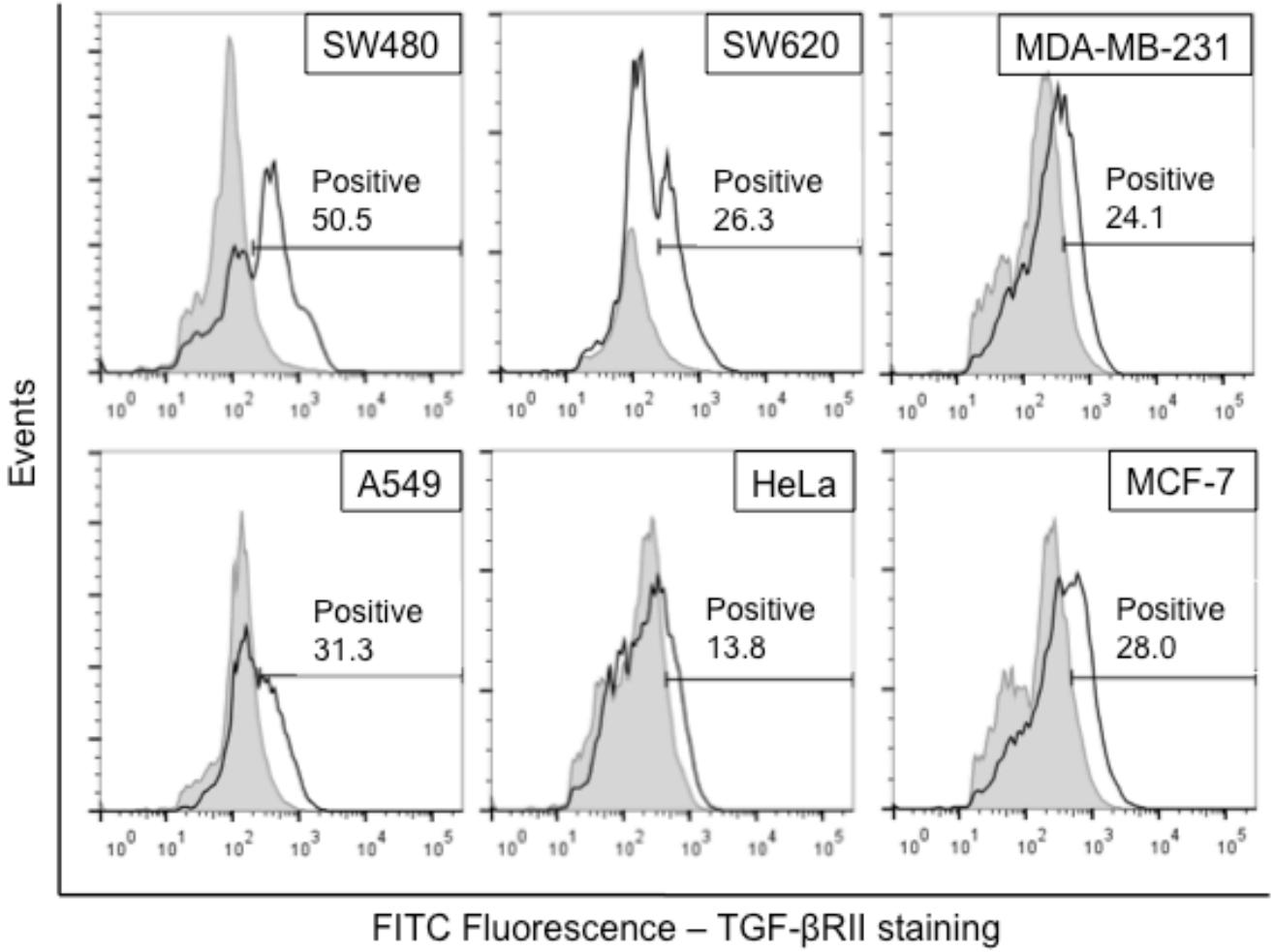

Figure 4. Screening of cancer cell lines for the expression of TGF-βRII on the cell surface. SW480, SW620, MDA-MB-231, MCF-7, A549 and HeLa cancer cells were seeded at a density of 5 x 10^6 cells/ml and stained for the presence of TGF-βRII using a Fluorescein isothiocyanate (FITC) conjugated TGF-βRII antibody. Fluorescence was detected using the FACSAria III flow cytometer (BD Biosciences). The 488 nm Coherent® laser (BD Biosciences) was used with the wavelengths of 488 nm and 519 nm for excitation and emission, respectively. A negative control for each cell type was included and consisted of cells incubated with a fluorophore-conjugated IgG1 isotype control. Data was analysed using FlowJo software version 10.0.4 (Tree Star Inc., 2013). Histograms from isotype controls were gated for 5% TGF-βRII positive events and then copied onto the histograms for the corresponding stained samples. The histograms for the cell samples were overlaid onto each respective isotype control and therefore show the normalised levels of FITC fluorescence for each cell line, where solid black lines represent each antibody-stained sample and the filled grey peaks represent the respective isotype control.

Equal total protein concentrations (50 µg) from SW480, SW620, MDA-MB-231, MCF-7, A549 and HeLa whole cell lysates were analysed for expression levels of intracellular TGF-βRII and Hsp90 using western blot analysis (Figure 5A). Densitometry was performed using Image J, normalising to total protein loaded. These levels were compared between the various cell line lysates and are shown in Figure 5B. The highest levels of intracellular TGF-βRII were detected in the lysates derived from the SW480 and MDA-MB-231 cell lines, with arbitrary units of 467.6 and 449.9; respectively (Figure 5B), followed by reduced levels observed in the SW620, MCF-7, A549 and HeLa cell lines, with ratios of 219.4, 304.2, 298.9 and 226.8; respectively (Figure 5B). SW480 cells displayed twice the level of intracellular TGF-βRII in comparison to SW620 cells (Figure 5B), which corresponds to the data regarding extracellular TGF-βRII derived using flow cytometry (Figure 4). A positive control of 2 ng Hsp90β was used to validate the Hsp90α/β antibody and was detected at a molecular weight corresponding to the anticipated size of 90 kDa. The α and β isoforms are too similar in size and therefore did not resolve. Densitometry for the Hsp90α/β signal was performed in the same manner as for TGF-βRII using total amount of protein loaded (50 µg). The expression levels of total intracellular Hsp90 (both α and β isoforms) were higher in MCF-7 cells (arbitrary unit per µg of protein of 382.3; Figure 5C) when compared to the other five cells lines, which ranged from arbitrary units per µg of protein of 73.8 to 189.6 (Figure 5C).

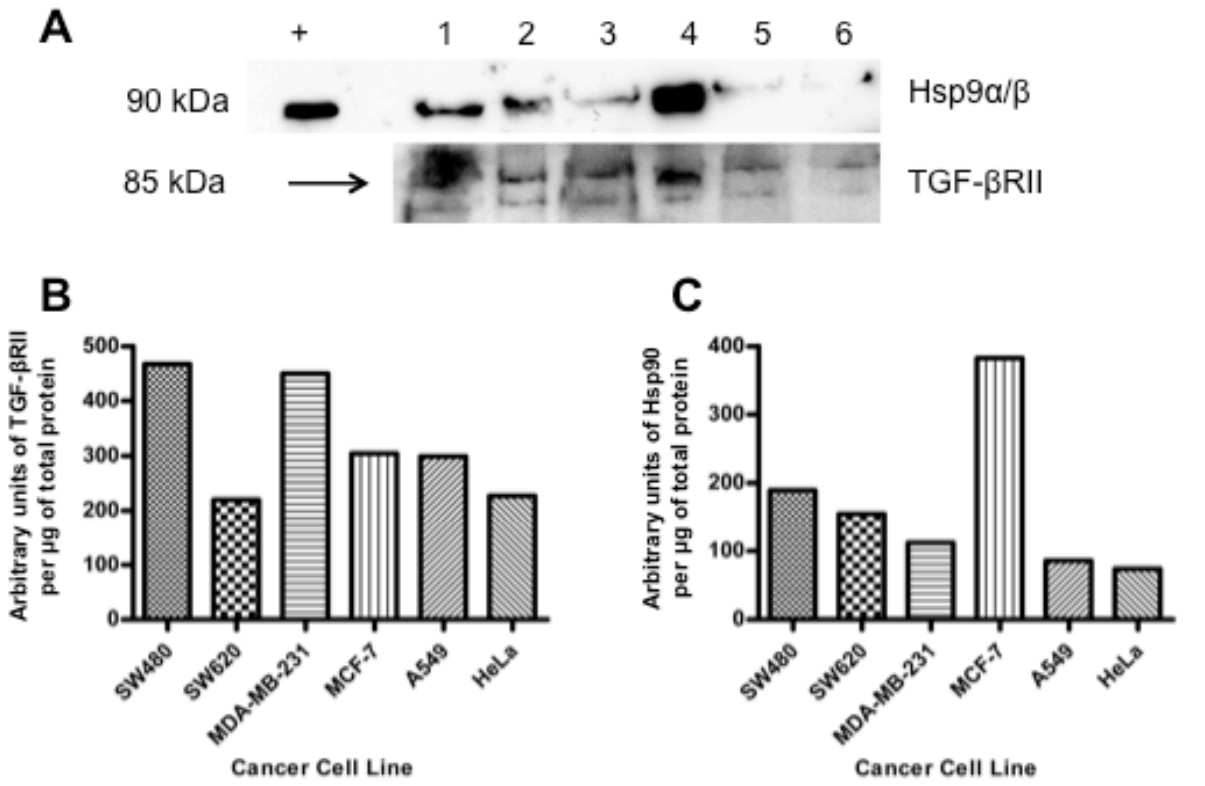

Figure 5. Screening of cancer cell lines for intracellular/total TGF-βRII and Hsp90 expression. (A) Whole cell lysates from SW480, SW620, MDA-MB-231, MCF-7, A549 and HeLa cancer cells were analysed for intracellular/total TGF-βRII and Hsp90 by western blot analysis using the intensity of the tubulin signal as a loading control. The lanes on the western blot in A correspond to: a positive control (+) of 2 ng of purified recombinant Hsp90β and whole cell lysates from SW480 (1), SW620 (2), MDA-MB-231 (3), MCF-7 (4), A549 (5) and HeLa (6) cells. The graphs in (B) and (C) show the densitometry for TGF-βRII and Hsp90, respectively, relative to the loading control as determined in Image J (NIH). These data are representative of one screening experiment.

To assess the expression of soluble extracellular TGF-β1 secreted by SW480, SW620, MDA-MB-231, MCF-7, A549 and HeLa cancer cell lines, an ELISA was performed on spent media using the human TGF-β1 DuoSet Development ELISA kit (Figure 6A and B). A standard curve was generated from eight serial dilutions of recombinant human TGF-β1 ranging in concentration from 31.25 - 2000 pg/ml (Figure 6A) and used to determine the concentration of soluble extracellular TGF-β1 in samples from each cell line. When corrected for cell number, it was discovered that HeLa cells exhibited the highest level of TGF-β1 secretion with a concentration of 444.0 pg/ml, while SW480 cells displayed low levels of TGF-β1 secretion (87.3 pg/ml; Figure 6B). SW620 and A549 cells displayed relatively similar levels of secretion of TGF-β1 (191.9 pg/ml and 252.3 pg/ml, respectively; Figure 6B). The breast cancer cell lines MCF-7 and MDA-MB-231 had similar TGF-β1 levels, although the concentrations determined were slightly higher than that of the other cell lines (296.1 pg/ml and 365.8 pg/ml, respectively; Figure 6B). When comparing TGF-β1 secretion by the

genetically paired cell lines SW480 and SW620, it was noted that SW620 cells secreted approximately twice the level of TGF-β1 than the SW480 cells (191.9 pg/ml vs. 87.3 pg/ml, respectively; Figure 6B). This is the opposite trend to that observed for the receptor TGF-βRII above (Figure 4).

Western blot analysis was performed to determine the expression levels of intracellular TGF-β1 in each of the six cancer cell lines (Figure 6C). Equal protein concentrations from whole cell lysates of SW480, SW620, MDA-MB-231, MCF-7, A549 and HeLa cancer cell lines were probed for TGF-β1. A positive control of 2 ng/ml of recombinant human TGF-β1 was loaded for comparison with the TGF-β1 detected in the lysates, and also included to validate the antibody detection (Figure 6C). The levels of TGF-β1 in each cell lysate were compared using densitometry after normalisation to histone H3 (Figure 6D). This quantification revealed that the SW620 and MCF-7 cell lines had a higher level of intracellular TGF-β1 (Arbitrary units per µg of protein of 451.9 and 309.9, respectively; Figure 6D) in comparison to the remaining cell lines, which demonstrated a similar level of expression between them (SW480: 241.4, MDA-MB-231: 188.9, A549: 212.9 and HeLa: 140.1, Figure 6D). The positive control of recombinant human TGF-β1 employed in the western blot analysis was detected at a molecular weight of approximately 13 kDa, whereas the TGF-β1 in the cell lysates was detected at a molecular weight of approximately 95 kDa (Figure 6C).

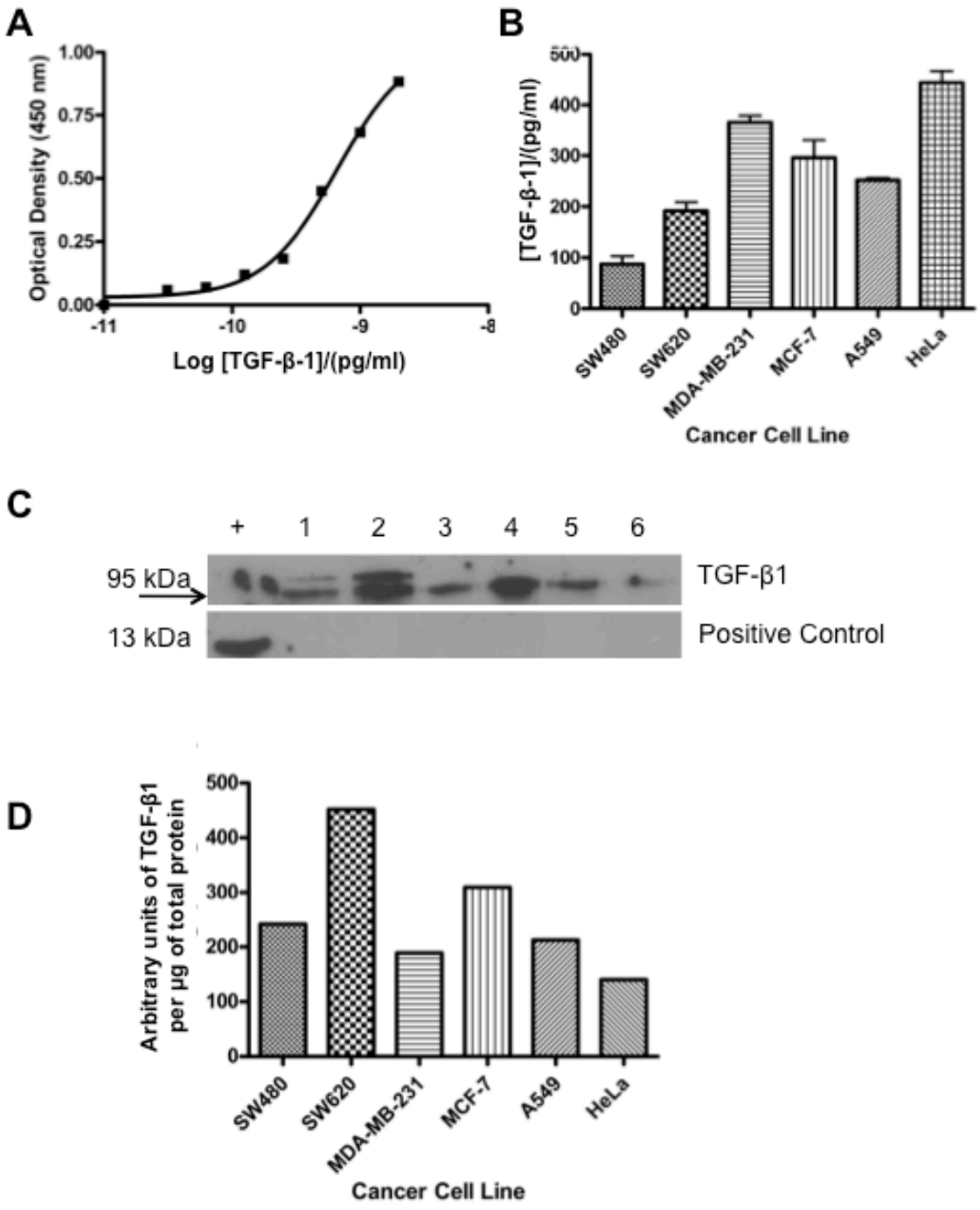

Figure 6. Screening of cancer cell lines for the expression of secreted, intracellular and membrane associated TGF-β1. (A) Recombinant human TGF-β1 was diluted to an eight point range between 31.25 pg/ml and 2000 pg/ml. The absorbance of these samples was read at 450 nm on a microtitre plate reader and the resultant concentration range used to create a standard curve from which the level of TGF-β1 in each sample was quantified. (B) Spent media collected from SW480, SW620, MDA-MB-231, MCF-7, A549 and HeLa cancer cells was analysed for the expression of extracellular, soluble ie. not membrane associated TGF-β1 using a human TGF-β1 DuoSet Development ELISA kit. Data was analysed using GraphPad Prism 4.03 software (GraphPad Inc., California). Data represent the average of three independent experiments performed in triplicate and error bars indicate the standard error in the mean. (C) Cell lysates from the abovementioned cancer cells were analysed for intracellular/total TGF-β1 by western blot analysis using the intensity of histone H3 as a loading control. The lanes on the western blot in A correspond to: a positive control (+) of 2 ng/ml of purified human TGF-β1 and whole cell lysates from SW480 (1); SW620 (2); MDA-MB-231 (3); MCF-7 (4); A549 (5) and HeLa (6) cells. The graph in (D) shows the densitometry for TGF-β1 relative to the Histone H3 loading control as determined in Image J. These data are representative of one experiment.

When TGF-β1 is produced as a recombinant protein it is in its active form, which as a disulphide linked homodimer is 26 kDa in size (Fortunel *et al*., 2000). Thus when this dimer is denatured with SDS-PAGE sample buffer and boiling during the sample preparation for western blot analysis, the disulphide bonds are broken producing a 13 kDa monomeric protein as detected for this recombinant TGF-β1 sample (Figure 6C). Intracellular TGF-β1 from lysates, on the other hand, may still be in the inactive form prior to secretion. When TGF-β1 is synthesised as a proprotein it is in combination with LAP and a signal peptide, which together have a molecular weight of 100 kDa (the processing of TGF-β1 is described in detail in Chapter 1, section 1. 6). It is therefore likely that it is the proprotein form of TGF-β1 being detected in the cell lysates as the denaturant in SDS-PAGE sample buffer should break all disulphide bonds and acidification steps are needed to release the mature peptide from LAP (Annes, 2003; Fontana *et al*., 2005; Fortunel *et al*., 2000; Munger *et al*., 1999).

3.2 Analysis of the expression and localisation of TGF-β1, TGF-βRII and Hsp90 isoforms in the paired SW480 and SW620 colon cancer cell lines

After the comparison of soluble and intracellular TGF-β1 and TGF-βRII, as well as intracellular Hsp90, in six cancer cell lines from four different cancers; the SW480 and SW620 cells were selected for further study due to the differences in the levels of TGF-βRII, TGF-β1 and Hsp90 observed in Figure 4, 5 and 6 above. In addition, these are genetically paired cell lines with the SW480 line derived from a primary colon tumour and the SW620 cells derived from a secondary site where the cancer had migrated to the lymph nodes (Leibovitz *et al*., 1976) making this system an established model for studying changes associated with metastasis *in vitro* and an ideal system to explore the interaction between TGF-βRII, TGF-β and Hsp90 in cancer cell biology.

Expression and localisation of TGF-βRII, TGF-β1 and four of the potentially five known isoforms of Hsp90 (Hsp90α, Hsp90β, TRAP1 and Grp94, described in section 1.3.2) were analysed in SW480 and SW620 cells using fluorescence microscopy (Figure 7, see Appendix 4 – Electronic image 1 for a more detailed figure). The images obtained using Zen Lite Software (2011) revealed that TGF-βRII was dispersed throughout the cell, but also seemed to be concentrated around the nucleus. SW480 cells had a higher level of expression of TGF-βRII, as more intense staining was observed in

comparison to the SW620 cells. On the other hand, TGF-β1 was located around the nucleus and near/on the cell surface in both cell lines, and displayed punctate staining. Expression levels of intracellular TGF-β1 as measured by fluorescent intensity appeared similar in the two cell lines. In terms of Hsp90 localisation, both the Hsp90α and Hsp90β isoforms were dispersed evenly throughout the cytosol in the SW480 as well as the SW620 cells, while the Grp94 and TRAP-1 isoforms were found to both have punctate staining in the cytosol in distinct areas of the cell, consistent with their organelle locations. In the cells stained with the TRAP-1 antibody, organelle staining could be seen more evidently. Expression levels of all Hsp90 isoforms appeared similar in both SW480 and SW620 cells (Figure 7).

Western blot analysis was performed to quantify the levels of Hsp90α and Hsp90β expressed within SW480 and SW620 cells. This was carried out in order to determine if the levels were similar to those seen in the fluorescence images in Figure 7 and to identify any difference between the intracellular expressions of these Hsp90 isoforms. Histone H3 was used as a loading control to ensure equal levels of total protein between samples (Figure 8A). The levels of Hsp90α and Hsp90β were compared using densitometry after normalisation to histone H3 (Figure 8B). As illustrated in Figure 8B, the expression levels of Hsp90α were found to be similar in the two colon cancer cell lines and while a slight difference in Hsp90β levels between cell lines was observed.

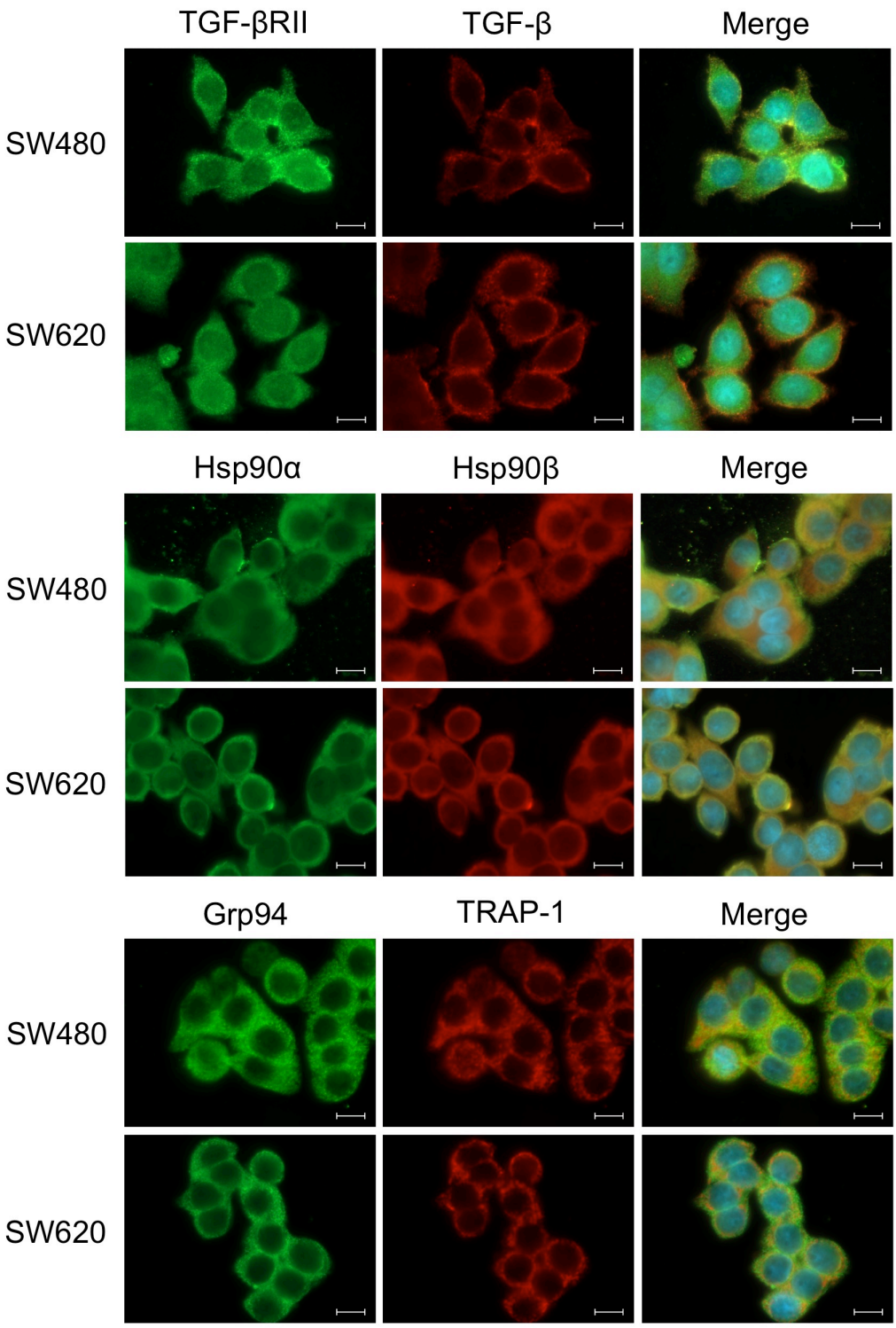

Figure 7. Localisation of TGF-β1, TGF-βRII, and Hsp90 isoforms in SW480 and SW620 colon cancer cells. SW480 and SW620 cancer cells were seeded at a density of 1 x 10^4 cells/ml onto gelatin-coated coverslips, incubated for 72 hours at 37°C and fixed with methanol. The cells were incubated with mouse anti-human TGF-β1, mouse anti-Hsp90β, rat anti-Hsp90α, mouse anti-TRAP-1 and rat anti-Grp94 primary antibodies overnight at 4 °C. This was followed by incubation in donkey anti-mouse Alexa-Fluor-550 (red), and donkey anti-rat Alexa-Fluor-488 (green) secondary antibodies as appropriate overnight at 4 °C. Carboxyfluorescein (CFS)-conjugated mouse anti-human TGF-βRII was incubated overnight at 4 °C. Nuclei were stained with 1 µg/ml Hoechst 33342 (blue). Immunofluorescence was detected using the Zeiss Axio Vert.A1 Fluorescence LED Microscope and the images analysed using Zen Lite Software 2012 (Zeiss, Germany). Cells are shown at 100x magnification. Scale bars represent 20 µm. Data are representative of triplicate images obtained showing similar results. (See Appendix 4, Electronic Image 1)

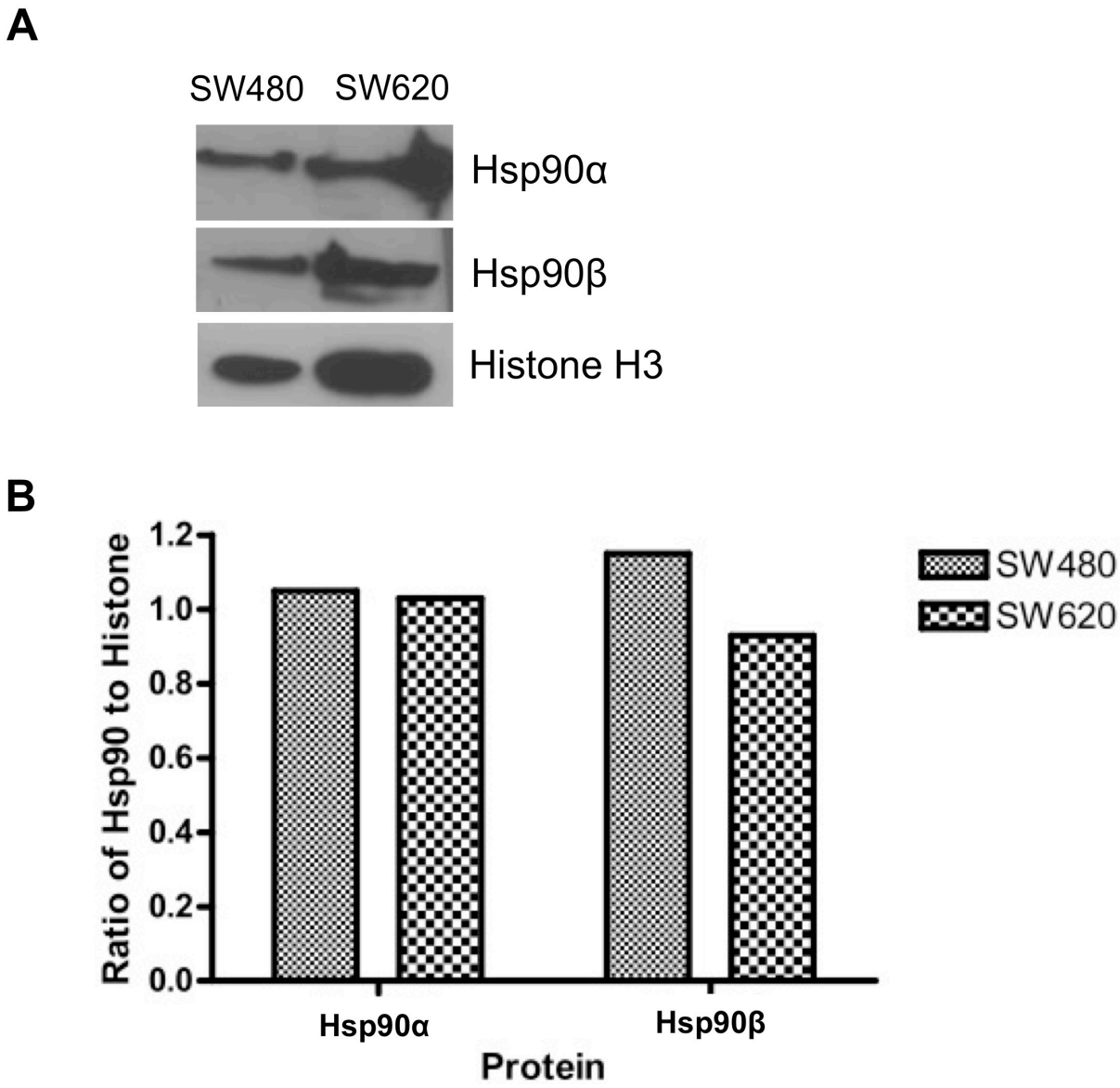

Figure 8. Comparison of the levels of Hsp90α and Hsp90β expression in SW480 and SW620 colon cancer cells. (A) Whole cell lysates from SW480 and SW620 cells were analysed for Hsp90α and Hsp90β expression using western blot analysis performed once. (B) Densitometry used to quantify the Hsp90 signal calculated using the intensity of the histone H3 band (shown in A) as a loading control carried out using Image J.

3.3 Cytotoxicity analysis of inhibitors of the TGF-β Receptor I and Hsp90 in SW480 and SW620 cell lines

To determine the half maximal inhibitory concentrations (IC_{50}) for SB 431542, a TGF-β type I receptor inhibitor; novobiocin, a C-Terminal Hsp90 inhibitor and geldanamycin, an N-Terminal Hsp90 inhibitor; a WST-1 cytotoxicity assay was performed. The colon cancer cell lines were treated with a range of concentrations between 25 and 800 nM for SB 431542 and geldanamycin and between 25 and 600 µM for novobiocin, for 96 hours in order to develop survival curves from which IC_{50} values were calculated using GraphPad Prism 4.03 software (Figure 9). When the SW480 cells were treated with a range of concentrations of the SB 431542 TGF-βRI inhibitor, an IC_{50} of 207.1 nM was obtained, although the standard deviation is relatively high and the R^2 value indicates that this graph is a poor fit to the survival curve generated by GraphPad (0.116, Figure 9A). This suggests that this compound may be non-toxic to the cells, however the poor fit of the survival curve means that any data generated must be interpreted with caution, as it may be unreliable. Analysis of the cytotoxicity of SB 431542 in SW620 cells produced an IC_{50} of 474.6 nM. However, in these cells the standard deviation was not as high as that calculated for SW480 cells (1.4 vs 2.4, respectively) and the fit to the cytotoxicity curve was better, with a R^2 value of 0.615 (Figure 9A). Since an R^2 value of close to 1 is preferable in terms of producing reliable cytotoxicity data, the latter result must again be interpreted with caution. It is possible, however, that the compound is not toxic to the SW620 cells as the IC_{50} is at a high concentration. In retrospect the data could perhaps have been improved using a larger range of concentrations, which may have produced a better curve, however the data served the purpose of determining the survival of the cells at specific concentrations of the inhibitor even though the non-linear regression to determine the IC_{50} may be inaccurate. Nonetheless it was decided to use a concentration of 100 nM for further treatments with SB 431542 as this treatment resulted in reasonable cell survival and was below the IC_{50} values of SB 431542 determined for the SW480 and SW620 cells lines, although, as discussed above, these values may be unreliable.

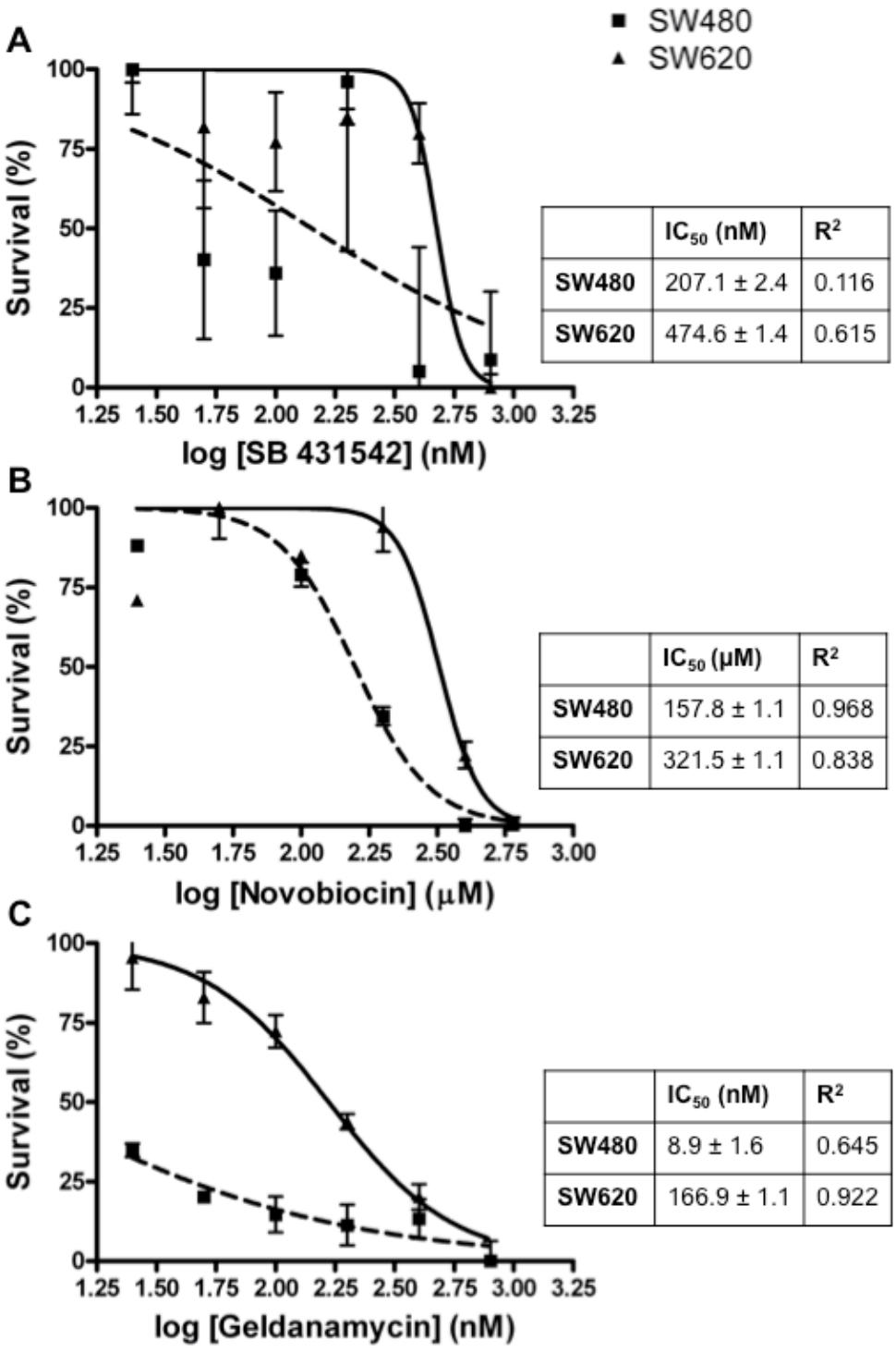

	IC_{50} (nM)	R^2
SW480	207.1 ± 2.4	0.116
SW620	474.6 ± 1.4	0.615

	IC_{50} (μM)	R^2
SW480	157.8 ± 1.1	0.968
SW620	321.5 ± 1.1	0.838

	IC_{50} (nM)	R^2
SW480	8.9 ± 1.6	0.645
SW620	166.9 ± 1.1	0.922

Figure 9. Cytotoxicity study of the TGF-βRI receptor inhibitor (SB 431542), and Hsp90 Inhibitors (novobiocin and geldanamycin) in SW480 and SW620 colon cancer cells. SW480 and SW620 cells were seeded at $6x10^3$ cell/well in 96-well plates at 37°C and allowed to adhere and grow for 48 hours. Cells were then treated with a 6-point serial dilution of three inhibitors in triplicate for 96 hours. These inhibitors included: (A) SB 431542, a TGF-β type I receptor inhibitor used at a concentration range from 25-800 nM; (B) novobiocin, a C-Terminal Hsp90 inhibitor, (25-600 μM) and (C) geldanamycin a N-Terminal Hsp90 inhibitor (25-800 nM). After 96 hours, 10 μl of WST-1 reagent was added to each well and incubated at 37°C for 3 hours. The absorbance at 440nm was read on a Powerwave microtitre plate reader (BioTek Instruments) and data were analysed using KC Junior software (Bio-Tek Instruments) prior to the determination of percentage cell viability relative to the untreated controls. Half maximal inhibitory concentration (IC_{50}) values and R^2 values were calculated using a non-linear regression equation determined using GraphPad Prism 4.03 software (GraphPad Inc.). Data represent the average of triplicate experiments and error bars and ± concentrations indicate the standard error in the mean.

When the cytotoxicity of the Hsp90 inhibitors was analysed, it was determined that novobiocin had an IC_{50} value of 157.8 µM in the SW480 cells and 321.5 µM in SW620 cells. There was a small standard deviation of 1.1 µM in both SW480 and SW620 cells (Figure 9B). The R^2 values derived for these graphs indicated that both the SW480 and SW620 cells produced a very good fit to the cytotoxicity curve (0.968 and 0.838, respectively; Figure 9B), reflecting reliable IC_{50} values. A concentration of 100 µM of novobiocin was used for further studies as it was below the IC_{50} of both the SW480 and SW620 cell lines and should thus not display too high a toxicity to the cells during treatments up to 96 hours. Geldanamycin, on the other hand, had a much greater effect on both cells lines in comparison to SB 431542 and novobiocin, with an IC_{50} of 8.9 nM in the SW480 cells and 166.9 nM in SW620 cells (Figure 9C). A good fit for the cytotoxicity curve was found for geldanamycin treatment in SW620 cells (R^2 value of 0.922, Figure 9C), while treatment in SW480 cells showed a moderate fit (R^2) and a very low IC_{50} value of 8.9 nM (Figure 9C). As geldanamycin was toxic to SW480 cells at very low concentrations and the IC_{50} values differed greatly between the two cells lines (twenty fold lower in the SW480 cells compared to the SW620 cells) the compound was not used in further experiments in this study. Overall, SW620 cells were found to be more resilient to SB 431542, novobiocin and geldanamycin, as the IC_{50} levels determined for this cell line were between two and twenty times higher than that of the IC_{50} values for SW480 cells. The concentrations of SB 431542 and novobiocin selected for further studies were chosen such that the compounds would cause an inhibitory effect on TGF-βRI and Hsp90, respectively, while not being overly toxic to the SW480 and SW620 cells.

3.4 Detection of a putative interaction between Hsp90β and TGF-β1 *in vitro* and *in vivo*

3.4.1 Co-immunoprecipitation of TGF-β1 with Hsp90β

Once the levels of expression of TGF-β1 and Hsp90β had been determined in SW480 and SW620 colon cancer cells as well as in the other four cell lines (MDA-MB-231, MCF-7, A549 and HeLa cells; Figures 6 and 7), the ability of TGF-β1 and Hsp90β to interact directly was assessed. This was performed using a pull down assay with purified recombinant human TGF-β1 and Hsp90β proteins (Figure 10). By incubating these proteins together and linking Hsp90β protein to an Hsp90α/β antibody that binds

strongly to protein A/G-coupled agarose beads, the interaction could be verified if TGF-β1 was pulled down in the bead-bound fraction and not the unbound fraction/flow through. The unbound fraction (depicted as U in Figure 10) was the sample separated from the beads by centrifugation once TGF-β1, Hsp90β, the Hsp90α/β antibody and the beads had interacted overnight and should contain any Hsp90β that did not bind to the Hsp90α/β antibody, any TGF-β1 not interacting with Hsp90β, as well as any excess antibody. The bound fraction (depicted as B in Figure 10) was the final fraction of the experiment after removal of proteins bound to the beads by boiling and denaturation. Any TGF-β1 in the bound sample which had not interacted with Hsp90β was washed off (shown as W in Figure 10A) prior to boiling. A negative control was performed by excluding the Hsp90α/β antibody to determine if the proteins bound to the beads non-specifically.

Western blot analysis was used to identify the proteins in the various fractions following the pull down assay (Figure 10A). A TGF-β1 antibody was used to detect if any TGF-β1 had interacted with the Hsp90β bound via the Hsp90 antibody to the beads. An Hsp90α/β antibody from a different species (mouse) compared to the antibody bound to the beads used for the pull down assay (goat) was utilised to prevent cross species reactions in the western blot. To determine whether the pull down assay had worked i.e. if the Hsp90β had bound to the Hsp90α/β antibody bound to the beads, it was important that Hsp90β be detected. The input of recombinant human TGF-β1 and Hsp90β, containing 2 ng of each protein, in the first lane of the western blot verified that the antibodies would detect the correct proteins (Figure 10A). The unbound (U) samples containing any proteins not interacting with the antibody coupled beads showed a similar amount of TGF-β1 in the analysis with and without the Hsp90 antibody (Figure 10A). In contrast, the level of Hsp90 detected in the unbound sample without the antibody was much greater, indicating that without the antibody the Hsp90β protein did not bind non-specifically to the beads. In the lane labeled B on the western blot (Figure 10A) containing the sample with the Hsp90 antibody, Hsp90β was detected indicating that the pull down was successful, because Hsp90β bound to the antibody and remained on the beads until it was removed by denaturation. Due to the fact that TGF-β1 was detected (at a molecular weight corresponding to 13 kDa) in the Bound (B) fraction containing the Hsp90 antibody, it could be concluded that TGF-β1 was pulled down/co-immunoprecipitated by Hsp90β.

This indicated that there was a direct interaction between the two proteins. The sample without the antibody had either no or very low levels of Hsp90β and TGF-β1 in the bound sample, thus verifying that the interaction was not simply a non-specific interaction of TGF-β1 with the beads.

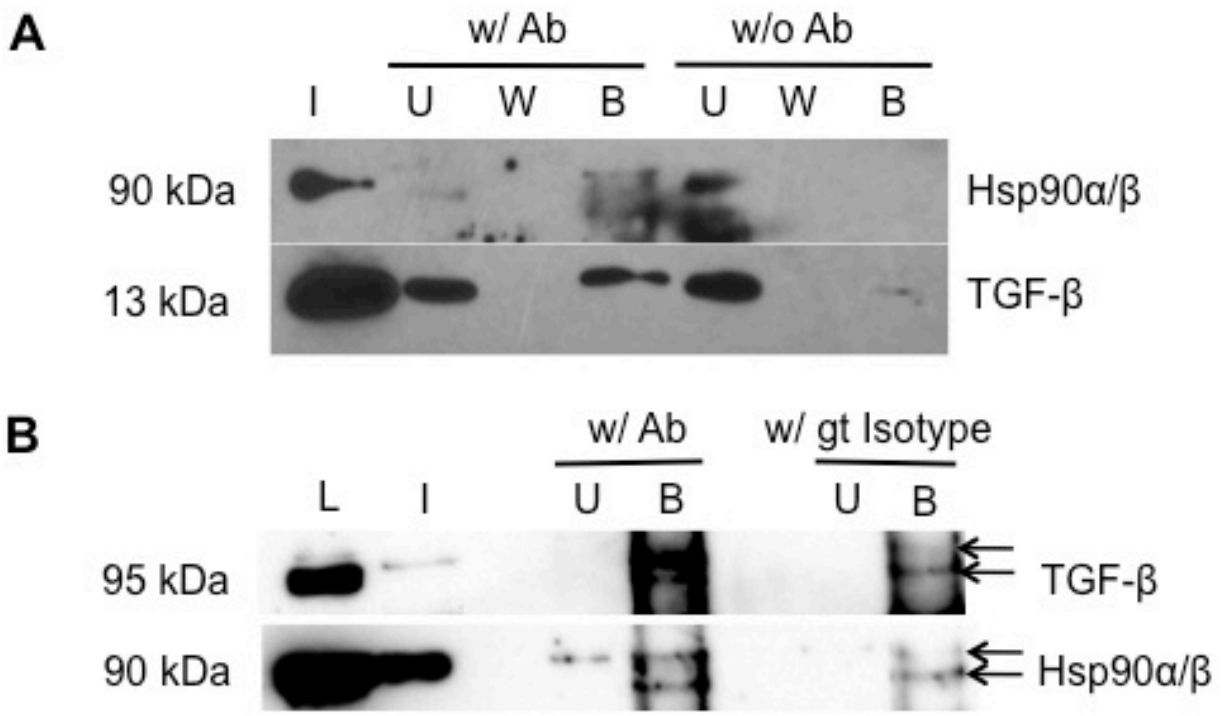

Figure 10. Hsp90β and TGF-β1 interact directly *in vitro* and *in vivo*. (A) Recombinant human Hsp90β (2 µg), recombinant human TGF-β1 (2 µg), goat anti-Hsp90α/β antibody and resuspended Protein A/G PLUS-Agarose were incubated over night at 4 °C. A negative control containing all components of the interaction except the antibody was used. Immunoprecipitates were collected by centrifugation at 1000 x *g* for 5 minutes at 4 °C. The pellet was washed four times with TBS, each time undergoing the centrifugation step mentioned above. After the final wash the pellet was resuspended in 40 µl of SDS-PAGE sample buffer, boiled, and centrifuged to pellet out the agarose beads. Flow through and elution samples were analysed using western blot analysis. Lanes correspond to: I- Input, U-Unbound, W- Wash 1, B- Bound. Experiments with and without the Hsp90 antibody are indicated by w/ Ab and w/o Ab, respectively. Data is representative of triplicate experiments. (B) SW620 cells in a confluent T150 flask were placed at 4°C for 1 hour, washed and then incubated in 3 mg/ml DTSSP with 1% Triton-X at 4°C for 2 hours The DTSSP was quenched with 1M Tris-HCl (pH 7.5) for 15 minutes. The cell were lysed with RIPA buffer and gentle scraping. Goat anti-Hsp90α/β antibody (5 µg), or normal goat IgG (5 µg) (a negative control) was added to 1 mg of cell lysate and allowed to interact for an hour at 4°C with gentle agitation. Resuspended Protein A/G PLUS-Agarose was added to the mixture and processed as above, with the exception of TBS-T as wash buffer. Lanes correspond to: L- Lysate, I- Input, U-Unbound, B- Bound. Experiments with the Hsp90 antibody is indicated by w/ Ab, while experiments with the goat isotype control is indicated by w/gt isotype. The black arrows in (B) indicate the two bands of interest in each experiment. These western blots are representative of triplicate experiments showing similar results.

This *in vitro* interaction was confirmed *in vivo* using a cell lysate made from SW620 colon cancer cells, as these cells were shown to have a higher level of soluble TGF-β1 (Figure 6B), as well as a higher level of expression of intracellular TGF-β1 (Figure 6B) in comparison to SW480 cells. The pull down was carried out in the same manner as for the recombinant proteins, except for the addition of the insoluble DTSSP crosslinker. DTSSP crosslinks cell surface proteins by binding to primary amines on proteins within 12.0 Å of each other at pH7-9 to form stable amine bonds (Cheng *et al*., 2004; Hunter *et al*., 2014). The crosslinked proteins can subsequently be separated by treatment with reducing agent. Triton-X 100 was included during the crosslinking process to allow for the crosslinker to penetrate the cell membranes, ensuring that if TGF-β1 and Hsp90β were interacting intracellularly they would be also connected by the crosslinker. An isotype control was included as the negative control; this contains the same Fc chain as the antibody from the same species (in this case goat) with the same antibody type (IgG). This accounts for any non-specific binding to the Fc receptor and confirms the specificity of the antibody binding.

A goat Hsp90α/β antibody was used to bind to the Hsp90α/β protein present in the SW620 cell lysate. If any TGF-β1 was interacting with Hsp90 (either the α or β isoforms) within the cells it would be pulled down/co-immunoprecipitated with the Hsp90 bound to the Hsp90α/β antibody, which is in turn, bound to the Protein A/G-coupled beads. Western blot analysis was once again performed, using a TGF-β1 antibody, to determine if a complex had formed between the two proteins. A SW620 cell lysate (50 µg) labeled L, shown in the first lane (Figure 10B) was used as a positive control for total protein to ensure that the antibody detected Hsp90. This sample would also indicate whether crosslinking Hsp90 had changed the conformation of the protein, thus preventing the antibody from detecting it. The lysate used for the pull down assay (crosslinked by DTSSP with Triton-X 100) was also included and is shown in the second lane labeled I (Figure 10B). These lysates showed that both TGF-β1 and Hsp90α/β were present in both the lysate and the crosslinked lysate (although TGF-β1 was detected at very low levels), and were thus used as further positive controls. The fact that TGF-β1 and Hsp90α/β were detected in the crosslinked lysate meant that the proteins were available for the interaction.

The unbound (U) samples on the western blot in Figure 10B contained no TGF-β1 and only a small amount of Hsp90α/β, the latter of which indicates the presence of residual Hsp90α/β protein that did not bind to the antibody. In this fraction, Hsp90α/β was detected as two bands of slightly different molecular weights shown with the two arrows. The presence of these two bands for Hsp90 may be due to the Hsp90α/β antibody detecting the two isoforms, Hsp90α and Hsp90β, at slightly different sizes (Figure 10B). It is also possible that the lower band could be a protein that has bound non-specifically. In the isotype control sample (I, Figure 10B), only the lower molecular weight band, potentially a non-specific band was detected in the bound fraction, while the sample containing antibody (w/ Ab, Figure 10B) showed Hsp90α/β at both molecular weights in the bound (B) fraction or only Hsp90α/β. This indicated that the immunoprecipitation was successful because Hsp90 was pulled down by the Hsp90α/β antibody bound to the beads (Figure 10B). Two bands for TGF-β1 were detected in the bound fraction with the antibody as well as with the isotype control (shown by two arrows in Figure 10B), however the level of protein present in the sample with the antibody had substantially more of this protein than in the sample with the isotype control. This indicated that there was an interaction between Hsp90 and TGF-β1 in the cell lysate (Figure 10B). This confirmed that the direct interaction found between recombinant TGF-β1 and Hsp90β (Figure 10A) also occurred in SW620 colon cancer cells. As the antibody used binds to both Hsp90α and Hsp90β, it is not certain which isoform of Hsp90 TGF-β1 interacts with *in vivo.* The likelihood that the two bands detected for Hsp90 represent Hsp90α and Hsp90β suggest that TGF-β1 could be bound to either isoform. In addition, the detection of TGF-β1 at molecular weights corresponding to both the active and inactive forms of the protein (13 kDa and 95 kDa, Lane B (w/Ab), Figure 10 A and B) suggest that TGF-β1 is capable of directly binding to Hsp90 in either of the latter forms. The differences in the mature and proprotein forms of TGF-β1 in recombinant and cell lysate-derived samples were noted in the screening of cancer cell lines for intracellular TGF-β1 (Figure 6A) and the derivation of the forms of TGF-β1 during maturation is described in detail in the introduction (Figure 2).

3.4.2 Colocalisation study of TGF-β1 and Hsp90α/β in SW480 and SW620 cells

A colocalisation study was done to verify that Hsp90 and TGF-β1 do in fact occur in the same regions of the cell providing a greater likelihood of interaction. SW480 and SW620 cells were seeded onto gelatin, fixed with ethanol and stained using Hsp90α/β and TGF-β1 antibodies. Samples containing cells treated with either SB 431542 or novobiocin were included to determine if inhibiting the TGF-β pathway (via TGF-βRI) or Hsp90 (via its C-terminus) would affect their localisation. The images obtained using confocal microscopy seen in Figure 11 show that both Hsp90α/β (stained in red in the first panel) and TGF-β1 (stained in green in the second panel) localised throughout the cell. The TGF-β1 protein, however, appeared to be more concentrated near the edges of the cell (Figure 11; see Appendix 4 – Electronic image 2 for a more detailed figure). In the SW480 cells, novobiocin changed the cellular morphology, causing round vesicles, protrusions or possible cell retractions or extensions near the cell surface and these areas showed a high level of colocalisation between the two proteins. This effect was also seen in SW620 cells treated with SB 431542 or novobiocin (Figure 11).

The images depicted in Figure 11, together with several similar images not included in the figure, were analysed for colocalisation using Image J (Zinchuk *et al*., 2007). The images in the fourth column of Figure 11 show PDM values. Positive PDM values are shown in yellow and imply colocalisation between TGF-β1 and Hsp90α/β. Negative PDM values indicate no colocalisation or complete exclusion and are shown in blue (Reitan *et al*., 2012) (Figure 11). The frequency plot in the fifth column shows colocalisation where the two colours (green and red) are correlated in a linear manner by the intensity of each colour and by overlapping the pixels. The more yellow (green and red combined) signal in the frequency scatterplot, and the more linear the scattergram, the more the proteins colocalise (Zinchuk *et al*., 2007).

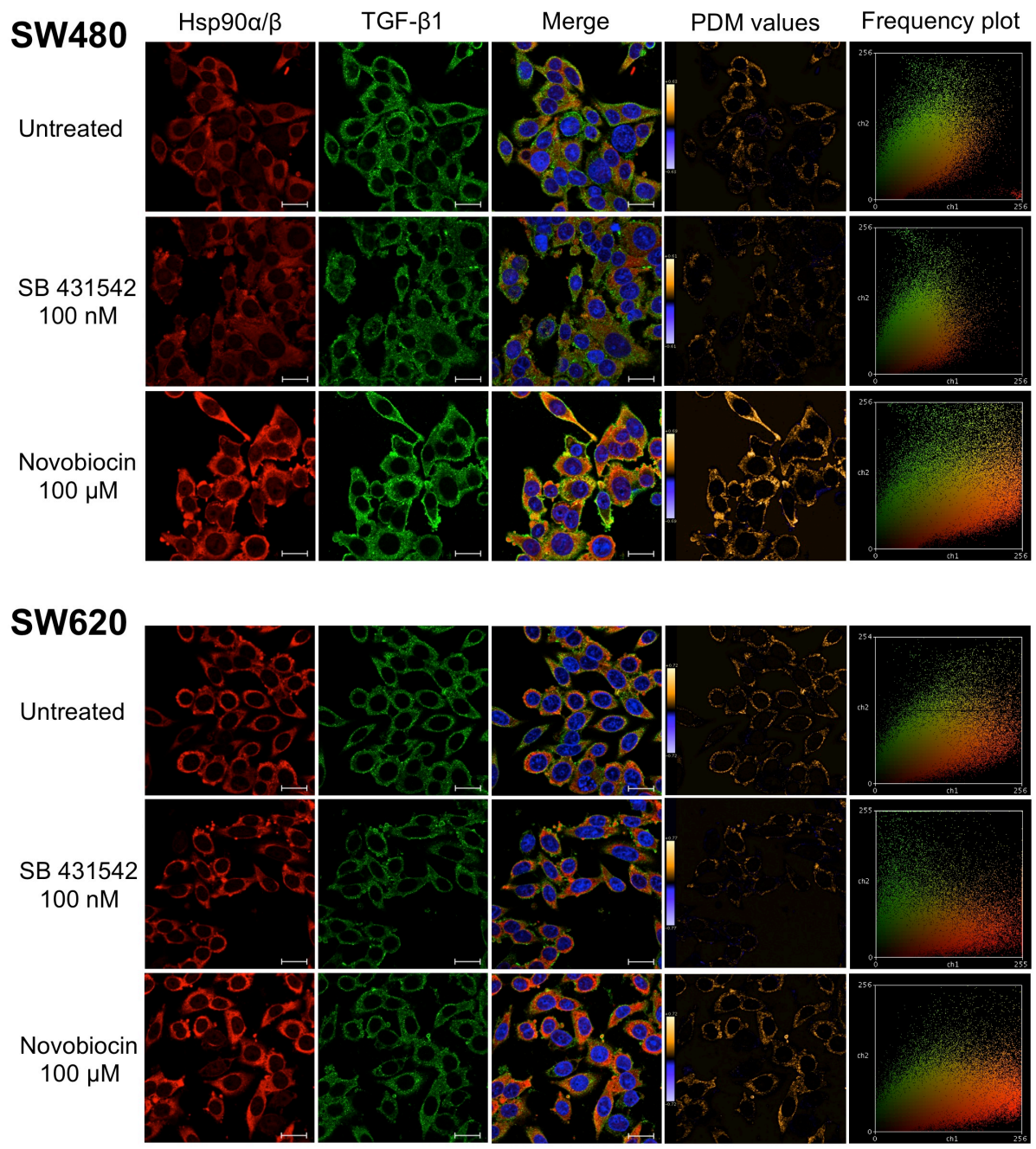

Figure 11. Colocalisation of TGF-β1 and Hsp90α/β in SW480 and SW620 colon cancer cells by confocal microscopy. SW480 and SW620 cancer cells were seeded at a density of 3 x 10^5 cells/ml on gelatin coated 15-well μ-Slide angiogenesis plates and incubated at 37°C for 24 hours. Cells were treated with novobiocin and SB 431542 at the concentrations indicated on the figure for 24 hours. Cells were fixed with ethanol and stained with mouse anti-human TGF-β1 and goat anti-Hsp90 primary antibodies overnight at 4 °C. This was followed by incubation in donkey anti-goat DY660 (first panel-pseudo-coloured red) and donkey anti-mouse IgG DY488 (second column– green) secondary antibodies overnight at 4 °C. Nuclei were stained with 1 μg/ml Hoechst 33342 (blue). Immunofluorescence was detected using the Zeiss LSM 780 confocal microscope and the images analysed using Zen Lite Software 2012 (Zeiss, Germany). Images are shown at 63x magnification. The fourth column shows the product of the differences from the mean (PDM) values and the fifth column shows frequency scattergrams both obtained using colocalisation analysis on Image J, representing triplicate z-stack images individually analysed. Scale bars represent 20 μm. Data are representative of triplicate images obtained showing similar results. **(**See Appendix 4 – Electronic image 2)

The untreated SW480 cells showed good colocalisation of TGF-β1 and Hps90 around the periphery of the cells as seen by the positive yellow PDM values (fourth column), as well as a strong linear correlation seen in the frequency scattergram (fifth column, Figure 11). This correlation was decreased upon treatment with 100 nM of SB 431542 for 24 hours. There was, however, some positive PDM values in the PDM graph indicating that there is a fair level of colocalisation, while the frequency plot displays lower levels when comparing to the untreated cells indicating that TGF-β1 and Hps90 do not colocalise at the same level compared to untreated cells when the TGF-βRI is inhibited.

However the novobiocin (100 μM) treated cells on the other hand, showed much stronger positive PDM values, throughout the cell excluding the nucleus. There was an increase in bright yellow positive PDM values in the vesicles and protrusions mentioned above indicating that there is a possibility that there is an increase of colocalisation of TGF-β1 and Hps90 in those areas of the cell. The frequency scattergram also shows a much higher level of correlation and an increase in signal of both the TGF-β1 and Hps90 proteins in the SW480 cells.

The untreated SW620 cells displayed a higher correlation between TGF-β1 and Hps90 when looking at the frequency scattergram, specifically when comparing this scattergram to that of the untreated SW480 cells. The PDM value output shows that the colocalisation potentially occurs near the cell surface, which is similar to what was seen for the SW480 cells. Treatment with SB 431542 once again caused a decrease in the colocalisation between TGF-β1 and Hps90, which can clearly be seen in both the PDM value output and the frequency scattergram where fewer positive values and reduced linear correlation can be seen, respectively. The level of Hsp90 increased with novobiocin treatment, although TGF-β1 did not increase to the same extent. The positive PDM values are increased with novobiocin treatment, especially in the vesicle-like structures, indicating that there is a higher level of colocalisation of TGF-β1 and Hps90 in SW620 cells after novobiocin treatment, which is similar to the effect that novobiocin had on SW480 cells. The frequency scattergram, however, showed a similar level of linear correlation to that of the untreated SW620 cells. These data support the finding of a direct interaction between TGF-β1 and Hsp90 shown in Figure

10 since the two proteins were found in the same areas of the cells and have strong colocalisation within both SW480 and SW620 cells.

3.5 Investigation of the role of the TGF-β pathway and Hsp90 on key cellular responses in SW480 and SW620 colon cancer cells

3.5.1 The effect of the TGF-β pathway and Hsp90 on cell growth

A growth assay was performed to determine the effect of a range of concentrations of recombinant TGF-β1 and Hsp90β proteins as well as the inhibitors SB 431542 and novobiocin on the growth of SW480 and SW620 cells. Cells were seeded into 96-well plates and subjected to the aforementioned treatments at the time of seeding for 24 hours. Proliferation was assessed at each endpoint using the WST-1 assay, which measures metabolic activity as an indicator of actively proliferating cells. For the purposes of this study the term growth refers to proliferation. The normalised absorbance levels indicative of cellular proliferation in comparison to untreated controls (taken at 100%) are shown in Figure 12.

After 24 hours of treatment with exogenous TGF-β1, a decrease in growth was observed in SW480 cells at low concentrations (0.2 ng/ml) of TGF-β1, although a dose dependent increase in proliferation was observed as the concentration of the protein increased (12.0±5.1% at 0.2 ng/ml, 35.6±0.4% at 2 ng/ml and 49.1±12.5% at 20 ng/ml relative to the untreated control, Figure 12A). In contrast, in SW620 cells, the low concentration of TGF-β1 (0.2 ng/ml) increased growth to 122.0±7.8%, while 2 ng/ml decreased cell growth at 24 hours to 56.4±6.4% of the control. The higher concentration of TGF-β1 (20 ng/ml) had no effect on the growth of SW620 cells in comparison to untreated cells. When SW480 and SW620 cells were treated for 24 hours with a range of Hsp90β concentrations (2 ng/ml, 20 ng/ml and 20 ng/ml, Figure 12), a dose-dependent decrease in growth was seen in SW480 cells in comparison to untreated cells (102.7±2.6%, 69.7±7.1% and 41.2±6.2% vs 100%, respectively; Figure 12). Similarly, the growth of SW620 cells decreased to 56.6±14.1% with treatment of the low concentration of Hsp90β (2 ng/ml), however no effect was seen when cells were treated with higher concentrations of Hsp90β (20 ng/ml and 200 ng/ml, Figure 12).

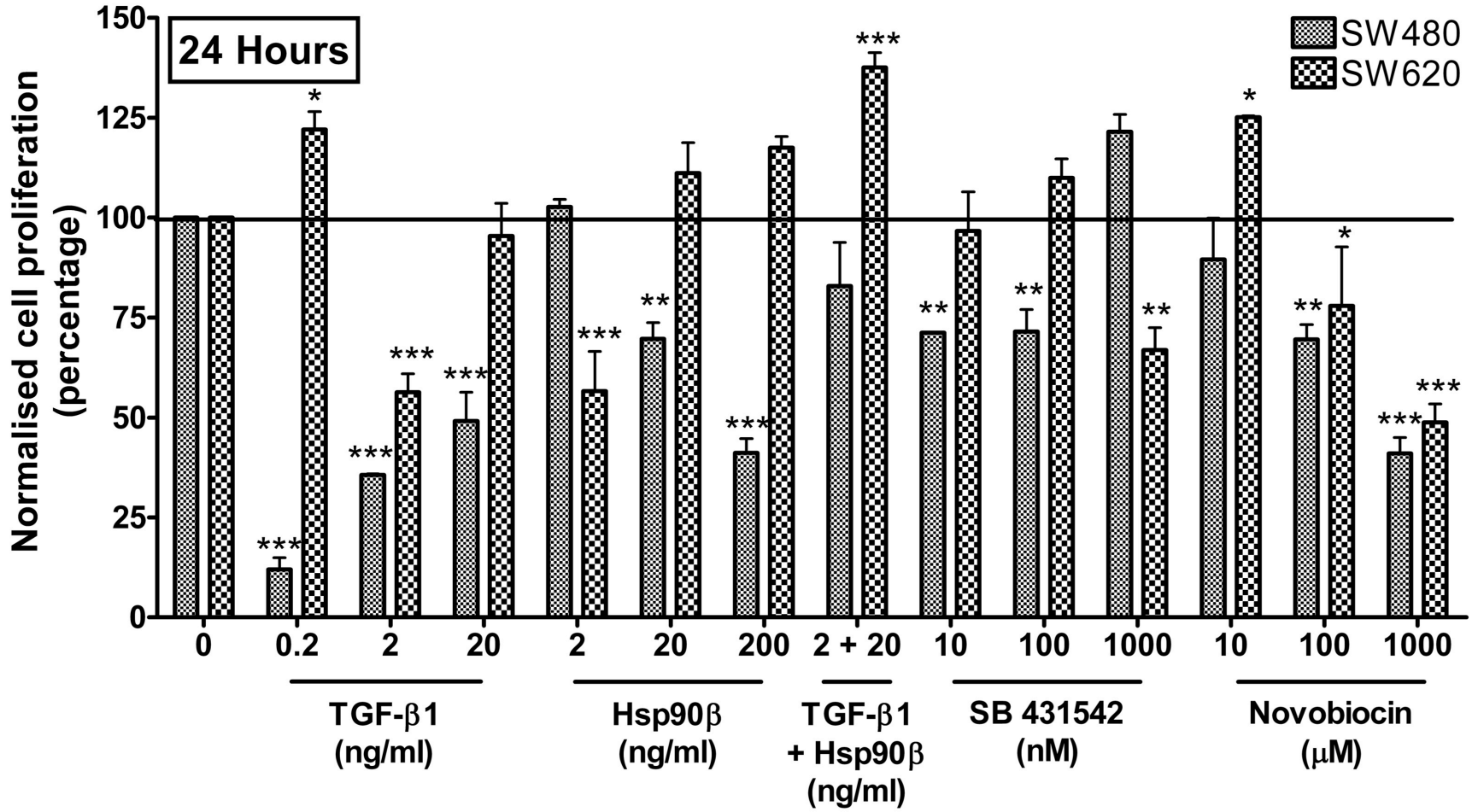

Figure 12. Determination of the effect of the addition and inhibition of TGF-β1 and Hsp90β on the growth of SW480 and SW620 colon cancer cells. SW480 and SW620 cells were seeded at a density of 1.2 x 10^5 cells/ml into 96-well plates and treated with TGF-β1 (0.2 ng/ml, 2 ng/ml and 20 ng/ml), Hsp90β (2 ng/ml, 20 ng/ml and 200 ng/ml), a combination of TGF-β1 and Hsp90β (2 ng/ml and 20 ng/ml), SB 431542 (10 nM, 100 nM and 1000 nM) and novobiocin (10 μM, 100 μM and 1000 μM). In independent experiments 10 μl of WST-1 reagent was added to each well at 24 hours and incubated for 3 hours at 37°C. The absorbance at 440nm was read using a spectrophotometer (PowerWaveX^{TM}, BioTek) and data were analysed using KC Junior software (Bio-Tek Instruments) prior to the determination of percentage cell proliferation relative to untreated cells, given as 100%, and depicted by the solid horizontal line in each graph. Statistical analysis was done using GraphPad Prism 4.03 software (GraphPad Inc., California). A two-way analysis of variance (ANOVA) with Bonferroni post tests was performed and significance between untreated and treatments are shown as follows: ($p<0.05$)*, ($p<0.01$)**, ($p<0.001$)***. Data is representative of triplicate experiments.

The combination treatment of 2 ng/ml of TGF-β1 and 20 ng/ml of Hsp90β over 24 hours appeared to show a decrease in growth of SW480 cells in comparison to untreated cells, although this was not found to be statistically signifiant. When the combination treatment was compared to the TGF-β1 treatment alone there was a significant increase in growth (82.8±18.9% growth relative to the individual treatment of TGF-β1 - 35.6±0.5%; Figure 12). This may suggest that, at these concentrations, TGF-β1 and Hsp90β may be working synergystically to increase the growth of SW480 cells. In SW620 cells, on the other hand, the combination treatment of TGF-β1 and Hsp90β caused a substantial increase in growth in comparison to the untreated cells (137.6±6.5% growth, Figure 12). Due to the fact that TGF-β1 alone at this concentration caused 56.4±14.1% growth relative to the untreated control, while Hsp90β treatment alone cause no effect it may suggest that the addition of Hsp90β rescued the SW620 cells from the decrease in growth caused by TGF-β1.

SB 431542, used to inhibit TGF-βRI, decreased the growth of SW480 cells in comparison to untreated cells to 71.3±0.1% growth and 71.5±9.5% at 10 nM and 100 nM concentrations, respectively; while the higher concentration of 1000 nM of SB 431542 caused a slight non-significant increase in growth to 121.5±6.1% [$p>0.05$] (Figure 12). Conversely, SW620 cells showed no change in growth after 24 hours of treatment with 10 nM and 100 nM of SB 431542, but 66.9±7.9% growth in comparison to the untreated cells was seen after treatment with the higher 1000 nM concentration (Figure 12A). Novobiocin, a C-terminal Hsp90 inhibitor, on the other hand, caused a dose dependent decrease in the growth of SW480 cells (89.6±14.6% cell growth relative to the untreated control after 10 μM, 69.5±6.4% after 100 μM and 41.1±6.8% after 1000 μM, Figure 12A) and a similar trend was seen in SW620 cells although there was an initial increase in growth to 125.1±0.6% with the lower concentration of 10 μM of novobiocin. The growth then decreased, although not statistically significant [$p>0.05$], to 78.0±25.5% relative to the control after 100 μM and to 48.8±6.5% after 1000 μM of novobiocin.

3.5.2 The effect of the TGF-β pathway and Hsp90 on cell adhesion and migration

Following on from the growth studies above, the effect of the TGF-β pathway and Hsp90β on adhesion and migration, key processes in metastasis, in SW480 and

SW620 cells was analysed (Figure 13, 14 and 15). Due to that fact that both TGF-β1 and SB 431542 caused changes in growth, specifically contrasting changes, which one would not expect, it was decided to include a blocking antibody against an alternate receptor (as opposed to TGF-βRI, one of the canonical TGF-β receptors) to determine if TGF-β1 was perhaps causing an effect via a different signaling pathway. The αvβ6-integrin receptor was chosen due to an established link between αvβ6-integrin and TGF-β1, where αvβ6-integrin has been found to activate TGF-β1 specifically in SW480 cells (Wipff and Hinz, 2008). Using a blocking antibody to prevent the function of αvβ6-integrin may also inhibit the function of TGF-β1 (Wipff and Hinz, 2008). The blocking antibody has specific binding to both αv and β6, and does not recognise other αv integrins (Abcam).

Adhesion of SW480 and SW620 cells was assessed at 8 hours post seeding (a time point where it was unlikely effects could be associated with growth) by crystal violet staining of adherent cells after washing to remove floating cells and adhesion values reflect absorbances at 590 nm. Migration, on the other hand, was studied using Ibidi micro-insert 4 well chambers. The culture inserts were lifted after 24 hours and floating cells were removed by washing. Images were taken of the intersection between the vertical and horizontal wounds generated by removal of the micro-inserts at 0, 12 and 24 hours. The particles per area (mm^2) were normalised to each treatment at 0 hours. Statistical analysis was performed between the levels of migration (particles per mm^2 in the wound) of treated cells at 24 hours. First, the differences in the intrinsic rates of adhesion and migration within the paired cell lines SW480 and SW620 were assessed. These analyses revealed that SW480 cells displayed a significantly higher rate of adhesion than SW620 cells (0.91±0.27 vs 0.58±0.24 particles per mm^2 in the wound [$p<0.01$], respectively; Figure 13A), while SW620 cells migrated at a significantly greater rate (three-fold) than that of SW480 cells after 24 hours in comparison to 0 hours (30.2±27.7 vs 10.6±4.0 particles per mm^2 in the wound [$p<0.05$], respectively; Figure 13B). These opposing trends between the cell lines stand to reason and lend weight to the hypothesis that if there is less adhesion of the cells they are more likely to migrate (Bogenrieder and Herlyn, 2003; Huttenlocher *et al*., 1995; Kopfstein and Christofori, 2006). It should also be noted that the SW620 cells are the metastases (Leibovitz *et al*., 1976), and this means that these

cells may be more aggressive, which would also explain these differences in adhesion and migration.

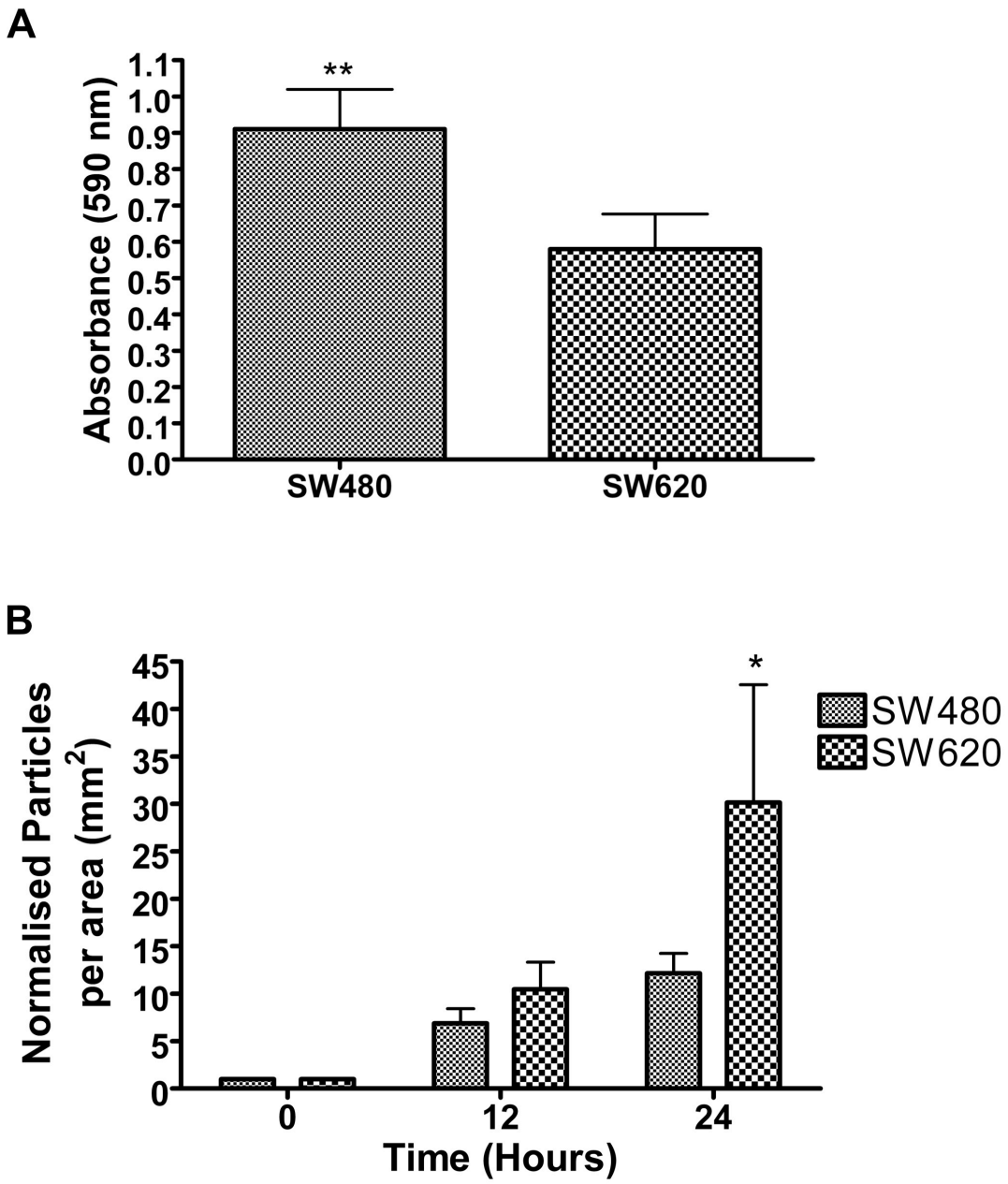

Figure 13. Comparison of the adhesion and migration capacities of SW480 and SW620 colon cancer cells. The absorbance at 590 nm of crystal violet-stained SW480 and SW620 cells, indicating adherence is shown in (A). SW480 and SW620 cells were seeded at a density of 1.2 x 10^6 cells/ml into a 96-well plate. The cells were left to adhere for 8 hours at 37°C. Cells were washed with PBS and then fixed with 4% [v/v] paraformaldehyde. Cells were stained with 10% [w/v] crystal violet in 5% ethanol for 20 minutes, washed with deionised water and solubilised with 5% [w/v] SDS and 1% [v/v] Triton-X overnight. In (B) the migration of untreated cells is shown comparing migration of SW480 to that of SW620 cells. Cells were seeded at a density of 1.2 x 10^6 cells/ml into each individual well of a micro-Insert 4 well chamber and left to adhere overnight. Each entire insert was then filled with L-15 medium and after 24 hours, the inserts were lifted and the cell area was washed to remove floating cells. Photos of the intersection between the vertical and horizontal wounds generated by the micro-inserts were taken under a 10x objective using a SkyLight at 0, 12, and 24 hours. Images were analysed in Image J. The graph shows the change in normalised particles per area determined in Image J. All graphs are representative of the average of three independent experiments performed in triplicate and error bars indicate the standard error in the mean. Statistical analysis was done using GraphPad Prism 4.03 software (GraphPad Inc., California). A two-way analysis of variance (ANOVA) with Bonferroni post tests was performed and significance between the two cell lines are shown as follows; ($p<0.05$)*, ($p<0.01$)**, ($p<0.001$)***.

The effect of addition or inhibition of TGF-β1 and Hsp90β on the adhesion of SW480 and SW620 cells was analysed by normalisation to untreated cells (taken as a 100%) as depicted in Figure 14. Adhesion studies, at 8 hours post seeding, revealed that treatment with 2 ng/ml of TGF-β1 did not significantly affect cell adhesion in SW480 and SW620 cells in comparison to the untreated cells (85.9±34.2% [$p>0.05$] and 121.1±31.1% [$p>0.05$] adhesion, respectively; Figure 14). Similarly, Hsp90β treatment (20 ng/ml) did not have any effect on the adhesion of SW480 cells (106.5±32.8% [$p>0.05$], Figure 14), but the treatment caused a substantial increase in adhesion of SW620 cells to 145.2±32.4% when compared to untreated cells although this was not significantly different [$p>0.05$]. Treatment with a combination of 2 ng/ml TGF-β1 and 20 ng/ml Hsp90β again showed no significant change in the adhesion of SW480 cells compared to untreated cells [$p>0.05$]. There was however a significant decrease in the adhesion of SW620 cells when comparing TGF-β1 treatment alone and in combination with Hsp90β (121.1±31.1% and 73.3±7.7% [$p<0.05$], respectively; Figure 14). This decrease in adhesion of SW620 cells is even greater when comparing Hsp90β treatment alone to the combination treatment with TGF-β1 (125.7±32.4% and 73.3±7.7% adhesion [$p<0.01$], respectively; Figure 14). This data may suggest that the proteins together stimulate an alternate pathway (we have shown that they interact), while causing different effects when added alone.

Inhibiting the receptor TGF-βRI with 100 nM SB 431542, either with or without the addition of exogenous TGF-β1, had no effect on the adhesion capacity of either SW480 or SW620 cells in comparison to the untreated cells. On the other hand, when SB 431542 treatment was combined with both TGF-β1 and Hsp90β, this caused a decrease in the adhesion of SW480 and SW620 cells in comparison to the untreated cells (71.8±33.2% and 68.1±11.9% vs 100% adhesion [$p<0.05$], respectively; Figure 14) although this was not significantly different to the effect seen after treatment with the two proteins TGF-β1 and Hsp90β alone (73.3±7.7% adhesion [$p>0.05$]), again suggesting that the TGR receptor inhibitor has no effect on adhesion.

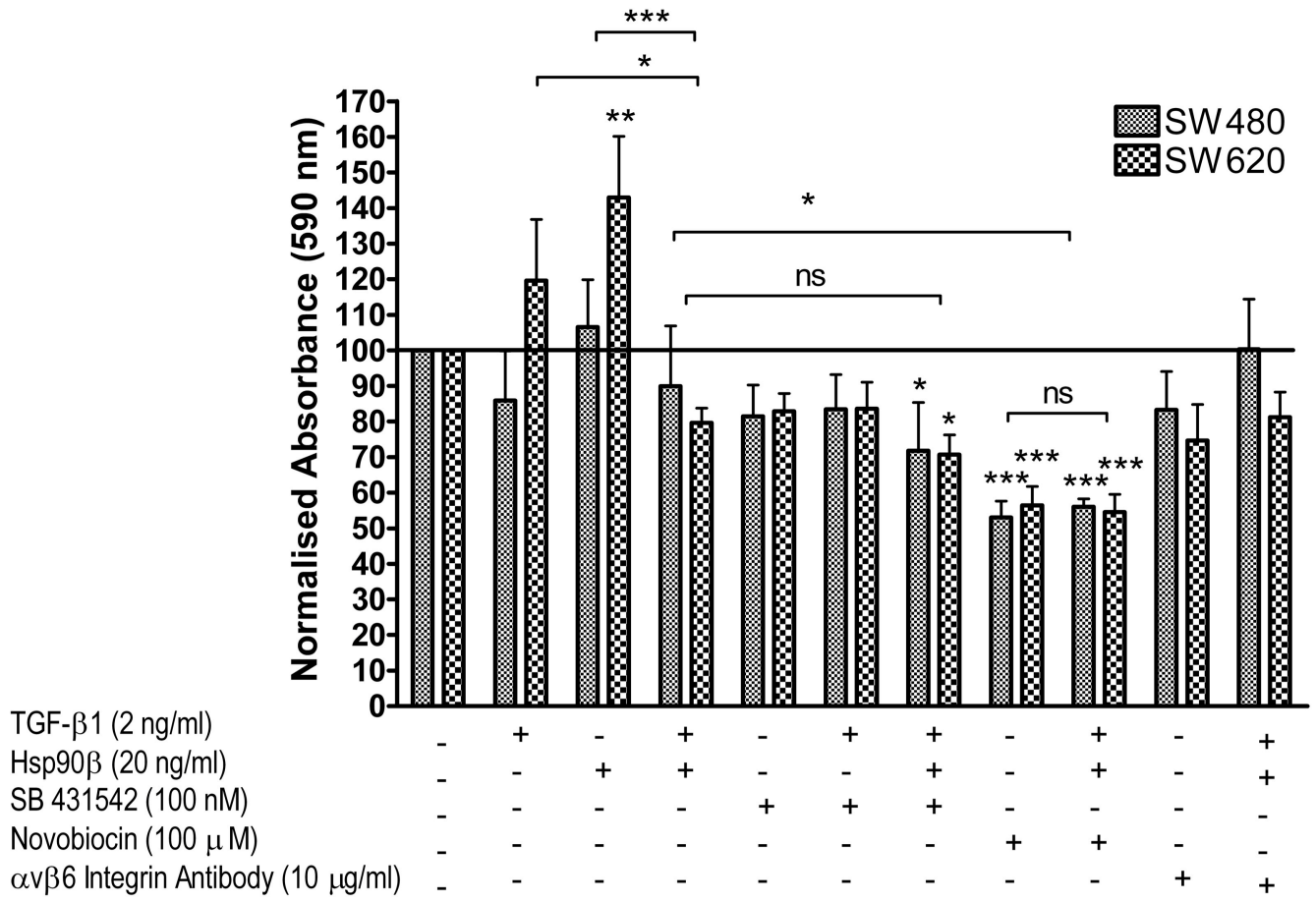

Figure 14. Determination of the effect of TGF-β, Hsp90β, SB 431542, novobiocin and αvβ6 integrin blocking antibody on the adhesion of SW480 and SW620 colon cancer cells. The y-axis represents absorbance at 590 nm of crystal violet stained SW480 and SW620 cells, indicating adherence. SW480 and SW620 cells were seeded at a density of 1.2 x 10^6 cells/ml into a 96-well plate and treated with 2ng/ml TGF-β1, 20 ng/ml Hsp90, 100 nM SB 431542, 100 μM novobiocin and 10 μg/ml αvβ6 integrin blocking antibody singly or in combinations as indicated in the figure. The cells were left to adhere for 8 hours at 37°C. Cells were washed with PBS then fixed with 4% [v/v] paraformaldehyde. Cells were stained with 10% [w/v] crystal violet in 5% ethanol for 20 minutes, washed with deionised water and solubilised with 5% [w/v] SDS and 1% [v/v] Triton-X overnight. Absorbance at 590 nm of crystal violet stained cells was normalized to the untreated cells, given as 100%, and depicted by the solid horizontal line in the graph, showing the changes in adherence for each treatment. The graph is representative of the average of three independent experiments performed in triplicate and error bars indicate the standard error in the mean. Statistical analysis was performed using GraphPad Prism 4.03 software (GraphPad Inc., California). A two-way analysis of variance (ANOVA) with Bonferroni post tests was performed and significance between untreated and each treatment within cell lines are shown, unless otherwise indicated; ($p<0.05$)*, ($p<0.01$)**, ($p<0.001$)***, ns – not significant.

The inhibition of intracellular Hsp90 by the addition of 100 μM novobiocin cause a significant decrease in the adhesion of both cell lines relative to the normalised untreated control (between 55% and 60% [$p<0.001$], Figure 14). The addition of exogenous Hsp90β and TGF-β1 in combination with novobiocin was not able to overcome the inhibition of intracellular or total Hsp90 by the drug although it was observed that in SW480 cells this decrease in adhesion was significantly less than TGF-β1 and Hsp90β treatments alone. The inhibition of the αvβ6 integrin alone as well as with the addition of exogenous Hsp90β and TGF-β1 in combination with the αvβ6 integrin antibody did not have any effect on the adhesion of either the SW480 or SW620 cells, suggesting that it may not play a role in the adhesion capacity of these cells.

Migration analysis was performed using Ibidi micro-insert 4-well chambers. Images were taken at 0, 12 and 24 hours, and the particles per area (mm^2) were normalised to each treatment at 0 hours and can be seen in Figure 15A and B. Statistical analysis was performed between the level of migration (particles per mm^2 in the wound) of treated cells at 24 hours in comparison to untreated cells at 24 hours.

Treatment with 2 ng/ml of TGF-β1 alone, 20 ng/ml of Hsp90β alone as well as the combination of TGF-β1 with Hsp90β caused no changes in the migration of SW480 cells [$p>0.05$] (Figure 15A). In contrast to this, the inhibition of the TGF-βRI using 100 nM of SB 431542 caused a two-fold increase in migration of SW480 cells in comparison to the untreated cells (23.9±4.1 vs 10.6±4.0 particles per mm^2 in the wound [$p<0.05$], respectively; Figure 15A). The addition of 2 ng/ml of exogenous TGF-β1 in combination with 100 nM SB 431542 had the same effect as treatment with SB 431542 alone (23.9±4.1 and 28.7±0.1 particles per mm^2 in the wound [$p<0.05$], respectively; Figure 15A), suggesting that the addition of TGF-β1 was unable to overcome the inhibition of the canonical TGF-β/ TGF-βR pathway. The addition of both TGF-β1 and Hsp90 with SB 431542 treatment, on the other hand, caused a significant three-fold increase compared the untreated cells (36.2±10.8 vs 10.6±4.0 and 23.9±4.1 particles per mm^2 in the wound [$p<0.05$], respectively; Figure 15A). This treatment was also statistically increased in comparison to the combination TGF-β1 and Hsp90β treatment (36.2±10.6 vs 13.4±5.6 particles per mm^2 in the wound [$p<0.001$], respectively; Figure 15A). The combination treatments, however, was not

significantly different to SB 431542 treatment alone. These data may suggest that blocking the TGF-βRI with SB 431542 may be pro-migratory and may be causing the SW480 cells to utilise a different pathway to the canonical TGF-βR1/R2/SMAD pathway, and that Hsp90 may enhance the stimulation of this alternative signaling pathway.

Novobiocin treatment (100 μM) caused an increase in migration in SW480 cells relative to the untreated control (29.7+35.6 vs 10.6±4.0 particles per mm^2 in the wound [$p<0.01$], respectively; Figure 15A). The addition of 2 ng/ml TGF-β1 and 20 ng/ml Hsp90β in combination with the novobiocin treatment caused no significant difference in comparison to novobiocin treatment alone suggesting that the addition of exogenous Hsp90β could not overcome the inhibition of intracellular Hsp90 by novobiocin. These treatments did however cause a substantial increase in migration, despite having large error bars from varying results, in comparison to the treatment using a combination of only TGF-β1 and Hsp90β (34.2±42.1 vs 13.4±5.6 particles per mm^2 in the wound [$p<0.001$], respectively; Figure 15A). This highlights that's it is the novobiocin specifically that is causing the increase. The inhibition of the αvβ6 integrin did not have any effect on the migration of SW480 cells, including when exogenous TGF-β1 and Hsp90β were added. This suggests that αvβ6 integrin likely does not play a part in the migration of these cells.

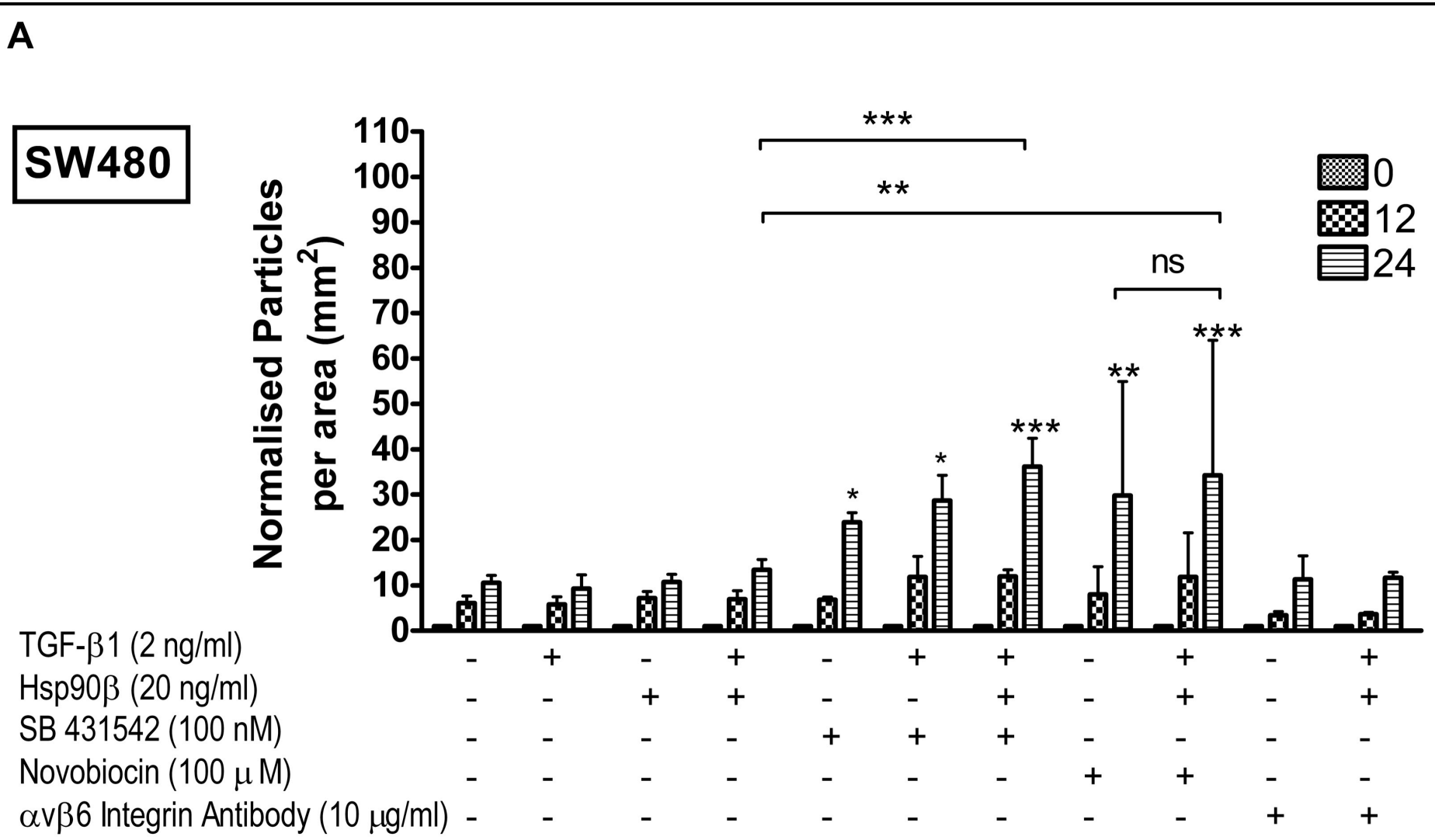

Figure 15. Determination of the effect of the TGF-β, Hsp90, SB 431542, novobiocin and αvβ6 integrin blocking antibody on migration of SW480 and SW620 colon cancer cells.

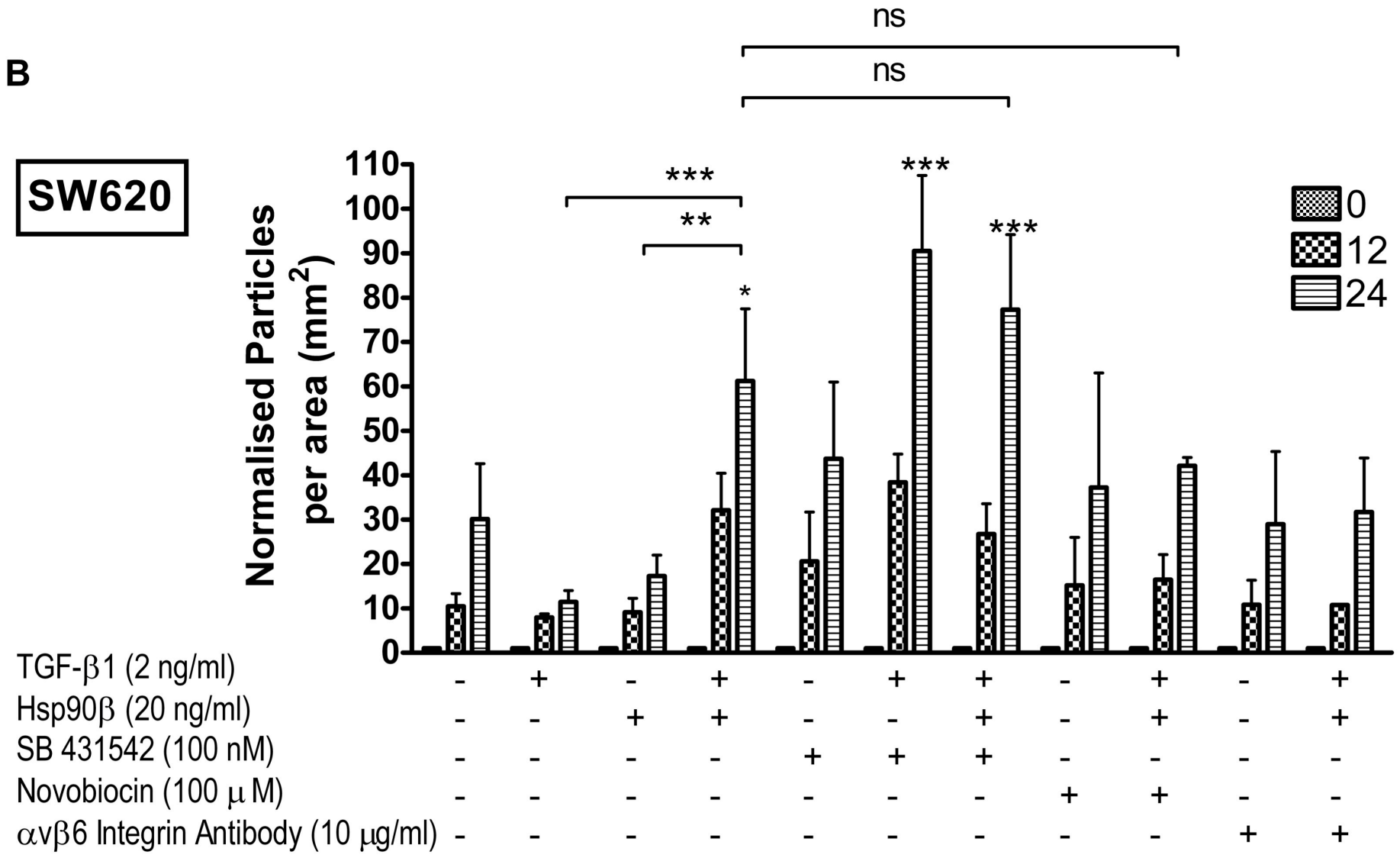

Figure 15. (Continued) Determination of the effect of the TGF-β, Hsp90, SB 431542, novobiocin and αvβ6 integrin blocking antibody on migration of SW480 and SW620 colon cancer cells.

Figure 15. (Continued) Determination of the effect of TGF-β, Hsp90, SB 431542, novobiocin and αvβ6 integrin blocking antibody on migration of SW480 and SW620 colon cancer cells. SW480 (A) and SW620 (B) cells were seeded at a density of 1.2 x 10^6 cells/ml into each individual well of a micro-Insert 4- well chamber and left to adhere overnight. Cells were treated with 2ng/ml TGF-β1, 20 ng/ml Hsp90, 100 nM SB 431542, 100 µM novobiocin and 10 µg/ml αvβ6 integrin blocking antibody singly and in various combination. After 24 hours the inserts were lifted and the cell area was washed to remove unattached cells. Photos of the intersection between the vertical and horizontal wounds generated by the micro-inserts were taken under a 10x objective using a SkyLight at 0, 12, and 24 hours. Images were analysed in Image J and show the change in normalised particles per area over 24 hours relative to particles at 0 hours. Both graphs are representative of the average of three independent experiments performed in triplicate and error bars indicate the standard error in the mean. Statistical analysis was done using GraphPad Prism 4.03 software (GraphPad Inc., California). A two-way analysis of variance (ANOVA) with Bonferroni post tests was performed and significance between untreated cells and those after each treatment are shown, unless otherwise indicated; ($p<0.05$)*, ($p<0.01$)**, ($p<0.001$)***, ns – not significant.

When analysing the migration of SW620 cells it was found that treatment for 24 hours with 2 ng/ml of TGF-β1 caused a decrease, although not significant, in the migration of these cells in comparison to the untreated cells (11.4±4.4 vs 30.2±27.7 particles per mm^2 in the wound [$p>0.05$], respectively; Figure 15B). While there appears to be a decrease in migration of SW620 cells after treatment with 20 ng/ml of Hsp90β in comparison to the untreated cells, it was not statistically significant (17.3±8.1 vs 30.1±27.7 particles per mm^2 in the wound [$p>0.05$], respectively; Figure 15B), it was found to be not significant. Treatment combining exogenous 2 ng/ml of TGF-β1 and 20 ng/ml of Hsp90β caused a statistically significant two-fold increase in migration of SW620 cells in comparison to untreated cells (61.2±36.3 vs 30.1±27.7 particles per mm^2 in the wound [$p<0.05$], respectively; Figure 15B). This increase in migration of SW620 cells caused by this combination treatment was significantly higher than either TGF-β1 or Hsp90β treatment alone (61.2±36.3 vs 11.4±4.4 [$p<0.001$] and 17.3±8.1 [$p<0.01$] particles per mm^2 in the wound, respectively; Figure 15B).

SB 431542 (100 nM) treatment alone did not cause a significant change in the rate of migration of SW620 cells relative to the untreated cells [$p>0.05$], while 100 nM treatment of SB431542 with the addition of 2 ng/ml of TGF-β1 as well as a combination of 2 ng/ml TGF-β1 and 20 ng/ml Hsp90β caused a substantial increase in migration of SW620 cells relative to the untreated cells (90.5±29.5 and 77.3±29.3 vs 30.1±27.7 particles per mm^2 in the wound [$p<0.001$], respectively; Figure 15B). This level of increase was however not statistically different to the combination treatment of TGF-β1 or Hsp90β alone. Once again the inhibition of TGF-βRI with SB 431542 caused an increase in the migratory capacity (Figure 15B). These data suggest that the pro-migratory effect of the combination of TGF-β1 and Hsp90β is not disrupted by inhibition of the receptor, suggesting that the canonical pathway is not being used and Hsp90 may not be required.

Treatment with 100 μM of novobiocin alone and in combination with 2 ng/ml of TGF-β1 and 20 ng/ml of Hsp90β showed no significant change in the migration of SW620 cells relative to the untreated cells [$p>0.05$], unlike in SW480 where the drug caused an increase. Although a similar observation to SW480 cells was noted, that exogenous TGF-β1 and Hsp90β was not able to overcome the effect of novobiocin (Figure 15B). This could mean that a different mechanism is being utilised, and

perhaps that novobiocin has decreased the stimulatory effect of TGF-β1 and Hsp90β in SW620 cells.

Disrupting αvβ6 integrin using a blocking antibody did not cause any change in the rate of migration relative to untreated cells in either of the cell lines and this trend was unaffected by the addition of 2 ng/ml of TGF-β1 and 20 ng/ml of Hsp90β (Figure 15B).

Finally when comparing the rates of adhesion and migration in response to the various treatments within each cell line revealed a number of interesting trends. The decrease in adhesion in both cell lines relative to the untreated cells, due to inhibition by 100 nM of SB 431542 in combination with 2 ng/ml of TGF-β1 and 20 ng/ml of Hsp90 (Figure 14) correlated with a significant increase in migration in both cell lines (Figure 15A and 15B). The inhibition of TGF-βRI thus caused cells to be more migratory and while SW480 cells seem to require Hsp90β to increase this further, SW620 cells only require TGF-β1 and are not stimulated further by the combination of the two proteins. Similarly, treatment with 100 μM of novobiocin singly or in combination with 2 ng/ml TGF-β1 and 20 ng/ml Hsp90β caused a decrease in adhesion in both cell lines, with a corresponding increase in migration in SW480 but not SW620 cells (Figure 15A and 15B). As the cell lines express similar levels of Hsp90 (Figure 8), this could be because the SW620 cell lines are more resistant to novobiocin (Figure 9) or suggest that SW620 cells are less reliant on Hsp90.

3.6 Determination of the effect of TGF-β1 and Hsp90β on the downstream members of the canonical TGF-β signaling pathway

In the TGF-β signaling pathway, described in detail in section 1.6.1 of the Introduction, TGF-β1 binds to TGF-βRII, recruiting TGF-βRI and leading to the phosphorylation of the transcription factors SMAD2 and SMAD3. These phosphorylated proteins bind to SMAD4 and translocate to the nucleus initiating gene transcription for several proteins as seen in the schematic diagram in Figure 3 (Massagué *et al*., 2005). SW480 and SW620 cells have an equivalent SMAD4 mutation, which is caused by a splice disruption, but showed no mutation of the TGF-βRII gene (Woodford-Richens *et al*., 2001). SMAD4 mutations have been found in several different colon cancer cell lines, however it has also been shown to regulate the transcription activity rather than the

translocation of pSMAD2/3 to the nucleus (Liu *et al*., 1997; Miyaki *et al*., 1999; Rosman *et al*., 2008; Subramanian *et al*., 2004).

After the role of TGF-β1 and Hsp90β in the metastatic processes of growth, adhesion and migration was analysed, the effect that these proteins had on the downstream proteins/signaling intermediates of the TGF-β pathway was investigated. This was achieved by staining cells for pSMAD2/3 and SMAD2/3 and analysing the levels and ratios of these two proteins using flow cytometry and confocal microscopy. Unfortunately the flow cytometry analysis was not reproducible and the data was contrasting (data not shown). The focus thus remained on the confocal microscopy, where SW480 and SW620 cells were grown on gelatin coated Ibidi 15-well µ-Slide angiogenesis plates and treated for 24 hours with 2 ng/ml TGF-β1, 20 ng/ml Hsp90β, 100 nM SB 431542 and 100 µM novobiocin alone and in combination. The effect of the αvβ6 integrin blocking antibody was not assessed as no effects were seen in the adhesion and migration studies. Images were obtained using a Zeiss LSM 780 confocal microscope and analysed using Zen Lite Software (2014) and Image J (Figure 16).

3.6.1 Colocalisation study between nuclei and pSMAD2/3 to determine the level of pSMAD2/3 activation

Due to the fact that when SMAD2 and SMAD3 are phosphorylated or activated they must move into the nucleus to exert their effect on target gene expression (Massagué *et al*., 2005) it was investigated if any of the treatments mentioned above affected the ratio of pSMAD2/3 in the Hoechst-stained nuclei of either the SW480 or the SW620 cells. The nuclear localisation of pSMAD2/3 was performed using Image J together with a colocalisation plug-in (Figure 16; see Appendix 4 – Electronic image 3 for a more detailed figure). This ‘colocalisation’ is depicted in the frequency scattergrams in the third column of each cell line in Figure 16. The nuclei were pseudo-coloured red and pSMAD2/3 staining was pseudo-coloured green, for ease of analysis. As mentioned in section 3.4.2, colocalisation is shown where the two colours (green – pSMAD2/3 and red – nucleus) are correlated in a linear manner in the scattergram, which can be seen by the intensity of each colour and done by overlapping the pixels. The more yellow (green and red combined) signal in the linear section of the

frequency scattergram, the higher the colocalisation of the regions of interest, in this case how much pSMAD2/3 was localized to the nucleus (Zinchuk *et al*., 2007). No changes were seen in total SMAD2/3 and these images were thus not shown.

In the untreated SW480 cells, a moderate level of nuclear localisation of pSMAD2/3 was observed in the frequency scattergram, and punctate structures of pSMAD2/3 were observed and are shown in the second column, which is a merged image between the nucleus and pSMAD2/3 (Figure 16A). This localisation was increased in SW620 cells as evidenced by the increase in linear correlation between green and red pixels in the frequency scattergram. The SW620 cells also had a markedly higher intensity of punctate staining of pSMAD2/3 in the nucleus (Figure 16A). This may allude to the fact that the pathway may be constitutively active in the SW620 cells.

With the addition of exogenous TGF-β1 (2 ng/ml), the nuclear localisation of pSMAD2/3 in both the SW480 and SW620 cells increased slightly. The pSMAD2/3 in the SW620 cells however became less punctate and more evenly distributed around the cell and, in some cells, localised near the cell surface. This may indicate that these cells are less sensitive to stimulation. Treatment of SW480 cells with 20 ng/ml of Hsp90β caused a similar effect as compared to treatment with TGF-β1 relative to the untreated cells (Figure 16A). In SW620 cells, the addition of exogenous Hsp90β showed no difference in the nuclear localisation of pSMAD2/3, although the punctate structures seemed to be less intense (Figure 16A). When 2 ng/ml of TGF-β1 and 20 ng/ml of Hsp90β were added in combination, the nuclear localisation of the pSMAD2/3 in SW480 cells increased greatly as can be seen in the frequency scattergram (Figure 16A). The intensity of the punctate pSMAD2/3 staining in the nucleus of SW480 cells in the image in the second column was also noticeably increased. The nuclear localization of pSMAD2/3 in SW620 cells, on the other hand, after treatment with both TGF-β1 and Hsp90β was very similar to the level of localisation with Hsp90β alone, and thus not different from the untreated cells (Figure 16A). This once again highlights the differences between the SW480 and SW620 cells in the pathway responsiveness to the two proteins.

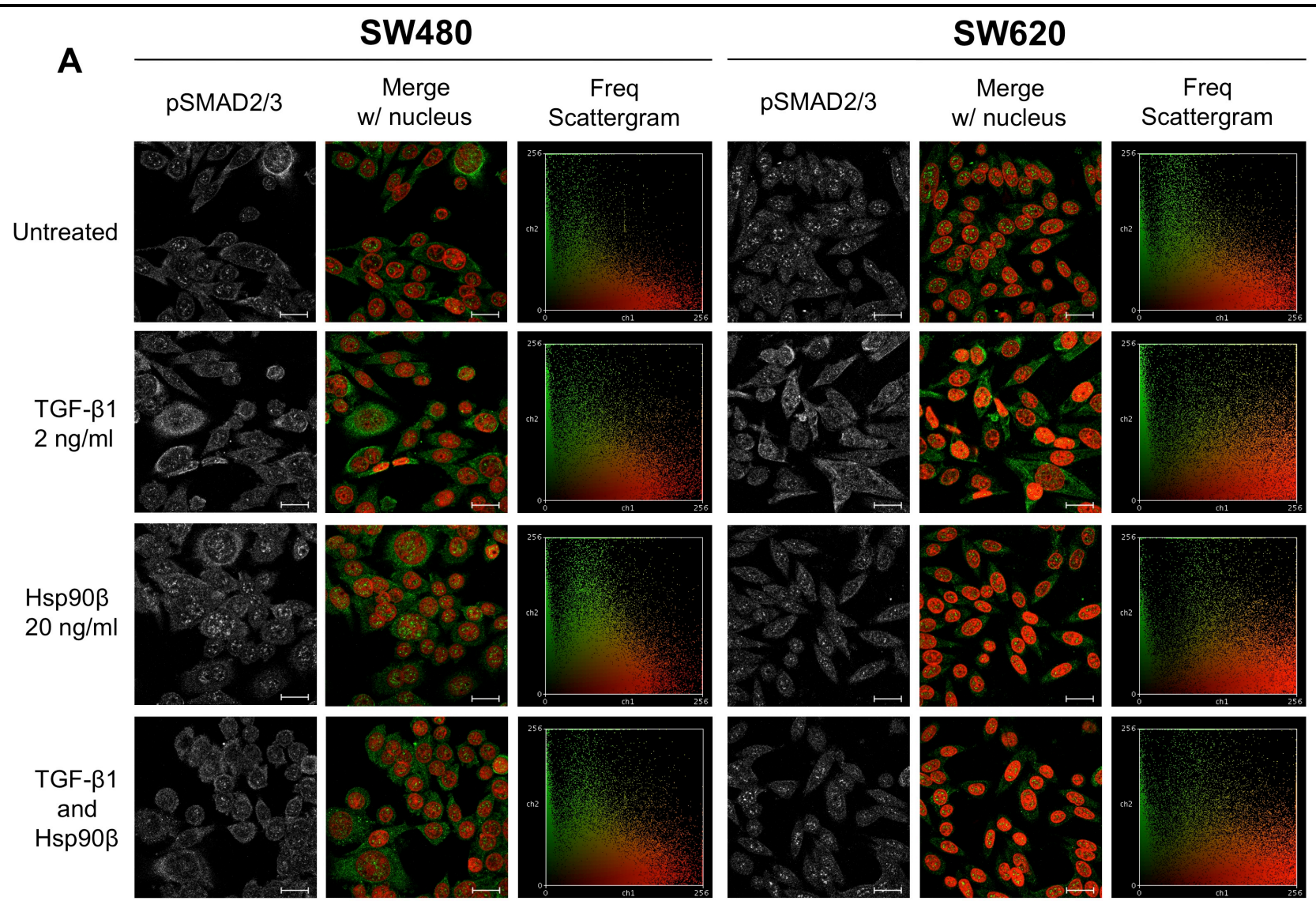

Figure 16. Analysis of the phosphorylation of SMAD2/3 after the addition and inhibition TGF-β1 and Hsp90 in SW480 and SW620 colon cancer cells by confocal microscopy.

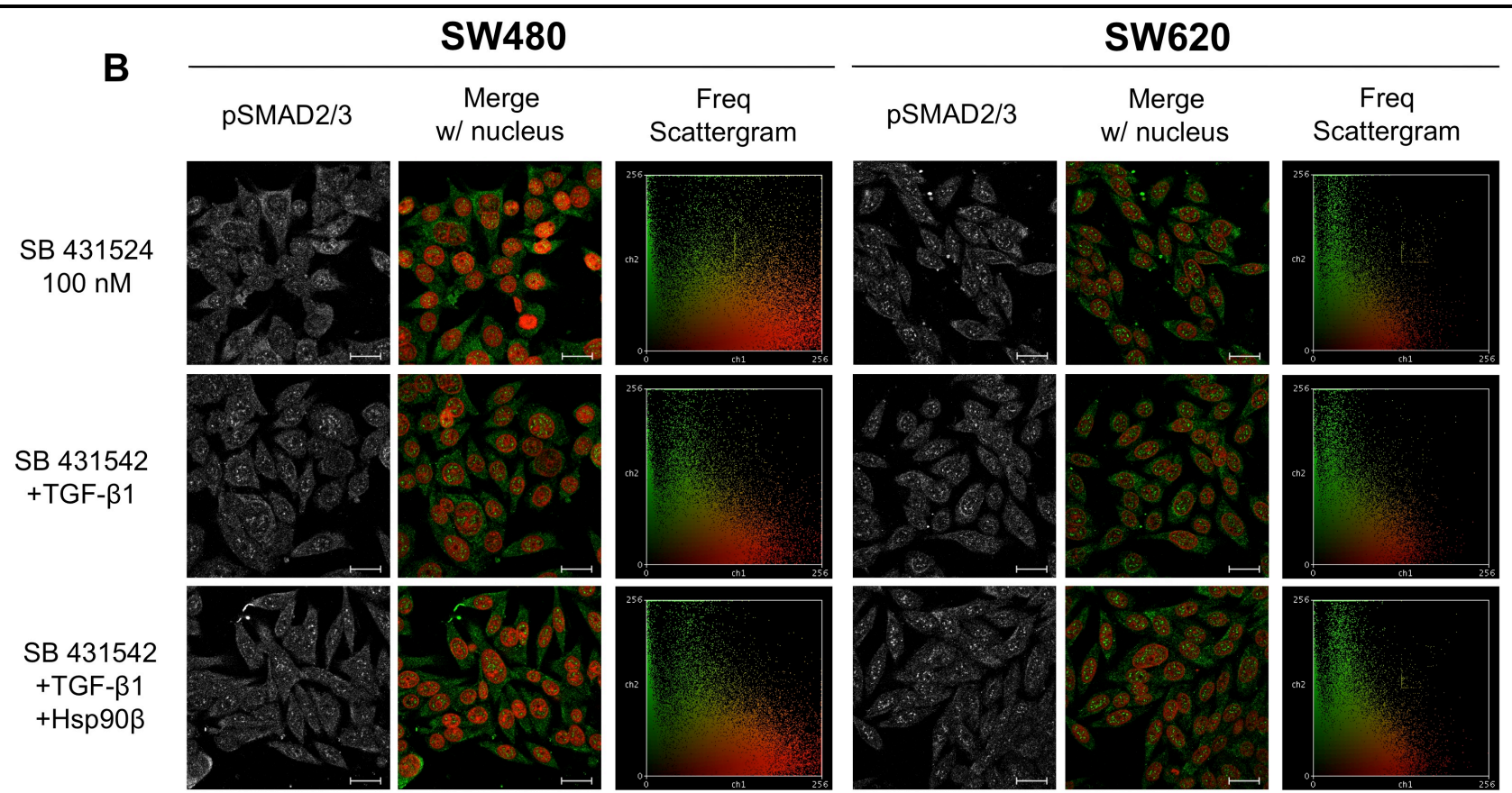

Figure 16. (Continued) Analysis of the phosphorylation of SMAD2/3 after the addition and inhibition TGF-β1 and Hsp90 in SW480 and SW620 colon cancer cells by confocal microscopy.

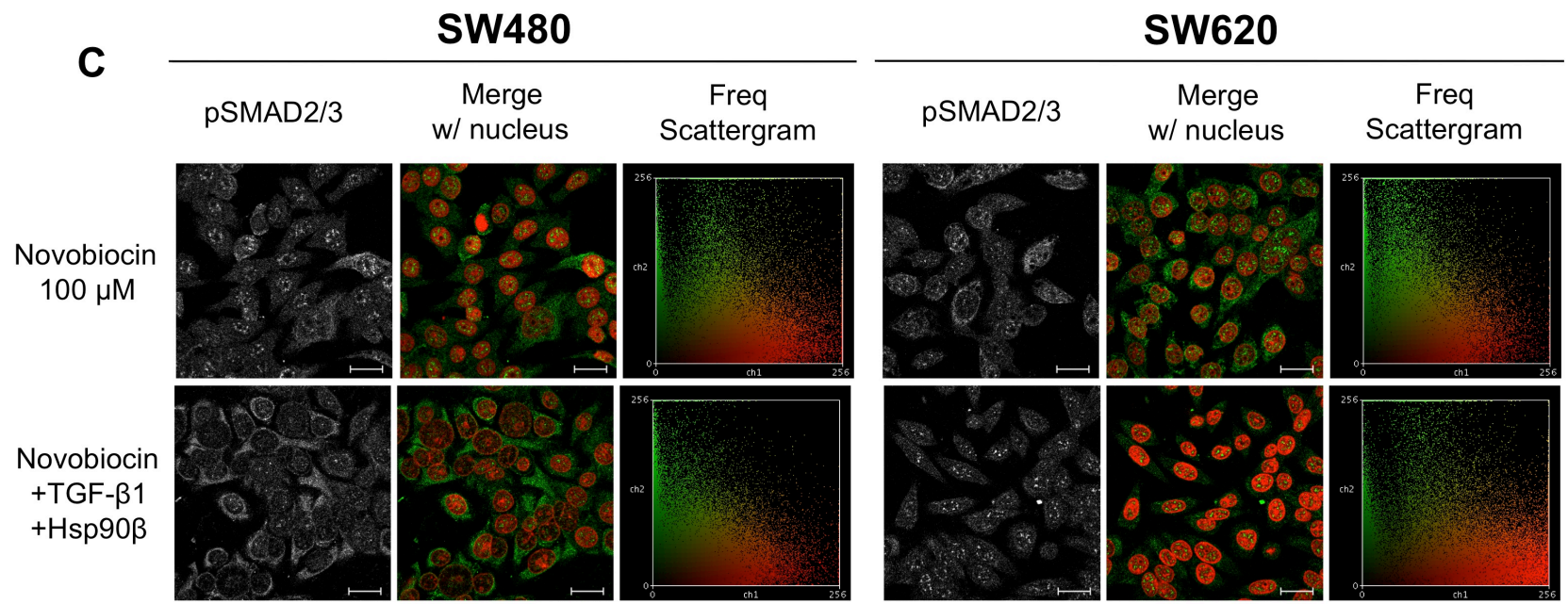

Figure 16. (Continued) Analysis of the phosphorylation of SMAD2/3 after the addition and inhibition of TGF-β1 and Hsp90 in SW480 and SW620 colon cancer cells by confocal microscopy. SW480 and SW620 cancer cells were seeded at a density of 3 x 10^5 cells/ml on gelatin coated 15-well µ-Slide angiogenesis plates and incubated at 37°C for 24 hours. Cells were treated with 2 ng/ml TGF-β1, 20 ng/ml Hsp90β, 100 nM SB 431542 and 100 µM novobiocin for 24 hours alone and in combinations. Cells were fixed with ethanol and stained with mouse anti-rabbit SMAD2/3 and goat anti-pSMAD2/3 primary antibodies overnight at 4 °C. This was followed by incubation with donkey anti-goat DY660 (first column -pseudo-coloured to white) secondary antibodies overnight at 4 °C. Nuclei were stained with 1 µg/ml Hoechst 33342 (blue). Immunofluorescence was detected using the Zeiss LSM 780 confocal microscope and the images analysed using Zen Lite Software 2014 (Zeiss, Germany). The second column shows a merged image of the nucleus pseudo-coloured to red and the pSMAD2/3 staining pseudo-coloured to green. The third column shows frequency scattergrams obtained using colocalisation analysis on Image J, representing triplicate images individually analysed. The Images are shown at 63x magnification. Scale bars represent 20 µm. Data are representative of triplicate images obtained showing similar results. The images in (A) shows the untreated cells in comparison to the addition of TGF-β1 and Hps90, while (B) SW480 and SW620 cells inhibited by SB 431542 and the images in (C) show the cells inhibited by novobiocin (See Appendix 4, Electronic image 3)

The inhibition of TGF-βRI by 100 nM of SB 431542 caused a substantial increase in the nuclear localization of pSMAD2/3 compared to the untreated cells in Figure 16A, as seen in the frequency scattergram in Figure 16B. The staining of pSMAD2/3, however, seemed to be dispersed rather than the punctate staining seen in the untreated cells (Figure 16A). Treatment with 100 nM of SB 431542 in SW620 cells cause a substantial decrease in the nuclear localisation of pSMAD2/3 (Figure 16B), although there continued to be punctate staining of pSMAD2/3 in the nucleus as can be seen in column 2 (Figure 16B). The addition of exogenous TGF-β1 with SB 431542 as well as a combination of SB 431542, 2 ng/ml TGF-β1 and 20 ng/ml Hsp90β had the same effect on SW480 cells. This was a slight increase in nuclear localisation compared to untreated cells, but a decrease in nuclear localisation compared to SB 431542 treatments alone. The frequency scattergrams for the SB 431542 treatments were also very similar to those of TGF-β1 and Hsp90β treatments alone. In SW620 cells the addition of TGF-β1 with SB 431542 and the combination of SB 431542 with TGF-β1 and Hsp90β showed no difference in the nuclear localisation of pSMAD2/3 in comparison to the SB 431542 treatment alone. All treatments with SB 431542 thus caused a decrease in nuclear pSMAD2/3 in comparison to untreated SW620 cells.

Novobiocin treatment (100 μM) caused an increase in the nuclear localization pSMAD2/3 in SW480 and SW620 cells, as seen in the frequency scattergrams in Figure 16C, although the increase in nuclear localisation in SW620 cells was not as substantial when compared to that in the SW480 cells. The pSMAD2/3 in the treated SW480 cells was observed to be concentrated in the nucleus, while in SW620 cells the pSMAD2/3 became more dispersed in the nucleus. The addition of exogenous 2 ng/ml of TGF-β1 and 20 ng/ml of Hsp90β was able to overcome the increase in pSMAD2/3 in the nucleus caused by the inhibition of novobiocin in SW480 cells. This was not observed in SW620 cells as the nuclear localisation decreased and pSMAD2/3 moved into more punctate structures in the nucleus.

3.6.2 Determination of the proportion of pSMAD2/3 in nucleus relative to the cytoplasm

While the previous colocalisation analysis gave insight into increasing levels of pSMAD2/3 in the nucleus, it did not take into account the level of pSMAD2/3 in the cytoplasm. This was addressed by developing profiles of the intensity of pSMAD2/3 in a line through the cells using Zen Lite Software. These could be compared to profiles along the same line of the nucleus identifying how much pSMAD2/3 was in the nucleus and in the cytoplasm; and this process has been described in Supplementary Figure 2. The intensity profiles generated revealed that there was a significant increase in the proportion of pSMAD2/3 in the nuclei of SW620 cells compared to the nuclei of SW480 cells (ratios of 0.82 and 0.67 [$p<0.01$], respectively; Figure 17). This can be seen in the images in Figure 16A described in section 3.6.1 and the difference in pSMAD2/3 in the nucleus is also seen in the increased colocalisation of pSMAD2/3 and the nucleus in SW620 cells (Figure 16A). SW480 cells showed no significant change [$p>0.05$] when comparing the untreated cells to the cells treated with 2 ng/ml of TGF-β1, while a significant move of pSMAD2/3 into the cytoplasm was seen in SW620 cells (ratios of 0.83±0.09 to 0.64±0.15 [$p<0.001$], respectively; Figure 17). This data explains the increase of pSMAD2/3 in the cytoplasm of the cells seen in Figure 16A. Treatment with exogenous Hsp90β (20 ng/ml) resulted in an increase in the proportion of pSMAD2/3 in the nucleus of SW480 cells in comparison to untreated cells (ratios of 0.79±0.11 vs 0.67±0.16; [p<0/05]), while a slight decrease was observed in SW620 cells after Hsp90β treatment (ratios of 0.79±0.10 vs 0.83±0.09, [p<0/05]; Figure 17). The addition of both 2 ng/ml of TGF-β1 and 20 ng/ml of Hsp90β had no effect [$p>0.05$] on the proportion of pSMAD2/3 in the nucleus of SW480 and SW620 cells compared to the untreated (Figure 17). In comparison to individual treatments, the combination of TGF-β1 and Hsp90β resulted in a greater level of pSMAD2/3 in the nucleus in comparison to TGF-β1 treatment in SW480 cells and less pSMAD2/3 in the nucleus in comparison to Hsp90β treatment in SW620 cells (Figure 17).

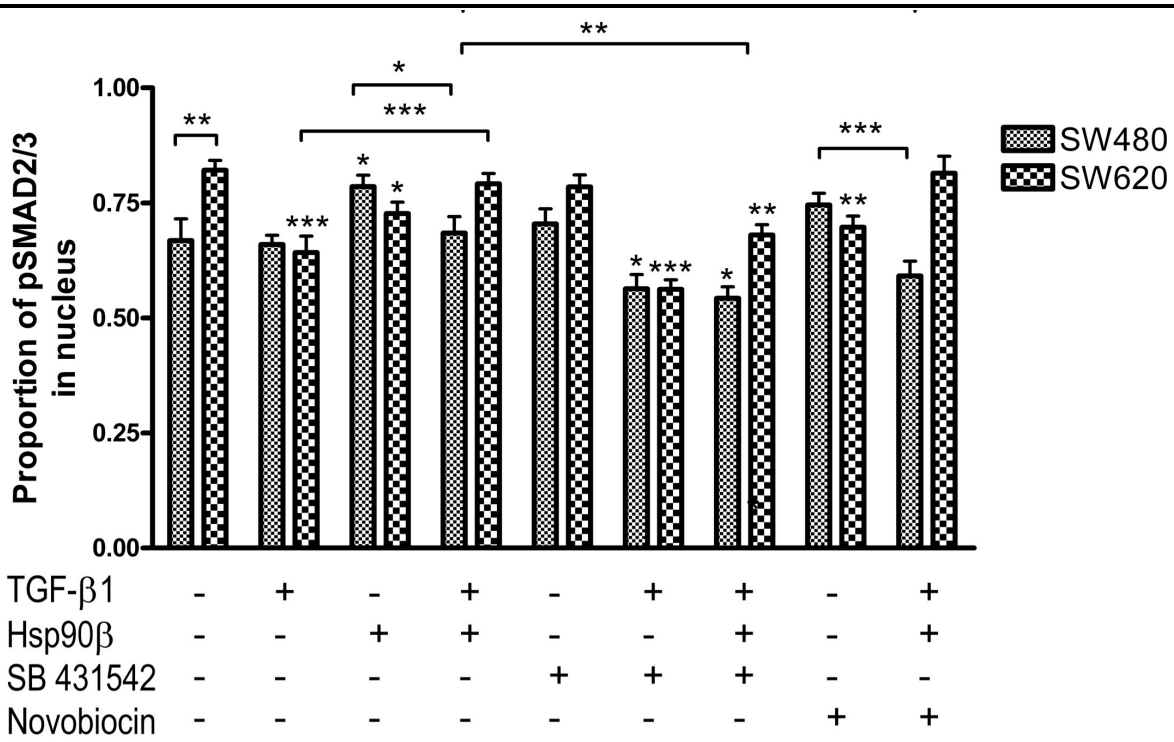

Figure 17. Analysis of the proportion of pSMAD2/3 in the nucleus after the addition and inhibition of TGF-β1 and Hsp90 in SW480 and SW620 colon cancer cells. SW480 and SW620 cancer cells were seeded at a density of 3 x 10^5 cells/ml on gelatin coated 15-well µ-Slide angiogenesis plates and incubated at 37°C for 24 hours. Cells were treated with 2 ng/ml TGF-β1, 20 ng/ml Hsp90β, 100 nM SB 431542 and 100 µM novobiocin for 24 hours alone and in combinations. Cells were fixed with ethanol and stained with mouse anti-rabbit SMAD2/3 and goat anti-pSMAD2/3 primary antibodies overnight at 4 °C. This was followed by incubation with donkey anti-rabbit 488 and donkey anti-goat DY660 secondary antibodies overnight at 4 °C. Nuclei were stained with 1 µg/ml Hoechst 33342 (blue). Immunofluorescence was detected using the Zeiss LSM 780 confocal microscope and the images analysed using Zen Lite Software 2014 (Zeiss, Germany). The graph indicates the proportion of total pSMAD2/3 that is found in the nucleus after each treatment. Errors bars indicate the standard error in the mean. Statistical analysis was done using GraphPad Prism 4.03 software (GraphPad Inc., California). A two-way analysis of variance (ANOVA) with Bonferroni post tests was performed, significance between untreated and each treatment within the different cell lines are shown, unless otherwise indicated connecting the two cell lines or between two treatments; ($p<0.05$)*, ($p<0.01$)**, ($p<0.001$)***, ns – not significant.

Treatment with 100 nM of SB 431542 had no effect [$p>0.05$] on the proportion of pSMAD2/3 in the nucleus of SW480 and SW620 cells compared to untreated cells. The addition of 2 ng/ml of TGF-β1 in combination with the inhibitor, however, caused a movement into the cytoplasm of pSMAD2/3 in both SW480 and SW620 cells (ratios of 0.56±0.13 vs 0.66±0.163 [$p<0.05$] and 0.56±0.08 vs 0.83±0.09 [$p<0.001$], respectively; Figure 17). SB 431542 treatment in combination with 2 ng/ml of TGF-β1 and 20 ng/ml of Hsp90β caused the same effect as SB 431542 with TGF-β1 in SW480 cells. The combination of TGF-β1 and Hsp90β in SB 431542 treated SW620 cells caused slightly more pSMAD2/3 to be found in the nucleus in comparison to SB 431542 treatment with only TGF-β1, although this was still less than the untreated cells (0.68±0.09 vs 0.56±0.08 [$p<0.01$], respectively; Figure 17).

SW480 cells treated with 100 μM of novobiocin had a slightly higher proportion of pSMAD2/3 in the nucleus, although this was not significantly different to untreated cells (ratios of 0.74±0.12 vs 0.67±0.16 [p>0.05], respectively; Figure 17). The addition of 2 ng/ml of TGF-β1 and 20 ng/ml of Hsp90β to novobiocin treated cells caused a significant decrease of pSMAD2/3 in the nucleus of SW480 cells, back to a similar proportion seen in untreated cells (ratios of 0.59±0.11 vs 0.67±0.16 [p<0.001], respectively; Figure 17). Although the novobiocin only treatment and the combination treatment were not significantly different to the untreated cells, the combination treatment was substantially lower than the novobiocin treatment alone (ratios of 0.74±0.12 vs 0.59±0.11 [p<0/001], respectively; Figure 17). The novobiocin treated SW620 cells however showed a decrease in the proportion of pSMAD2/3 in the nucleus compared to untreated cells (ratios of 0.69±0.10 vs 0.83±0.09 [p<0.01], respectively; Figure 17), and the addition of TGF-β1 and Hsp90β was enough to overcome the inhibition of Hsp90, bringing the proportion of pSMAD2/3 in the nucleus back to the same level as that of the untreated cells (ratios of 0.81±0.13 vs 0.83±0.09 [p>0.05], respectively; Figure 17).

Chapter 4

Discussion

4 Discussion

In this study, the expression levels of TGF-β1, TGF-βRII and Hsp90 in five different cancer types, namely of the colon, breast, lung, cervix and blood (leukemia), were analysed using six cell lines. The paired colon cancer cell lines SW480 and SW620 (from the colon and lymph node metastases, respectively) (Leibovitz *et al*., 1976) were chosen as the cell line model to study the effect of the TGF-β1 pathway and Hsp90 on growth, adhesion and migration. This was due to contrasting expression levels of TGF-β1 and TGF-βRII, where SW480 cells had twice the expression of TGF-βRII, compared to SW620 cells, while SW620 cells secreted double the level of TGF-β1 compared to SW480 cells. Changes in growth, migration and adhesion of SW480 and SW620 cells were analysed after either the addition or inhibition of TGF-β1 and Hsp90 and yielded a number of interesting trends when the two cells lines were compared. This is described in detail below. In addition, in light of the observed ability of the proteins to interact directly both *in vitro* and *in vivo* as determined in this study, the effects of a combination of TGF-β1 and Hsp90β as well as their inhibitors on adhesion and migration was investigated as this has not previously been reported in the literature.

4.1 A direct interaction between Hsp90β and the TGF-β1 was confirmed *in vitro* and *in vivo*

A potential interaction between Hsp90 and the TGF-β signaling pathway was first mentioned when a large scale interactome mapping analysis of *Caenorhabditis elegans* was performed (Savage-Dunn, 2005). Here an interaction between the gene DAF-21 (Hsp90β is the corresponding human othologue) and DAF-1 (TGF-βRI) as well as DAF-4 (TGF-βRII) was suggested (Savage-Dunn, 2005). These data were obtained using the yeast two-hybrid system, which is a genetic assay where one protein is bound to a DNA binding domain of a transcription factor and a second protein is bound to the activation domain. If the proteins interact, it will result in the activation of reporter genes (Braun, 2012). The interaction of Hsp90 with TGF-βRs was first determined experimentally in human cancer cells by co-immunoprecipitation both *in vitro,* using Glutathione S-transferase (GST)-tagged Hsp90, and *in vivo,* using human embryonic kidney (HEK293T) cell lysates (Wrighton *et al*., 2008). This team also determined that 17-AAG (a geldanamycin derivative) caused a degradation of both TGF-βRI and TGF-βRII, and it was thus concluded that Hsp90 could be

stabilising these TGF-β receptors (Wrighton *et al*., 2008). Haupt and colleagues in 2012 then confirmed this stabilisation of the TGF-β receptors by Hsp90. This was performed by treating Hs68 primary fibroblast cells, U2OS osteosarcoma cells, A549 lung adenocarcinoma cells and SW480 colon adenocarcinoma cells with geldanamycin for 12 or 24 hours and analysing the lysates using proteomic analysis (Haupt *et al*., 2012). Decreases in kinase populations were depicted on a heat map, and it was shown that both TGF-βRI and TGF-βII levels decreased in all four cell lines after treatment with 1.78 μM geldanamycin (Haupt *et al*., 2012). This concentration of geldanamycin is very high compared to our study and the effects of the toxicity of geldanamycin on the cell lines was not analysed.

The only report to date of a direct interaction between TGF-β1 and Hsp90β refers to the small latent complex (Suzuki and Kulkarni, 2010). This complex is formed between the active form of TGF-β in conjugation with the latency associated peptide (LAP) (Fortunel *et al*., 2000) and it is in this form that the interaction with Hsp90β was found, not necessarily active TGF-β (Suzuki and Kulkarni, 2010). Our study however reports an *in vitro* direct interaction between recombinant TGF-β1 (already in the active mature form) and Hsp90β. This is, to our knowledge, the first time this interaction has been reported. The interaction between TGF-β1 and Hsp90α/β was confirmed *in vivo* using SW620 colon cancer cells. In this experiment, the form of TGF-β1 detected during the immunoprecipitation assay was in fact larger than the mature form of TGF-β1 detected in the *in vitro* assay. As the latter protein was detected at a molecular weight corresponding to around 90/100 kDa it is likely that this is the proprotein, containing the LAP region that was found to interact with Hsp90 by Suzuki and Kulkarni (2010). Our study differs from that of Suzuki and Kulkarni because the interaction described by the latter was found using LAP to pull down Hsp90β, whereas our interaction was identified using Hsp90 to pull down TGF-β1, and a TGF-β1 antibody to detect this interaction by western blotting. From our findings it is possible that Hsp90 could be binding to either or both the mature form of TGF-β1 and LAP.

Our findings of an interaction between Hsp90 and TGF-β1, together with the earlier report by Wrighton and colleagues (2008) that Hsp90 and TGF-βRII are able to interact *in vivo*, have led us to hypothesise that there may be a complex formed between Hsp90, TGF-β1 and TGF-βRI/II, or that Hsp90 chaperones the latter proteins

at different points in the signaling process. Unfortunately, despite attempts to do so, we were unable to confirm the presence of such a complex. In addition, binding studies using Hsp90 inhibitors such as geldanamycin or novobiocin could also provide more insight into the interaction between Hsp90 and TGF-β1, and serve to verify the interaction. If Hsp90 is inhibited by novobiocin, the C-terminal is affected and Hsp90 should not be able to bind to TGF-β1. If geldanamycin inhibits Hsp90 at the N-terminal, this could prevent Hsp90 ATPase function and therefore inhibit the interaction between TGF-β1 and Hsp90. In either of the latter scenarios, TGF-β1 should not be pulled down in a complex with Hsp90. It would also be interesting to see if TGF-β1 is still able to interact with TGF-βRI if Hsp90 is inhibited, which would indicate whether Hsp90 assists in this interaction. This could be performed using novobiocin treated cells in immunoprecipitation assays and confocal microscopy. Studies determining the relative affinities of TGF-β1, Hsp90 and TGF-βRII for each other, such as surface plasmon resonance (SPR) spectroscopy, would also shed light on the interaction and perhaps even the mechanism as was performed in literature (Hunter *et al*., 2014).

4.2 Different levels of TGF-β1 and TGF-βRII expression may be linked to cancer progression

The major cause of cancer-associated mortality is often not the primary tumour, but rather metastasis of cancer cells to tissues elsewhere in the body (WHO, 2014). In the case of the paired SW480 and SW620 cell lines used in this study, the SW620 cells are derived from a lymph node metastases of a colon tumour (SW480 cells) and represent a more advanced stage of the disease (Leibovitz *et al*., 1976). Considering this, the contrasting expression levels of TGF-β1 and TGF-βRII in the two cell lines, namely the higher TGF-β1 and lower TGF-βRII expression in SW620 cells compared to SW480 cells, may potentially be linked to cancer progression. These contrasting changes in expression of TGF-β1 and TGF-βRII have been previously studied in other cancers, specifically esophageal carcinoma (Fukai *et al*., 2003), but also in colon cancer (Friedman *et al*., 1995). High levels of TGF-β1 in colon cancer have been correlated with a poor disease prognosis, specifically increasing metastasis and general invasiveness (Elliott and Blobe, 2005; Friedman *et al*., 1995), which is consistent with the findings in our study. Alterations in this signaling pathway could be one of the causes or consequences of the spread of the cancer from the colon

(SW480 cell line) to the lymph node (SW620 cell line) in the patient from whom the cell lines were derived. Furthermore, a low level of TGF-βR (both TGF-βRI and TGF-βRII) has also been demonstrated to correlate with disease progression (Fukai *et al*., 2003) and this is again consistent with the results reported in our study. The majority of latter studies on colon cancer reported in the literature differ from ours in that they have been carried out in resected tumours and their respective metastases and ours is thus the first study to our knowledge comparing genetically paired colon cancer cell lines.

4.3 Marked differences in the cellular responses of SW480 and SW620 colon cancer cells to TGF-β1 and Hsp90β reflect key changes in the functioning of this signaling machinery during the metastatic process

When comparing untreated SW480 and SW620 cells, it was found that SW480 cells had a higher level of adhesion, while SW620 cells had a much higher level of migration. Changes in the cytoskeleton and extracellular matrix proteins as well as weak adhesions may cause an increase in migration and may be required for cell motility (Bogenrieder and Herlyn, 2003; Huttenlocher *et al*., 1995; Kopfstein and Christofori, 2006). A proteomic study by Ghosh and colleagues (2011) identified several statistically significant levels of proteins associated to migration and adhesion, specifically the cytoskeleton, indicating that the SW620 line was more aggressive and migratory (Ghosh *et al*., 2011). Literature has shown SW620 cells to be more migratory during *in vivo* studies, which was performed in mice by injecting the cells and analysing the liver for metastases (Hewitt *et al*., 2000). *In vitro* migration studies on the other hand revealed that SW480 cells migrated substantially more than SW620 cells on various matrix proteins. These latter data were obtained using a transwell assay, which was performed by seeding cells onto a nucleopore polycarbonate membrane coated in several extracellular matrices and then observing how many cells had migrated to the other side of the membrane (Hewitt *et al*., 2000; Feng *et al*., 2012). SW480 cells were also more adherent on these matrices than SW620 cells over 4 hours (Hewitt *et al*., 2000). The extracellular matrices used in the latter studies may account for the difference in migratory capacity observed in comparison to our results, where uncoated wells were used for both adhesion and migration analysis. Here we found SW620 cells to be more migratory. It is important to note that the migration assay performed in the current study was linear migration which did not

account for invasion and this could be another aspect causing the contrasting data between this and published reports. The untreated cells also showed that the canonical TGF-β1/TGF-βRI/TGF-βRII pathway in SW620 cells may be constitutively active, as these cells display a higher level of nuclear pSMAD2/3 in comparison to the SW480 cell line. This may also be due to the higher level of TGF-RII in SW480 cells, while SW620 cells had a higher level of TGF-β1.

A summary comparing the cellular responses of SW480 and SW620 cells after addition or inhibition of TGF-β and Hsp90β, in comparison to untreated cells, can be seen in the heat map in Table II. All results shown are significant, with p values of 0.05 or less, and the red and blue indicate fold changes in the cellular responses of the cell lines. Single treatments with TGF-β1 and Hsp90β showed contrasting results in SW480 and SW620 cells, as did novobicoin treatment. SB 431542 treatment on the other hand showed a similar trend when comparing the two cell lines.

Table II. Comparison of the effects of the addition or inhibition of the TGF-β signaling pathway and Hsp90 on cellular responses of SW480 and SW620 colon cancer cells

CELL LINE:	SW480				SW620			
ASSAY→	Growth	Adhesion	Migration	Nuclear pSMAD2/3**	Growth	Adhesion	Migration	Nuclear pSMAD2/3**
EFFECT OF TREATMENT*								
TGF-β1 (2 ng/ml)								
Hsp90β (20 ng/ml)								
TGF-β1 and Hsp90β								
SB 431542 (100 nM)								
SB 431542 with TGF-β1								
SB 431542 with TGF-β1 and Hsp90β								
Novobiocin (100 μM)								
Novobiocin with TGF-β1 and Hsp90								
αvβ6 integrin (10 μg/ml)								
αvβ6 with TGF-β1 and Hsp90								

* Relative to untreated

** Proportion of pSMAD2/3 in the nucleus indicating activation of the downstream pathway

	Increase		No change	Decrease	
Fold Change:	2+	1-2	0	1-2	2+

4.3.1 Effect of the addition of TGF-β and Hsp90β on cellular responses

The addition of exogenous TGF-β1 caused a decrease in proliferation in both SW480 and SW620 cells, which was more prominent in SW480 cells (Table II). This inhibition of growth by TGF-β1 has been seen in a range of cancer cells, including MDA-MB-231 breast cancer cells, Mv1Lu lung epithelial cells, A549 lung adenocarcinoma cells, glioma and osteosarcoma cells using cell counting assays (Connolly *et al*., 2012; Halder *et al*., 2005). This addition of TGF-β1 also caused an increase in the activation of the canonical pathway in SW620 cells, which once again indicated that the pathway is constitutively activated in these cells. The addition of Hsp90 on the other hand activated the pathway in both cell lines, while decreasing growth in SW480 cells.

The effect of a combination of TGF-β1 and Hsp90β treatment on cancer cell growth has not previously been reported. This combination treatment had no effect on any responses in the SW480 cells, while causing an increase in growth and migration in SW620 cells. The stimulation of the growth of SW620 cells may suggest that the addition of exogenous Hsp90β had an overriding effect on the growth inhibitory effect of TGF-β1, because TGF-β1 treatment alone inhibited growth in SW620 cells at 24 hrs. When analyzing the pro-migratory effect it is important to take into account that the growth assay and migration assay were performed at the equivalent time point of 24 hrs. The fact that there was an increase in growth following this treatment compared to the control at 24 hours could indicate that the cells are not necessarily migrating, but rather proliferating. Perhaps the migration assay could be performed for a shorter time period, to account for the growth phenotype. The basal level of activated pSMAD2/3 in the nucleus with the combination treatment may suggest that extracellular Hsp90β may regulate TGF-β1 and thus control downstream signaling in SW620 cells. The SW620 cells are the metastases from SW480 cells so these data could also indicate that the cells are more aggressive in the presence of the TGF-β1 and Hsp90 complex (Hewitt *et al*., 2000; Kubens and Zanker, 1998). The SW620 cells may also have developed a way to overcome TGF-β1 growth inhibition using Hsp90, or express a specific receptor that the SW480 cells do not.

4.3.2 Effect of the inhibition of TGF-βRI on cellular responses

The same effects on growth, adhesion, migration and activation of pSMAD2/3 were seen in both SW480 and SW620 cells after the inhibition of TGF-βRI with SB 431542

(Table II). The decrease in growth has been seen in another colon cancer cell line, namely HT29, which also lacks the SMAD4 signaling intermediate of the TGF-β pathway (Arteaga, 2006). The decrease in adhesion is enhanced when exogenous TGF-β1 and Hsp90 was added in combination with SB 431542, as is the increase in migration. The increase in migration is correlated with a decrease in the activation of pSMAD2/3 (proportion of pSMAD2/3 in nucleus). The only difference was that in SW620 cells SB 431542 treatment alone caused no change in migration, which just indicates that the pathway may be more active or may correlate with the higher levels of TGF-β in these cells (Figure 5 and 6 as well as Table II). Several studies show that SB 431542 inhibits lung (A549) and breast (MDA-MB-231) cancer cell migration, especially inhibiting the increased migration associated with TGF-β1 treatment (Halder *et al*., 2005; Hjelmeland *et al*., 2004). This was not the case with our data. The inhibition of nuclear translocation of SMAD2 and SMAD3 by SB 431542 has been seen in literature as well as in our study (Halder *et al*., 2005; Hjelmeland *et al*., 2004; Matsuyama *et al*., 2003).

It was noted that, at 24 hours, separate treatments with either TGF-β1 or SB 431542 (alone) caused a decrease in proliferation. This is unexpected as SB 431542 should cause a decrease in TGF-β signaling as it is blocking the pathway at the receptor level; and should thus cause a different effect when compared to TGF-β1 treatment alone. Many studies have investigated the effect of SB 431542 on cancer cells after TGF-β growth stimulation/inhibition, but only in individual cell lines (Halder *et al*., 2005; Hjelmeland *et al*., 2004; Matsuyama *et al*., 2003; Watabe *et al*., 2003) Thus further studies using combinations of TGF-β1 and SB 431542 are required to analyse the effect of SB 431542 on growth of the paired cell lines SW480 and SW620.

4.3.3 Effect of the inhibition of Hsp90 on cellular responses

Novobiocin had different effects on the SW480 and SW620 cells. While the growth and adhesion phenotypes are the same, migration was enhanced with novobiocin in SW480 cells, correlated with no change in the amount of pSMAD2/3 in the nucleus. The novobiocin treatment in SW620 cells prevented pSMAD2/3 activation, but the addition of TGF-β1 and Hsp90β was enough to override this and return it to basal level (Table II). This may only be seen in SW620 cells because the pathway is

constitutively active and therefore the pathway is available to be inhibited, whereas the SW480 cells are not activated and therefore there is no change.

Novobiocin has been found to inhibit migration in MDA-MB-231 breast cancer cells (Luo *et al*., 2010). This data was obtained using a wound healing scratch assay and analysed at 12, 24 and 48 hours (Luo *et al*., 2010), which is different to our migration assay, where no wound was created and the cells were grown in separate areas and allowed to migrate towards one another. Our data suggests that novobiocin may increase migration, but this trend was only observed in SW480 cells. These differences in migration may be due to experimental design or may allude to the type of migration utilised by the different types of cells (breast versus colon). It was also discovered that adding exogenous Hsp90β in combination with TGF-β1 did not block the migration induced in the SW480 cells by novobiocin treatment at all. In fact, it increased the migration to some degree, which was the same effect seen with the inhibition of TGF-β1. In one study, the Hsp90 inhibitor 17-AAG prevented SMAD phosphorylation after TGF-β stimulation, although only 4 hours of treatment were performed. It was suggested that this was because Hsp90 was required for TGF-β receptor stabilisation (Reka *et al*., 2011). This effect of the inhibition of Hsp90 preventing the phosphorylation of SMAD2/3 was seen in SW620 cells and not in the SW480 cells, where novobiocin caused a decrease in the ratio of pSMAD2/3 in the nucleus. The inhibition of Hsp90 may be affecting TGF-β regulation, causing an increased migration of SW480 cells. Perhaps Hsp90 inhibition inhibits the TGF-βR1 and thus produces the same effect as inhibition with SB 431542. The effect of novobiocin treatment increasing migration in SW480 cells was not observed in SW620 cells, which might be due to the concentrations of novobiocin used (100 μM). This concentration is close to the IC_{50} of novobiocin observed in SW480 cells, but is much lower than the IC_{50} seen when novobiocin was tested in SW620 cells, which may account for the lack of migration. Alternatively, if the effect of novobiocin is via the TGF-βR1, the higher levels in SW620 may account for this effect and perhaps a different effect may be seen at a higher concentration of novobiocin. Further studies would be required to see if the effect is due to concentration of novobiocin, resistance to the effect of novobiocin on migration (due to the aggressive nature of the SW620 cells) or if there is a different mechanism used in SW620 cells compared to SW480 cells during migration.

4.4 Conclusions

Intrinsic differences between the SW480 primary and SW620 metastatic colon cancer cells (the latter cell line representing a more advanced form of the disease) in terms of the specific protein levels, drug sensitivity, growth, adhesion, migration, and pathway activation were seen in this study. Most notably that SW620 cells had a higher level of TGF-β, while SW480 cells had a higher level of the TGF-βRII. A novel interaction was found between mature form of TGF-β1 and Hsp90β and, when investigating the effect of this interaction on the biology of SW480 and SW620 cells, the metastatic cell line was found to be more aggressive and less susceptible to inhibition of the two proteins. Although there was no clear growth phenotype distinguishable between the two cells lines, SW480 cells were more adherent while SW620 cells were more migratory.

SB 431542 caused the same effects on SW480 and SW620 cells, suggesting that even though the canonical TGF-β1/TGF-βRI/TGF-βRII pathway may be constitutively active in SW620, the response to its inhibition may suggest an alternate pathway or receptor. An unintentional finding that the addition of TGF-β1, as well as inhibition of TGF-βRI, has the same effect is only feasible if it is not the TGF-β/TGF-βR/SMAD pathway that is causing the effect. In this scenario, blocking of the TGF-βR may direct the signals via an alternate pathway, which may also be activated due to the availability of higher levels of TGF-β1. Blocking the αvβ6 integrin had no effect on the migration, suggesting that the proposed alternative signaling pathway for TGF-β and Hsp90 under the conditions for migration was not one previously linked to this integrin receptor (Munger *et al*., 1999; Wipff and Hinz, 2008). The alternate pathway could potentially be activated by the TGF-β1 ligand and could be one of those mentioned in Figure 3, for example the JNK or ERK pathway, which are pathways also linked to migration. As the inhibition of TGF-βRI has no effect on the function of TGF-β1 and the fact that pSMAD2/3 levels in the nucleus were unchanged after treatment with SB 431542 substantiates this claim as well. Further research to answer these questions will be required and this is ongoing.

Chapter 5
References

5 References

Akhurst, R. J. (2004). TGF beta signaling in health and disease. *Nature Genetics*, *36*(8), 790–2.

Altieri, D. C., Stein, G. S., Lian, J. B., and Languino, L. R. (2012). TRAP-1, the mitochondrial Hsp90. *Biochimica et Biophysica Acta*, *1823*(3), 767–73.

Annamalai, B., Liu, X., Gopal, U., and Isaacs, J. S. (2009). Hsp90 is an essential regulator of EphA2 receptor stability and signaling: implications for cancer cell migration and metastasis. *Molecular Cancer Research : MCR*, *7*(7), 1021–32.

Annes, J. P. (2003). Making sense of latent TGFbeta activation. *Journal of Cell Science*, *116*(2), 217–224.

Arteaga, C. L. (2006). Inhibition of TGFbeta signaling in cancer therapy. *Current Opinion in Genetics and Development*, *16*(1), 30–7.

Bagatell, R., and Whitesell, L. (2004). Altered Hsp90 function in cancer : A unique therapeutic opportunity. *Molecular Cancer Therapeutics*, *3*, 1021–1030.

Barrot, J. J., and Haystead, T. A. (2013). Hsp90, an unlikely ally in the war on cancer. *NIH Public Access*, *280*(6), 1–24.

Belani, C. (2013). 17-DMAG in Treating Patients With Metastatic or Unresectable Solid Tumors or Lymphomas. Retrieved from http://clinicaltrials.gov/

Biaoxue, R., Xiling, J., Shuanying, Y., Wei, Z., Xiguang, C., Jinsui, W., and Min, Z. (2012). Upregulation of Hsp90-beta and annexin A1 correlates with poor survival and lymphatic metastasis in lung cancer patients. *Journal of Experimental and Clinical Cancer Research : CR*, *31*, 70.

Bierie, B., and Moses, H. L. (2006). TGF-beta and cancer. *Cytokine and Growth Factor Reviews*, *17*(1-2), 29–40.

Blagg, B. S. J., and Kerr, T. D. (2006). Hsp90 inhibitors: small molecules that transform the Hsp90 protein folding machinery into a catalyst for protein degradation. *Medicinal Research Reviews*, *26*(3), 310–38.

Bogenrieder, T., and Herlyn, M. (2003). Axis of evil: molecular mechanisms of cancer metastasis. *Oncogene*, *22*(42), 6524–36.

Braun, P. (2012). Interactome mapping for analysis of complex phenotypes: insights from benchmarking binary interaction assays. *Proteomics*, *12*(10), 1499–518.

Calderwood, S. K., Khaleque, M. A., Sawyer, D. B., and Ciocca, D. R. (2006). Heat shock proteins in cancer: chaperones of tumorigenesis. *Trends in Biochemical Sciences*, *31*(3), 164–72.

Chaffer, C., and Weinberg, R. (2011). A perspective on cancer cell metastasis. *Science*, *31*(6024), 1559–1564.

Chen, W.-S., Chen, C.-C., Chen, L.-L., Lee, C.-C., and Huang, T.-S. (2013). Secreted heat shock protein 90α (HSP90α) induces nuclear factor-κB-mediated TCF12 protein expression to down-regulate E-cadherin and to enhance colorectal cancer cell migration and invasion. *The Journal of Biological Chemistry*, *288*(13), 9001–10.

Cheng, C.-F., Fan, J., Fedesco, M., Guan, S., Li, Y., Bandyopadhyay, B., Bright, A. M., Yerushalmi, D., Liang, M., Chen, M., Han, Y-P., Woodley, D. T. and Li, W. (2008). Transforming growth factor alpha (TGFalpha)-stimulated secretion of HSP90alpha: using the receptor LRP-1/CD91 to promote human skin cell migration against a TGFbeta-rich environment during wound healing. *Molecular and Cellular Biology*, *28*(10), 3344–58.

Cheng, S. K., Olale, F., Brivanlou, A. H., and Schier, A. F. (2004). Lefty blocks a subset of TGFbeta signals by antagonizing EGF-CFC coreceptors. *PLoS Biology*, *2*(2), E30.

Ciocca, D. R., and Calderwood, S. K. (2005). Heat shock proteins in cancer: diagnostic, prognostic, predictive, and treatment implications. *Cell Stress and Chaperones*, *10*(2), 86–103.

Connolly, E. C., Freimuth, J., and Akhurst, R. J. (2012). Complexities of TGF-β targeted cancer therapy. *International Journal of Biological Sciences*, *8*(7), 964–78.

Csermely, P., Schnaider, T., Soti, C., Prohászka, Z., and Nardai, G. (1998). The 90-kDa Molecular Chaperone Family. *Pharmacology and Therapeutics*, *79*(2), 129–168.

Didenko, T., Duarte, A. M. S., Karagöz, G. E., and Rüdiger, S. G. D. (2012). Hsp90 structure and function studied by NMR spectroscopy. *Biochimica et Biophysica Acta*, *1823*(3), 636–47.

Elliott, R. L., and Blobe, G. C. (2005). Role of transforming growth factor Beta in human cancer. *Journal of Clinical Oncology : Official Journal of the American Society of Clinical Oncology*, *23*(9), 2078–93.

Eustace, B. K., and Jay, D. G. (2004). Extracellular roles for the molecular chaperone, HSP90. *Cell Cycle*, *3*(9), 1096–1098.

Eustace, B. K., Sakurai, T., Stewart, J. K., Yimlamai, D., Unger, C., Zehetmeier, C., Lain, B. Torella, C., Henning, S. W., Beste, G., Scroggins, B.T. Neckers, L., Ilag, L.L. andJay, D. G. (2004). Functional

proteomic screens reveal an essential extracellular role for hsp90 alpha in cancer cell invasiveness. *Nature Cell Biology*, *6*(6), 507–14.

Fallon, J., Reid, S., Kinyamu, R., Opole, I., Opole, R., Baratta, J., Korc, M., Endo, T. L., Duong, A., Nguyen, G., Karkehabadhi, M., Twardzik, D., Patel, S. and Loughlin, S. (2000). In vivo induction of massive proliferation, directed migration, and differentiation of neural cells in the adult mammalian brain. *Proceedings of the National Academy of Sciences of the United States of America*, *97*(26), 14686–91.

Feng, B., Dong, T. T., Wang, L. L., Zhou, H. M., Zhao, H. C., Dong, F., and Zheng, M. H. (2012). Colorectal cancer migration and invasion initiated by microRNA-106a. *PloS One*, *7*(8), e43452.

Fidler, I. J. (2003). The pathogenesis of cancer metastasis: the “seed and soil” hypothesis revisited. *Nature Reviews. Cancer*, *3*(6), 453–8.

Fontana, L., Chen, Y., Prijatelj, P., Sakai, T., Fässler, R., Sakai, L. Y., and Rifkin, D. B. (2005). Fibronectin is required for integrin alphavbeta6-mediated activation of latent TGF-beta complexes containing LTBP-1. *FASEB Journal : Official Publication of the Federation of American Societies for Experimental Biology*, *19*(13), 1798–808.

Fortunel, N. O., Hatzfeld, A., and Hatzfeld, J. A. (2000). Transforming growth factor-β : pleiotropic role in the regulation of hematopoiesis. *Blood*, *96*, 2022–2036.

Friedman, E., Gold, L., Klimstra, D., Winawer, S., and Cohen, A. (1995). High levels of transforming growth factor beta 1 correlate with disease progression in human colon cancer. *Cancer Epidemiology, Biomarkers and Prevention*, *4*, 549–554.

Fukai, Y., Fukuchi, M., Masuda, N., Osawa, H., Kato, H., Nakajima, T., and Kuwano, H. (2003). Reduced expression of transforming growth factor-beta receptors is an unfavorable prognostic factor in human esophageal squamous cell carcinoma. *International Journal of Cancer. Journal International Du Cancer*, *104*(2), 161–6.

Garon, E. B., Finn, R. S., Hamidi, H., Dering, J., Pitts, S., Kamranpour, N., Desai, A. J., Hosmer, W., Ide, S., Avsar, E., Jensen, M. R., Quadt, C., Liu, M. Dubinett, S. M. and Slamon, D. J. (2013). The HSP90 inhibitor NVP-AUY922 potently inhibits non-small cell lung cancer growth. *Molecular Cancer Therapeutics*, *12*(6), 890–900.

Ghosh, D., Yu, H., Tan, X. F., Lim, T. K., Zubaidah, R. M., Tan, H. T., and Lin, Q. (2011). Identification of key players for colorectal cancer metastasis by iTRAQ quantitative proteomics profiling of isogenic SW480 and SW620 cell lines. *Journal of Proteome Research*, *10*, 4373–4287.

Gopal, U., Bohonowych, J. E., Lema-Tome, C., Liu, A., Garrett-Mayer, E., Wang, B., and Isaacs, J. S. (2011). A novel extracellular Hsp90 mediated co-receptor function for LRP1 regulates EphA2 dependent glioblastoma cell invasion. *PloS One*, *6*(3), e17649.

Grad, I., Cederroth, C. R., Walicki, J., Grey, C., Barluenga, S., Winssinger, N., De Massy, B., Nef, S., and Picard, D. (2010). The molecular chaperone Hsp90α is required for meiotic progression of spermatocytes beyond pachytene in the mouse. *PloS One*, *5*(12), e15770.

Grammatikakis, N., Vultur, A., Ramana, C. V, Siganou, A., Schweinfest, C. W., Watson, D. K., and Raptis, L. (2002). The role of Hsp90N, a new member of the Hsp90 family, in signal transduction and neoplastic transformation. *The Journal of Biological Chemistry*, *277*(10), 8312–20.

Gupta, G. P., and Massagué, J. (2006). Cancer metastasis: building a framework. *Cell*, *127*(4), 679–95.

Halder, S. K., Beauchamp, R. D., and Datta, P. K. (2005). A Specific Inhibitor of TGF-β Receptor Kinase, SB-431542, as a Potent Antitumor Agent for Human Cancers. *Neoplasia*, *7*(5), 509–521.

Hanahan, D., and Weinberg, R. A. (2000). The Hallmarks of Cancer. *Cell*, *100*(1), 57–70.

Hanahan, D., and Weinberg, R. A. (2011). Hallmarks of cancer: the next generation. *Cell*, *144*(5), 646–74.

Hance, M. W., Nolan, K. D., and Isaacs, J. S. (2014). The double-edged sword: conserved functions of extracellular hsp90 in wound healing and cancer. *Cancers*, *6*(2), 1065–97.

Hartl, F. (2002). Molecular Chaperones in the Cytosol: from Nascent Chain to Folded Protein. *Science*, *295*(5561), 1852.

Haupt, A., Joberty, G., Bantscheff, M., Fröhlich, H., Stehr, H., Schweiger, M. R., Fischer, A., Kerick, M., Boerno, S. T. Dahl, A. Lappe, M., Lehrach, H., Gonzalez, C., Drewes, G. and Lange, B. M. (2012). Hsp90 inhibition differentially destabilises MAP kinase and TGF-beta signaling components in cancer cells revealed by kinase-targeted chemoproteomics. *BMC Cancer*, *12*(1), 38.

Hewitt, R. E., McMarlin, a, Kleiner, D., Wersto, R., Martin, P., Tsokos, M., Stamp, G. W., Stetler-Stevenson, W. G. and Tsoskas, M. (2000). Validation of a model of colon cancer progression. *The Journal of Pathology*, *192*(4), 446–54.

Hjelmeland, M. D., Hjelmeland, A. B., Sathornsumetee, S., Reese, E. D., Herbstreith, M. H., Laping, N. J., Friedman, H. S., Bigner, D. D., Wang, X-F. and Rich, J. N. (2004). SB-431542 , a small molecule transforming growth factor- β -receptor antagonist, inhibits human glioma cell line proliferation and motility factor. *Molecular Cancer Therapeutics*, *3*, 737–745.

Holzbeierlein, J. M., Windsperger, A., and Vielhauer, G. (2010). Hsp90: a drug target? *Current Oncology Reports*, *12*(2), 95–101.
Hui, A. Y., and Friedman, S. L. (2003). The transforming growth factor b (TGF-b) signaling pathway. *Expert Reviews in Molecular Medicine.* 5, 4
Hunter, M. C., O'Hagan, K. L., Kenyon, A., Dhanani, K. C. H., Prinsloo, E., and Edkins, A. L. (2014). Hsp90 binds directly to fibronectin (FN) and inhibition reduces the extracellular fibronectin matrix in breast cancer cells. *PloS One*, *9*(1), e86842.
Huttenlocher, A., Sandborg, R. R., and Horwitz, A. F. (1995). Adhesion in cell migration. *Current Opinion in Cell Biology*, *7*, 697–706.
Jensen, M. R., Schoepfer, J., Radimerski, T., Massey, A., Guy, C. T., Brueggen, J., Quadt, C., Buckler, A., Cozens, R., Drysdale, M. J., Garcia-Echeverria, C. and Chène, P. (2008).NVP-AUY922: a small molecule HSP90 inhibitor with potent antitumor activity in preclinical breast cancer models. *Breast Cancer Research : BCR*, *10*(2), R33.
Jin, S., Song, Y. C., Emili, A., Sherman, P. M., and Chan, V. L. (2003). JlpA of Campylobacter jejuni interacts with surface-exposed heat shock protein 90α and triggers signaling pathways leading to the activation of NF-κB and p38 MAP kinase in epithelial cells. *Cellular Microbiology*, *5*(3), 165–174.
Johnson, J. L. (2012). Evolution and function of diverse Hsp90 homologs and cochaperone proteins. *Biochimica et Biophysica Acta*, *1823*(3), 607–13.
Kopfstein, L., and Christofori, G. (2006). Metastasis: cell-autonomous mechanisms versus contributions by the tumor microenvironment. *Cellular and Molecular Life Sciences : CMLS*, *63*(4), 449–68.
Kubens, B. S., and Zanker, K. S. (1998). Differences in the migration capacity of primary human colon carcinoma cells (SW480) and their lymph node metastatic derivatives (SW620). *Cancer Letters*, *131*, 55–64.
Laemmli, U. K. (1970). Cleavage of structural proteins during the assembly of the head of bacteriophage T4. *Nature*, *227*(5259), 680–685.
Lee, E. Y., Parry, G., and Bissell, M. J. (1984). Modulation of secreted proteins of mouse mammary epithelial cells by the collagenous substrata. *The Journal of Cell Biology*, *98*(1), 146–55.
Lee, G. Y. H., and Lim, C. T. (2007). Biomechanics approaches to studying human diseases. *Trends in Biotechnology*, *25*(3), 111–8.
Lei, H., Romeo, G., and Kazlauskas, A. (2004). Heat shock protein 90alpha-dependent translocation of annexin II to the surface of endothelial cells modulates plasmin activity in the diabetic rat aorta. *Circulation Research*, *94*(7), 902–9.
Leibovitz, A., Stinson, J. C., Iii, W. B. M., Leibovltz, A., Stlnson, J. C., Mccombs, W. B., and Mabry, N. D. (1976). Classification of Human Colorectal Adenocarcinoma Cell Lines. *Cancer Research*, 4562–4569.
Li, J., Soroka, J., and Buchner, J. (2012a). The Hsp90 chaperone machinery: conformational dynamics and regulation by co-chaperones. *Biochimica et Biophysica Acta*, *1823*(3), 624–35.
Li, W., Li, Y., Guan, S., Fan, J., Cheng, C.-F., Bright, A. M., Chinn, C., Chen, M. and Woodley, D. T. (2007). Extracellular heat shock protein-90alpha: linking hypoxia to skin cell motility and wound healing. *The EMBO Journal*, *26*(5), 1221–33.
Li, W., Sahu, D., and Tsen, F. (2012b). Secreted heat shock protein-90 (Hsp90) in wound healing and cancer. *Biochimica et Biophysica Acta*, *1823*(3), 730–41.
Li, Y., Zhang, T., Schwartz, S. J., and Sun, D. (2009). New developments in Hsp90 inhibitors as anti-cancer therapeutics: mechanisms, clinical perspective and more potential. *Drug Resistance Updates : Reviews and Commentaries in Antimicrobial and Anticancer Chemotherapy*, *12*(1-2), 17–27.
Linehan, W. M. (2012). 17AAG to Treat Kidney Tumors in Von Hippel-Lindau Disease. Retrieved from http://clinicaltrials.gov/
Liu, F., Pouponnot, C., and Massague, J. (1997). Dual role of the Smad4 / DPC4 tumor suppressor in TGFβ -inducible transcriptional complexes. *Genes and Development,* 3157–3167.
Luo, X.-G., Zou, J.-N., Wang, S.-Z., Zhang, T.-C., and Xi, T. (2010). Novobiocin decreases SMYD3 expression and inhibits the migration of MDA-MB-231 human breast cancer cells. *IUBMB Life*, *62*(3), 194–9.
Makhnevych, T., and Houry, W. A. (2012). The role of Hsp90 in protein complex assembly. *Biochimica et Biophysica Acta*, *1823*(3), 674–82.
Martin, G. S. (2003). Cell signaling and cancer. *Cancer Cell*, *4*(3), 167–74.
Maruya, M., Sameshima, M., Nemoto, T., and Yahara, I. (1999). Monomer arrangement in HSP90 dimer as determined by decoration with N and C-terminal region specific antibodies. *Journal of Molecular Biology*, *285*(3), 903–7.

Marzec, M., Eletto, D., and Argon, Y. (2012). GRP94: An HSP90-like protein specialized for protein folding and quality control in the endoplasmic reticulum. *Biochimica et Biophysica Acta*, *1823*(3), 774–87.

Massagué, J. (2008). TGFbeta in Cancer. *Cell*, *134*(2), 215–30.

Massagué, J., Seoane, J., and Wotton, D. (2005). Smad transcription factors. *Genes and Development*, *19*(23), 2783–810.

Matsuyama, S., Iwadate, M., Kondo, M., Saitoh, M., Hanyu, A., Shimizu, K., Aburatani, H., Mishima, H. K., Imamura, T., Miyazono, K. and Miyazawa, K. (2003). SB-431542 and Gleevec Inhibit Transforming Growth Factor- β -Induced Proliferation of Human Osteosarcoma Cells SB-431542 and Gleevec Inhibit Transforming Growth Factor-β-Induced Proliferation of Human Osteosarcoma Cells. *Cancer Research*, *63*, 7791–7798.

McCready, J., Sims, J. D., Chan, D., and Jay, D. G. (2010). Secretion of extracellular hsp90alpha via exosomes increases cancer cell motility: a role for plasminogen activation. *BMC Cancer*, *10*, 294.

Meyer, P., Prodromou, C., Hu, B., Vaughan, C., Roe, S. M., Panaretou, B., Piper, P. W. and Pearl, L. H. (2003). Structural and Functional Analysis of the Middle Segment of Hsp90: Implications for ATP Hydrolysis and Client Protein and Cochaperone Interactions. *Molecular Cell*, *11*(3), 647–658.

Millson, S. H., Truman, A. W., Rácz, A., Hu, B., Panaretou, B., Nuttall, J., Mollapour, M. Söti, C. and Piper, P. W. (2007). Expressed as the sole Hsp90 of yeast, the alpha and beta isoforms of human Hsp90 differ with regard to their capacities for activation of certain client proteins, whereas only Hsp90beta generates sensitivity to the Hsp90 inhibitor radicicol. *The FEBS Journal*, *274*(17), 4453–63.

Minami, Y., Kawasaki, H., Miyata, Y., Suzuki, K., and Yahara, I. (1991). Analysis of native forms and isoform compositions of the mouse 90-kDa heat shock protein, HSP90. *The Journal of Biological Chemistry*, *266*(16), 10099–103.

Miyaki, M., Iijima, T., Konishi, M., Sakai, K., Ishii, A., Yasuno, M., Hishima, T., Koike, M., Shitara, K., Iwama, T., Utsunomiya, J., Kuroki, T., and Mori, T. (1999). Higher frequency of Smad4 gene mutation in human colorectal cancer with distant metastasis. *Oncogene*, *18*, 3098–3103.

Miyazono, K., Hellman, U., Wernstedt, C., and Heldins, C. (1988). Latent High Molecular Weight Complex of Transforming Growth Factor β1. *The Journal of Biological Chemistry*, *263*(13), 6407–6415.

Morimoto, R. I., Sarge, K. D., and Abravaya, K. (1992). Transcriptional regulation of heat shock genes. *The Journal of Biological Chemistry*, *267*(31), 21987–21990.

Munger, J. S., Huang, X., Kawakatsu, H., Griffiths, M. J. D., Dalton, S. L., Wu, J., Kaminski, N., Garat, C., Matthat, M. A., Rifkin, D. B., Sheppard, D. and Francisco, S. (1999). The Integrin αvβ6 Binds and Activates Latent TGFβ1 : A Mechanism for Regulating Pulmonary Inflammation and Fibrosis. *Cell*, *96*, 319–328.

Neckers, L., and Ivy, S. P. (2003). Heat shock protein 90. *Current Opinion in Oncology*, *15*(6), 419–24.

Padua, D., and Massagué, J. (2009). Roles of TGFbeta in metastasis. *Cell Research*, *19*(1), 89–102.

Pauwels, K., Van Molle, I., Tommassen, J., and Van Gelder, P. (2007). Chaperoning Anfinsen: the steric foldases. *Molecular Microbiology*, *64*(4), 917–22.

Picard, D. (2014). Hsp90 Facts and Literature. Retrieved from http://www.hsp90.org/resources

Pratt, W. B., and Toft, D. O. (2003). Regulation of signaling protein function and trafficking by the hsp90/hsp70-based chaperone machinery. *Experimental Biology and Medicine (Maywood, N.J.)*, *228*(2), 111–33.

Ramanathan, R. K., Egorin, M. J., Erlichman, C., Remick, S. C., Ramalingam, S. S., Naret, C., Helleran, J. L., TenEyck, C. J., Ivy, S. P. and Belani, C. P. (2010). Phase I Pharmacokinetic and Pharmacodynamic Study of an Inhibitor of Heat-Shock Protein 90, in Patients With Advanced Solid Tumors. *Journal of Clinical Oncology*, *28*(9), 1520–1526.

Reing, J., Zhang, L., Myers-Irvin, J., Cordero, K., Freytes, D., Heber-Katz, E., Bedelbaeva, K., McIntock, D., Dewilde, A., Braunhut, S. J. and Badylak, S. (2009). Degradation products of extracellular matrix affect cell migration and proliferation. *Tissue Engineering Part A*, *15*(3), 604–614.

Reitan, N. K., Sporsheim, B., Bjørkøy, A., Strand, S., and Davies, C. D. L. (2012). Quantitative 3-D colocalization analysis as a tool to study the intracellular trafficking and dissociation of pDNA-chitosan polyplexes. *Journal of Biomedical Optics*, *17*(2), 026015.

Reka, A. K., Kuick, R., Kurapati, H., Standiford, T., Omenn, G., and Keshamouni, V. (2011). Identifying Inhibitors of Epithelial-Mesenchymal Transition by Connectivity-Map Based Systems Approach.. *Journal of Thoracic Oncology, 6*(11), 1784–1792.

Reyes-Del Valle, J., Chávez-Salinas, S., Medina, F., and Del Angel, R. M. (2005). Heat shock protein 90 and heat shock protein 70 are components of dengue virus receptor complex in human cells. *Journal of Virology*, *79*(8), 4557–67.

Rich, J. N. (2003). The role of transforming growth factor-beta in primary brain tumors. *Frontiers in Bioscience*, *8*, 245–260.
Ritossa, F. (1962). A new puffing pattern induced by temperature shock and DNP in drosophila. *Cellular and Molecular Life Sciences*, *18*(12), 571–573.
Rosman, D. S., Phukan, S., Huang, C.-C., and Pasche, B. (2008). TGFBR1*6A enhances the migration and invasion of MCF-7 breast cancer cells through RhoA activation. *Cancer Research*, *68*(5), 1319–28.
Sarto, C., Binz, P. A, and Mocarelli, P. (2000). Heat shock proteins in human cancer. *Electrophoresis*, *21*(6), 1218–26.
Savage-Dunn, C. (2005). TGF-beta signaling. *The C. Elegans Research Community, WormBook*, 1–12.
Schlesinger, J. (1990). Heat Shock Proteins. *The Journal of Biological Chemistry, 265*(21), 12111–12114.
Schwartz, M. A., and Ginsberg, M. H. (2002). Networks and crosstalk: integrin signaling spreads. *Nature Cell Biology*, *4*(4), E65–8.
Sheppard, D. (2005). Integrin-mediated activation of latent transforming growth factor beta. *Cancer Metastasis Reviews*, *24*(3), 395–402.
Sidera, K., Gaitanou, M., Stellas, D., Matsas, R., and Patsavoudi, E. (2008). A critical role for HSP90 in cancer cell invasion involves interaction with the extracellular domain of HER-2. *The Journal of Biological Chemistry*, *283*(4), 2031–41.
Sidera, K., and Patsavoudi, E. (2009). Extracellular HSP90: An Emerging Target for Cancer Therapy. *Current Signal Transduction Therapy*, *4*(1), 51–58.
Sidera, K., Samiotaki, M., Yfanti, E., Panayotou, G., and Patsavoudi, E. (2004). Involvement of cell surface HSP90 in cell migration reveals a novel role in the developing nervous system. *The Journal of Biological Chemistry*, *279*(44), 45379–88.
Simms, N. A. K., Rajput, A., Sharratt, E. A, Ongchin, M., Teggart, C. A, Wang, J., and Brattain, M. G. (2012). Transforming growth factor-β suppresses metastasis in a subset of human colon carcinoma cells. *BMC Cancer*, *12*(1), 221.
Sims, J. D., McCready, J., and Jay, D. G. (2011). Extracellular heat shock protein (Hsp)70 and Hsp90α assist in matrix metalloproteinase-2 activation and breast cancer cell migration and invasion. *PloS One*, *6*(4), e18848.
Smith, J. R., and Workman, P. (2007). Targeting the cancer chaperone HSP90. *Drug Discovery Today: Therapeutic Strategies*, *4*(4), 219–227.
Sorger, P. K., and Pelham, H. R. B. (1988). Yeast heat shock factor is an essential DNA-binding protein that exhibits temperature-dependent phosphorylation. *Cell*, *54*(6), 855–864.
Sottile, J., and Chandler, J. (2005). Fibronectin matrix turnover occurs through a caveolin-1-dependent process. *Molecular Biology of the Cell*, *16*(2), 757–68.
Sreedhar, A., Kalmár, É., Csermely, P., and Shen, Y.-F. (2004). Hsp90 isoforms: functions, expression and clinical importance. *FEBS Letters*, *562*(1-3), 11–15.
Stellas, D., Hamidieh, A. El, and Patsavoudi, E. (2010). Monoclonal antibody 4C5 prevents activation of MMP2 and MMP9 by disrupting their interaction with extracellular HSP90 and inhibits formation of metastatic breast cancer cell deposits. *BMC Cell Biology*, *11*(51), 1–9.
Subramanian, G., Schwarz, R. E., Higgins, L., Dugar, S., and Reiss, M. (2004). Targeting Endogenous Transforming Growth Factor β Receptor Signaling in SMAD4-Deficient Human Pancreatic Carcinoma Cells Inhibits Their Invasive Phenotype 1. *Cancer Research*, *64*, 5200–5211.
Suzuki, S., and Kulkarni, A. B. (2010). Extracellular heat shock protein HSP90beta secreted by MG63 osteosarcoma cells inhibits activation of latent TGF-beta1. *Biochemical and Biophysical Research Communications*, *398*(3), 525–31.
Taipale, M., Krykbaeva, I., Koeva, M., Kayatekin, C., Westover, K. D., Karras, G. I., and Lindquist, S. (2012). Quantitative analysis of HSP90-client interactions reveals principles of substrate recognition. *Cell*, *150*(5), 987–1001.
Terasawa, K., Minami, M., and Minami, Y. (2005). Constantly updated knowledge of Hsp90. *Journal of Biochemistry*, *137*(4), 443–7.
Tissieres, A., Mitchell, H. K., and Tracy, U. M. (1974). Protein synthesis in salivary glands of Drosophila melanogaster: relation to chromosome puffs. *Journal of Molecular Biology*, *84*, 389.
Towbin, H., Staehelin, T., and Gordon, J. (1979). Electrophoretic transfer of proteins from polyacrylamide gels to nitrocellulose sheets: procedure and some applications. *Proceedings of the National Academy of Sciences*, *76*(9), 4350–4354.
Trepel, J., Mollapour, M., Giaccone, G., and Neckers, L. (2010). Targeting the dynamic HSP90 complex in cancer. *Nature Reviews. Cancer*, *10*(8), 537–49.

Triantafilou, M., and Triantafilou, K. (2004). Heat-shock protein 70 and heat-shock protein 90 associate with Toll-like receptor 4 in response to bacterial lipopolysaccharide. *Biochemical Society Transactions*, *32*(Pt 4), 636–9.

Tsutsumi, S., Beebe, K., and Neckers, L. (2009). Impact of heat-shock protein 90 on cancer metastasis. *Future Oncology*, *5*(5), 679–688.

Tsutsumi, S., and Neckers, L. (2007). Extracellular heat shock protein 90: a role for a molecular chaperone in cell motility and cancer metastasis. *Cancer Science*, *98*(10), 1536–9.

Ullrich, A., Coussens, L., Hayflick, J. S., Dull, T. J., Gray, A., Tam, A. W., Lee, J., Yarden, Y., Libermam, T.A., Schlesseinger, J., Downward, J., Mayes, E. L. V., Whittle, N., Watrfield, M. D. and Seeburg, P. H. (1984). Human epidermal growth factor receptor cDNA sequence and aberrant expression of the amplified gene in A431 epidermoid carcinoma cells. *Nature*, *309*(5967), 418–425.

Voss, A. K., Thomas, T., and Gruss, P. (2000). Mice lacking HSP90 β fail to develop a placental labyrinth, *11*, 1–11.

Watabe, T., Nishihara, A., Mishima, K., Yamashita, J., Shimizu, K., Miyazawa, K. Nishikawa, S-I. and Miyazono, K. (2003). TGF-beta receptor kinase inhibitor enhances growth and integrity of embryonic stem cell-derived endothelial cells. *The Journal of Cell Biology*, *163*(6), 1303–11.

Wipff, P.J., and Hinz, B. (2008). Integrins and the activation of latent transforming growth factor beta1 - an intimate relationship. *European Journal of Cell Biology*, *87*(8-9), 601–15.

Witsch, E., Sela, M., and Yarden, Y. (2013). Roles for Growth Factors in Cancer Progression. *Physiology*, *25*, 85–101.

Woodford-Richens, K. L., Rowan, A. J., Gorman, P., Halford, S., Bicknell, D. C., Wasan, H. S., Roylance, R. R., Bodmer, W. F. and Tomlinson, I. P. (2001). SMAD4 mutations in colorectal cancer probably occur before chromosomal instability, but after divergence of the microsatellite instability pathway. *Proceedings of the National Academy of Sciences of the United States of America*, *98*(17), 9719–23.

World Health Organization. (2014). World Cancer Report. *GLOBOCAN (IARC)*.

Wrighton, K. H., Lin, X., and Feng, X.-H. (2008). Critical regulation of TGFbeta signaling by Hsp90. *Proceedings of the National Academy of Sciences of the United States of America*, *105*(27), 9244–9.

Xu, Y., and Pasche, B. (2007). TGF-β signaling alterations and susceptibility to colorectal cancer. *Human Molecular Genetics*, *16*(2), R14–R20.

Young, J. C. (2001). Hsp90: a specialized but essential protein-folding tool. *The Journal of Cell Biology*, *154*(2), 267–274.

Yu, X. M., Shen, G., Neckers, L., Blake, H., Holzbeierlein, J., Cronk, B., and Blagg, B. S. J. (2005). Hsp90 inhibitors identified from a library of novobiocin analogues. *Journal of the American Chemical Society*, *127*(37), 12778–9.

Zinchuk, V., Zinchuk, O., and Okada, T. (2007). Quantitative colocalization analysis of multicolor confocal immunofluorescence microscopy images: pushing pixels to explore biological phenomena. *Acta Histochemica et Cytochemica*, *40*(4), 101–11.

Zurawska, A., Urbanski, J., and Bieganowski, P. (2008). Hsp90n - An accidental product of a fortuitous chromosomal translocation rather than a regular Hsp90 family member of human proteome. *Biochimica et Biophysica Acta*, *1784*(11), 1844–6.

Appendices

Appendices

Appendix 1: Additional materials

A1.1 Tissue culture reagents

Dulbecco's Modified Eagle Medium [DMEM] and Leibovitz's L-15 Medium with GlutaMAX™ were from Gibco, Invitrogen. L-glutamine, trypsin-EDTA, Accutase and Penicillin/Streptomycin/Amphotericin (PSA) were from Sigma-Aldrich. Roswell Park Memorial Institute (RPMI) medium was from Lonza, heat-inactivated fetal calf serum (FCS) was from BioWest, and tissue culture plasticware was from Corning Incorporated, Greiner CELLSTAR®, and Porvair Sciences.

A1.2 Biochemical and molecular biology reagents

General reagents and chemicals (e.g. NaCl, Tris etc) were purchased from Sigma-Aldrich unless otherwise stated. Hybond nitrocellulose membrane, western blotting and SDS-PAGE apparatus and Clarity Western ECL Substrate (170-5061) were from Bio-Rad. SB431542 (1614) was from Tocris Bioscience, novobiocin (N1838), geldanamycin (G3381) and dimethyl sulfoxide (DMSO) were from Sigma-Aldrich.

A1.3 Proteins and antibodies

Recombinant native endotoxin-free human Hsp90β protein (SPR-102C) was from StressMarq Biosciences Inc., recombinant Human TGF-β1 (carrier-free) (580704) was from BioLegend, and Bovine Serum Albumin (BSA) (10735078001) was from Roche. See Table 1 for a complete list of antibodies used.

Table III. Summary of the relevant antibody details including supplier and individual experimental details used in this study

Antibody	Species	Type	Supplier and catalogue number		Experimental details*
Anti-human Hsp90α/β [F-8]	Mouse	Primary antibody	Santa Cruz Biotechnology	sc-13119	WB: 1:1000
Anti-human Hsp90α/β [N17]	Goat	Primary antibody	Santa Cruz Biotechnology	sc-1055	IP: 1 µg, C: 1:100
Anti-human TGF-β1 [500-M66]	Mouse	Primary antibody	Santa Cruz Biotechnology	sc-65378	WB: 1:1000, F and C: 1:100
Anti-human TGF-β RII [L21]	Rabbit	Primary antibody	Santa Cruz Biotechnology	sc-400	WB: 1:500
Anti-human pSMAD2/3	Goat	Primary antibody	Santa Cruz Biotechnology	sc-11769	C: 1:100, FC: 2 µg
Anti-human SMAD2/3	Rabbit	Primary antibody	Santa Cruz Biotechnology	sc-8332	C: 1:100, FC: 2 µg
Anti-human Hsp75 [TR1]	Mouse	Primary antibody	Santa Cruz Biotechnology	sc-13557	F: 1:500
Anti-histone H3	Rabbit	Primary antibody	Cell Signaling Technologies	9715L	WB: 1:5000
Anti-human Hsp90α	Rat	Primary antibody	Enzo life sciences	ADI-SPA-840-F	WB: 1:5000, F: 1:100
Anti-human Hsp90β	Mouse	Primary antibody	StressMarq Biosciences Inc.	SMC-107A	WB: 1:1000, F: 1:100
Anti-Grp94 [9G10]	Rat	Primary antibody	StressMarq Biosciences Inc.	SMC-105B	WB: F: 1:300
Anti-alpha tubulin [DM1A]	Mouse	Primary antibody	Abcam	ab7291	WB: 1:5000
Anti-integrin alpha V + beta 6 [10D5]	Mouse	Blocking antibody	Abcam	ab77906	B: 10 µg/ml
Normal Goat IgG	Goat	Isotype control	Santa Cruz Biotechnology	sc-2028	IP: 1 µg
FITC-conjugated mouse IgG_1	Mouse	Isotype control	BD Biosciences	11-4714-42	FC: 1 µg
FITC-conjugated anti-human TGF-βRII	Mouse	Directly conjugated	R&D systems	FAB241F	FC: 1 µg, F: 1:100
HRP-conjugated anti-mouse	Donkey	Secondary antibody	Santa Cruz Biotechology	sc-2314	WB: 1:5000
HRP-conjugated anti-rat	Donkey	Secondary antibody	Santa Cruz Biotechology	sc-2032	WB: 1:5000
HRP-conjugated anti-goat	Donkey	Secondary antibody	Abcam	ab97110	WB: 1:5000
HRP-conjugated anti-rabbit	Donkey	Secondary antibody	Abcam	ab16294	WB: 1:5000
Alexa-Fluor-488 conjugated anti-rat	Donkey	Fluorescent secondary antibody	Invitrogen	A21208	F: 1:100
Alexa-Fluor-550 conjugated anti-mouse	Donkey	Fluorescent secondary antibody	Abcam	ab96876	F: 1:1000
Anti-mouse DY488	Donkey	Fluorescent secondary antibody	Abcam	ab96934	C: 1:500
Anti-goat DY660	Donkey	Fluorescent secondary antibody	Abcam	ab96875	C: 1:500, FC: 2 µl
Anti-rabbit DY550	Donkey	Fluorescent secondary antibody	Abcam	ab96892	FC: 2 µl
Anti-rabbit DY488	Donkey	Fluorescent secondary antibody	Abcam	ab96891	C: 1:500

*WB= Western Blot Analysis, IP= Immunoprecipitation, F= Fluorescence Microscopy, C= Confocal Microscopy, B= Protein Blocking, FC= Flow Cytometry

Appendix 2: Example of the method used to quantify the migration of SW480 and SW620 cells over 24 hours

Example: SW620 cells treated for 24 hours with 2ng/ml TGF-β and 20 ng/ml Hsp90β. Photo taken at 12 Hours under a 10x objective using an iPhone in conjunction with the SkyLight

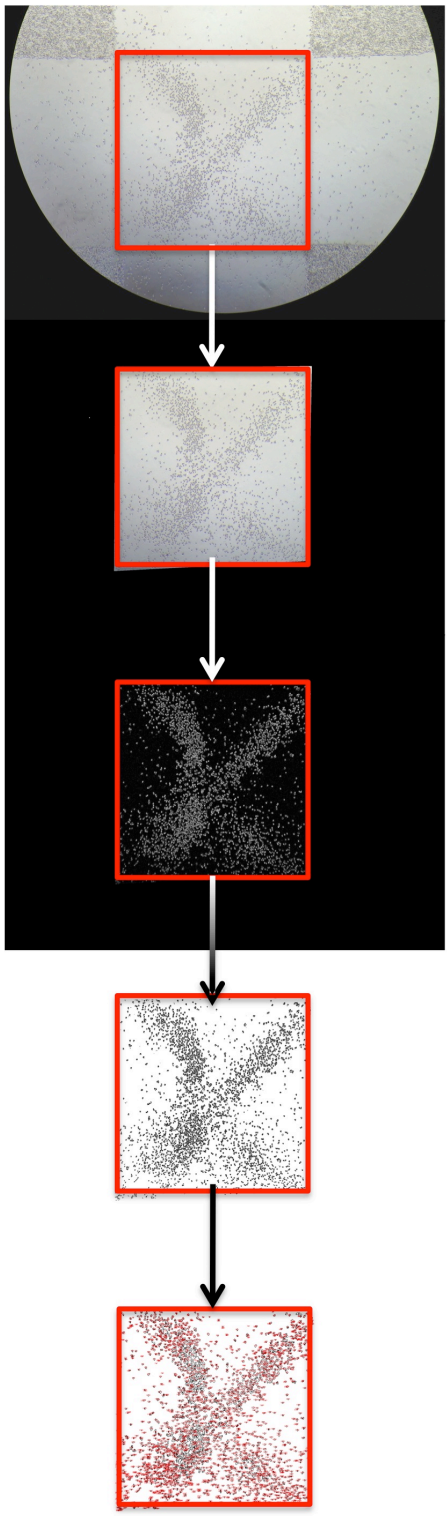

1 The image was opened in Image J, a square was created between the four cell areas from which the cells moved, and the area of this square was measured
(Scale set at 500 pixels = 1mm)

2 Everything outside the square was deleted. The image was converted to 8-bit and the 'find edges' function is used to outline all cells individually.

3 The threshold of the cells was determined and applied highlighting each cell.

4 The 'analyze particles' function was used with all cells smaller than 3E-6 being excluded, the outlines and counts are shown in (5).

5 The count was 2693 cells in 5.1mm^2. Each count was divided by the area to obtain cells per area (mm^2), and each image was normalised to each time=0 image

Supplementary Figure 1. Step by step example of quantitation of the cellular migration of SW480 and SW620 cells over 24 hours

Supplementary Figure 1. Step by step example of quantitation of the cellular migration of SW620 cells over 24 hours. The migration of SW620 cells treated cells with 2ng/ml TGF-β1 and 20 ng/ml Hsp90β is shown. Cells were seeded at a density of 1.2 x 10^6 cells/ml into each individual well of an Ibidi micro-Insert four-well chamber and left to adhere overnight. Each entire insert was filled with L15 medium with treatments. After 24 hours the inserts were lifted and the cell area was washed to remove unattached cells. Photos of the intersection between the vertical and horizontal wounds generated by the micro-inserts were taken under a 10x objective using a SkyLight adapter at 0, 12, and 24 hours. Images were analysed in Image J. The square between the four-well inserts containing cells was blocked off and measured (scale: 500 pixels = 1 mm). Everything in the square was converted to 8-bit and the edges were identified. Using the threshold function, each cell was highlighted and counted by analysing the particles. Each count was divided by its area and normalised to time=0 for each treatment. This data was statistically analysed using GraphPad Prism 4.03 software (GraphPad Inc., California) and a two-way analysis of variance (ANOVA) with Bonferroni post tests was performed to compare the different treatments to untreated cells.

Appendix 3: Example of the method used to determine the intensity of pSMAD2/3 and nuclei stained in confocal images of SW480 and SW620 cells

Example: SW620 cells treated for 24 hours with 2ng/ml TGF-β1, and stained for pSMAD2/3 and nuclei (see Figure 14 for details).

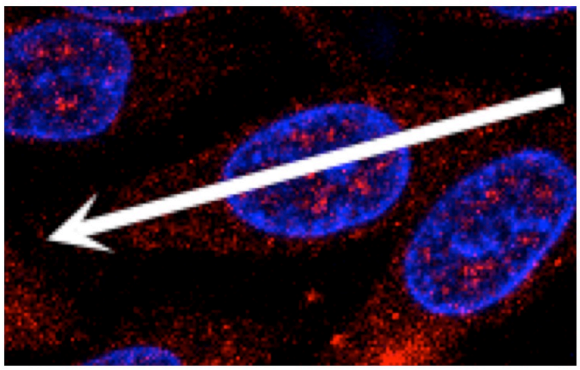

1 The image stained for pSMAD2/3 (in red) and nuclei (in blue) was opened in Zen Lite 2014, in profile mode an arrow is drawn through the length of several cells 5 pixels wide. This data is exported to create a graph.

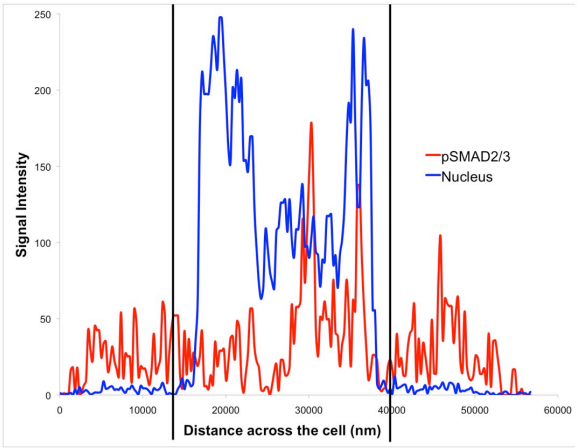

2 Each scatter plot graph was created using coordinates from the nucleus and pSMAD2/3 intensities. Two black lines were drawn on either side of the nucleus (shown as a blue line).

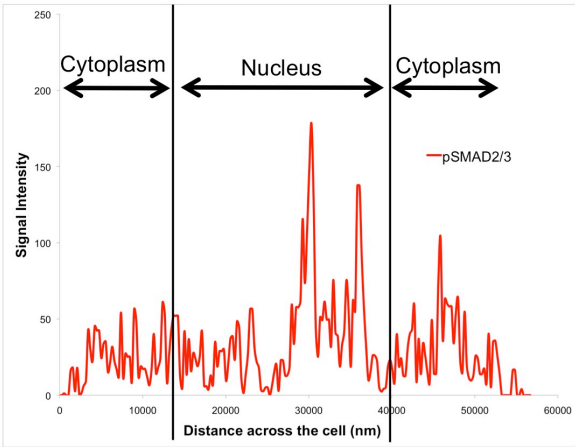

3 The lines were deleted and the images were imported into Image J, where the area under the pSMAD2/3 graph (shown as a red line) was analysed between the lines (in the nucleus) and on either side of the lines (in the cytoplasm).

Supplementary Figure 2. Step by step example of the method used to determine pSMAD2/3 distribution in SW480 and SW620 cells, by determining signal intensity of confocal images.

Supplementary Figure 2. Step by step example of the method used to determine pSMAD2/3 distribution in SW480 and SW620 cells, by determining signal intensity of confocal images. SW480 and SW620 cancer cells were seeded at a density of 3 x 10^5 cells/ml on gelatin coated 15-well µ-Slide angiogenesis plates and incubated at 37°C for 24 hours. Cells were treated with 2 ng/ml TGF-β1, 20 ng/ml Hsp90β, 100 nM SB 431542 and 100µM novobiocin for 24 hours alone and in combinations. Cells were fixed with ethanol and stained with rabbit anti-SMAD2/3 and goat anti-pSMAD2/3 primary antibodies overnight at 4 °C. This was followed by incubation with donkey anti-goat DY660 (pseudo-coloured to red) secondary antibodies overnight at 4 °C. Nuclei were stained with 1 µg/ml Hoechst 33342 (blue). Immunofluorescence was detected using the Zeiss LSM 780 confocal microscope and the images analysed using Zen Lite Software 2014 (Zeiss, Germany), where profiles were created using an arrow (5 pixels wide) as seen in step 1. Graphs were made using profiles of the nucleus and pSMAD2/3, thereafter two lines were drawn containing the nucleus as seen in step 2. Step 3 consisted of measuring the area under the graph between the lines (in the nucleus) and on either side of the lines (in the cytoplasm). The ratio of pSMAD2/3 was analysed using GraphPad Prism 4.03 software (GraphPad Inc., California) and a two-way analysis of variance (ANOVA) with Bonferroni post tests was performed to compare untreated cells to treated cells.